UNIVERSITY OF SÃO PAULO
SÃO CARLOS SCHOOL OF ENGINEERING

FERNANDO LUIZ LAVOIE

Study on the durability of HDPE geomembranes applied to geotechnics and the environment using laboratory aged samples and in situ exhumed samples

São Carlos
2021

FERNANDO LUIZ LAVOIE

Study on the durability of HDPE geomembranes applied to geotechnics and the environment using laboratory aged samples and in situ exhumed samples

Doctor dissertation presented to the Graduate Program in Geotechnics at the São Carlos School of Engineering at the University of São Paulo, as part of the requirements for obtaining the title of Doctor of Science.

Concentration Area: Geotechnics

Supervisor: Prof. Dr. Jefferson Lins da Silva

Co-supervisor: Prof. Dr. Marcelo Kobelnik

São Carlos

2021

Ficha catalográfica elaborada pela Biblioteca Prof. Dr. Sérgio Rodrigues Fontes da EESC/USP com os dados inseridos pelo(a) autor(a).

Lavoie, Fernando Luiz
L363s Study on the durability of HDPE geomembranes applied to geotechnics and the environment using laboratory aged samples and in situ exhumed samples / Fernando Luiz Lavoie; orientador Jefferson Lins da Silva; coorientador Marcelo Kobelnik. São Carlos, 2021.

Tese (Doutorado) - Programa de Pós-Graduação e Área de Concentração em Geotecnia -- Escola de Engenharia de São Carlos da Universidade de São Paulo, 2021.

1. HDPE geomembrane. 2. Durability. 3. Physical analysis. 4. Thermal analysis. 5. Aging. I. Título.

Eduardo Graziosi Silva - CRB - 8/8907

Candidato: Engenheiro **FERNANDO LUIZ LAVOIE.**

Título da tese: "Estudo sobre a durabilidade de geomembranas de PEAD aplicadas na geotecnia e meio ambiente por meio de amostragens envelhecidas em laboratório e exumadas in situ".

Data da defesa: 19/11/2021.

Comissão Julgadora	**Resultado**
Prof. Associado **Jefferson Lins da Silva (Orientador)** (Escola de Engenharia de São Carlos/EESC-USP)	APROVADO
Prof. Titular **Ennio Marques Palmeira** (Universidade de Brasília/UnB)	APROVADO
Profa. Dra. **Maria de Lurdes da Costa Lopes** (Universidade do Porto/UP-Portugal)	APROVADO
Profa. Dra. **Marta Pereira da Luz** (Pontifícia Universidade Católica de Goiás/PUC)	APROVADO
Prof. Dr. **Guilherme Wolf Lebrão** (Instituto Mauá de Tecnologia/IMT)	APROVADO

Coordenadora do Programa de Pós-Graduação em Geotecnia:
Profa. Associada **Valéria Guimarães Silvestre Rodrigues**

Presidente da Comissão de Pós-Graduação:
Prof. Titular **Murilo Araujo Romero**

DEDICATION

To Ingrid, my wife, and the love of my life.

ACKNOWLEDGEMENTS

I thank my parents, Cybelli Lavoie and Luiz Paulo Lavoie, for providing me a solid familiar education, which enabled me to aim at a high education level.

I would like to thank my ex-supervisor, Prof. Dr. Benedito de Souza Bueno, for open the geosynthetics laboratory door for the first time in 2001. He was a Brazilian geosynthetics pioneer; I am so proud to have been his student.

I would like to thank my friend and supervisor, Prof. Dr. Jefferson Lins da Silva, for open the geosynthetics laboratory door for the second time in 2019. Jefferson gave me the conditions to develop my research, supporting me and believing in me during the whole process.

I am grateful to my co-supervisor, Prof. Dr. Marcelo Kobelnik, for teaching me thermal analysis and supporting my work from the first day until the last one.

I want to express my gratitude to Prof. Dr. Maria de Lurdes Lopes, for the knowledge about geosynthetics durability transmitted during this time.

I want to show my gratefulness to MSc. Clever Aparecido Valentin, for the support and collaboration with my work.

I thank MSc. Érica Fernanda da Silva Tirelli, for supporting me in the thermal and physical analyses of my research.

I would like to thank the Brazilian manufacturers who donated the virgin samples of HDPE geomembranes used in this research.

I want to express my gratitude to the engineers and friends who helped me collect the exhumed HDPE geomembrane samples utilized in my work.

I would like to thank Prof. Dr. Cássia de Silveira Assis, for encouraging me to grow academically.

Special thanks to Mauá Institute of Technology (IMT) for the fund provided to my research.

ABSTRACT

LAVOIE, F. L. **Study on the durability of HDPE geomembranes applied to geotechnics and the environment using laboratory aged samples and in situ exhumed samples**. 2021. Doctor Dissertation – São Carlos School of Engineering, University of São Paulo, São Carlos, 2021.

The polymer demand for geotechnical applications has been growing. The geomembrane is a geosynthetic, manufactured, polymeric product and is often specified in environmental and hydraulic projects. Over the past forty years, millions of square meters of HDPE geomembrane have been used in different applications. One of the most important issues for HDPE geomembranes is the durability, involving very long-term property requirements. This work analyzed exhumed and laboratory aged HDPE geomembrane samples using physical and thermal analyses. The virgin samples evaluated in this research were smooth and with nominal thicknesses of 1.0 (1L sample), 1.5 (1.5L sample) and 2.0 mm (2L sample). The exhumed samples were collected in different Brazilian construction works in many geotechnical and environmental applications. The CLIQ sample was exhumed from an industrial water pond after 2.25 years of field exposure. The LTE sample was exhumed from an aeration pond by sewage treatment after 2.75 years of exposure. The LCH sample was exhumed from a municipal landfill leachate pond after 5.17 years of exposure. The MIN and MIN2 samples were exhumed from mining facilities after, respectively, 7.92 and 10.08 years of exposure. The LDO sample was exhumed from a biodegradable waste pond after 15.17 years of exposure. The CAM, CAM1 and CAM2 samples were exhumed from shrimp farming ponds, that the CAM and CAM1 samples were exhumed from the same pond, but the CAM sample was taken from the bottom liner and the CAM1 sample from the slope liner, both after 8.25 years of exposure. The CAM2 sample was taken from another shrimp farming pond after 3.0 years of field exposure. The analyzed exhumed geomembranes demonstrated several changes in their properties, including low stress crack resistance (SCR) values and low Std. OIT (oxidative-induction time), which could conduct a liner rupture in a short-term, except for the LCH sample, the thickest exhumed sample, which presented good performance in the physical properties, but some changes in thermal decomposition. For the UV fluorescent radiation, after 8760 h of exposure, the 1L sample demonstrated losses in tensile properties and a considerable antioxidant depletion, changing its performance as a liner. It was observed that the 1.5 mm-thick HDPE geomembrane had losses in SCR, high antioxidant consumption, a change in the thermal behavior before the melting point, but maintained the viscosity of the polymer and preserved the ductility. The virgin samples presented several changes in some evaluated properties after the thermal

exposure (8760 h) and the synergy exposure to UV radiation (8760 h) and thermal aging (4380 h), highlighting for the MFI (melt flow index) results, which demonstrated the occurrence of cross-linking reactions for all samples. Moreover, all samples presented considerable changes in SCR behavior and high antioxidant depletion. Finally, this research evidenced the necessity to homogenise the resins and additives of the Brazilian HDPE geomembranes to guarantee products with long-term durability, avoiding losses in terms of human lives, environmental impacts, and financial costs.

Keywords: HDPE geomembrane. Durability. Physical analysis. Thermal analysis. Aging.

RESUMO

LAVOIE, F. L. **Estudo sobre a durabilidade de geomembranas de PEAD aplicadas na geotecnia e meio ambiente por meio de amostragens envelhecidas em laboratório e exumadas in situ**. 2021. Tese (Doutorado) – Escola de Engenharia de São Carlos, Universidade de São Paulo, São Carlos, 2021.

A demanda de polímeros para aplicações geotécnicas vem crescendo. A geomembrana é um produto geossintético, manufaturado, polimérico e frequentemente especificado em projetos ambientais e hidráulicos. Nos últimos quarenta anos, milhões de metros quadrados de geomembrana de PEAD foram usados em diferentes aplicações. Uma das questões mais importantes para geomembranas de PEAD é a durabilidade, envolvendo requisitos de propriedade de muito longo prazo. Este trabalho analisou amostras de geomembrana de PEAD exumadas em campo e envelhecidas em laboratório usando análises físicas e térmicas. As amostras virgens avaliadas nesta pesquisa eram lisas e com espessuras nominais de 1,0 (amostra 1L), 1,5 (amostra 1,5L) e 2,0 mm (amostra 2L). As amostras exumadas foram coletadas em diferentes obras brasileiras em diversas aplicações geotécnicas e ambientais. A amostra CLIQ foi exumada de uma lagoa de água industrial após 2,25 anos de exposição em campo. A amostra LTE foi exumada de uma lagoa de aeração de uma estação de tratamento de esgoto após 2,75 anos de exposição. A amostra de LCH foi exumada de uma lagoa de chorume de um aterro sanitário após 5,17 anos de exposição. As amostras MIN e MIN2 foram exumadas de obras de mineração após, respectivamente, 7,92 e 10,08 anos de exposição. A amostra LDO foi exumada de uma lagoa de resíduos biodegradáveis após 15,17 anos de exposição. As amostras CAM, CAM1 e CAM2 foram exumadas de lagoas de carcinicultura, As amostras CAM (base) e CAM1 (talude) foram exumadas da mesma lagoa, ambas após 8,25 anos de exposição. A amostra CAM2 foi retirada de outra lagoa de carcinicultura após 3,0 anos de exposição em campo. As geomembranas exumadas analisadas demonstraram várias alterações em suas propriedades, incluindo baixos valores de resistência ao *stress cracking* (SCR) e baixos valores de OIT padrão (tempo de indução oxidativa), podendo conduzir a ruptura da barreira de fluxo em curto prazo, exceto para a amostra LCH, a mais espessa, que apresentou bom desempenho nas propriedades físicas, mas algumas alterações na decomposição térmica. Para a radiação UV fluorescente, após 8760 h de exposição, a amostra 1L demonstrou perdas nas propriedades de tração e um considerável consumo de antioxidantes, alterando seu desempenho como barreira de fluxo. Observou-se que a geomembrana de PEAD de 1,5 mm de espessura apresentou perdas no SCR, alto consumo de antioxidantes, alteração do comportamento térmico antes do ponto de fusão, mas manteve a viscosidade do polímero e preservou a ductilidade. As amostras

virgens apresentaram diversas alterações em algumas propriedades avaliadas após a exposição térmica (8760 h) e exposição sinérgica à radiação UV (8760 h) e envelhecimento térmico (4380 h), com destaque para os resultados de índice de fluidez (MFI), que demonstraram a ocorrência de reações de ligação cruzada para todas as amostras. Além disso, todas as amostras apresentaram mudanças consideráveis no comportamento do SCR e alto consumo de antioxidantes. Por fim, esta pesquisa evidenciou a necessidade de homogeneizar as resinas e aditivos das geomembranas brasileiras de PEAD para garantir produtos com durabilidade de longo prazo, evitando perdas em vidas humanas, impactos ambientais e custos financeiros.

Palavras-chave: Geomembrana de PEAD. Durabilidade. Análise física. Análise térmica. Envelhecimento.

LIST OF FIGURES

LIST OF TABLES

LIST OF ABBREVIATIONS

Abs	–	Absorbance
ASTM	–	American Society for Testing and Materials
ATAC	–	Almost the Total Antioxidant Consumption
BB	–	Brittle Behavior
BCE	–	Baseline Change Event
BOD	–	Biochemical Oxygen Demand
Deriv.	–	Derivative
CAM	–	Shrimp Farming Pond HDPE Geomembrane Sample
CAM1	–	Shrimp Farming Pond HDPE Geomembrane Sample
CAM2	–	Shrimp Farming Pond HDPE Geomembrane Sample
CB	–	Combustion
CBC	–	Carbon Black Content
CBD	–	Carbon Black Dispersion
CCDM	–	Material Characterization and Development Center
CCL	–	Compacted Clay Liner
CEC	–	Cation Exchange Capacity
CLIQ	–	Industrial Water Pond HDPE Geomembrane Sample
CSPE	–	Chlorosulfonated Polyethylene
CTD	–	Changes in Thermal Decomposition
DEV	–	Deviation in DSC Curve
DMA	–	Dynamic Mechanic Analysis
DSC	–	Differential Scanning Calorimetry
DTA	–	Differential Thermal Analysis
DTB	–	Distinct Thermal Behavior
DTG	–	Derivative Thermogravimetry
EESC-USP	–	São Carlos School of Engineering, University of São Paulo
Elong.	–	Elongation
f-HDPE	–	Fluorinated High-Density Polyethylene
FTIR	–	Fourier Transform Infrared Spectroscopy
GCL	–	Geosynthetic Clay Liner
GM	–	Geomembrane

GMB	–	Geomembrane
GRI	–	Geosynthetic Research Institute
HALS	–	Hindered Amine Light Stabilizer
HDPE	–	High-Density Polyethylene
HP OIT	–	High-Pressure Oxidative-Induction Time
IBRA	–	Brazilian Institute of Analysis
IMT	–	Mauá Institute of Technology
INT	–	Interaction between the Polymer and the Solution
IQ-UNESP	–	Chemical Institute, São Paulo State University
IQSC-USP	–	São Carlos Chemical Institute, University of São Paulo
LDO	–	Biodegradable Waste Pond HDPE Geomembrane Sample
LCH	–	Municipal Landfill Leachate Pond HDPE Geomembrane Sample
LLDPE	–	Linear Low-Density Polyethylene
LTE	–	Sewage Treatment Aeration Pond HDPE Geomembrane Sample
MDPE	–	Medium-Density Polyethylene
MFI	–	Melt Flow Index
MIN	–	Mining Facility HDPE Geomembrane Sample
MIN2	–	Mining Facility HDPE Geomembrane Sample
MNP	–	Most Probable Number
MQC	–	Manufacturing Quality Control
MWCNT	–	Multiwall Carbon Nanotubes
NCTL	–	Notched Constant Tensile Load
NTU	–	Nephelometric Turbidity Unit
OIT	–	Oxidative-Induction Time
OVL	–	Overlapped Reactions
PE	–	Polyethylene
PTFE	–	Polytetrafluoroethylene
Resist.	–	Resistance
SEM	–	Scanning Electron Microscopy
SCR	–	Stress Crack Resistance
Std. OIT	–	Standard Oxidative-Induction Time
TBB	–	Tendency to Brittle Behavior
TBF	–	Tendency to Brittle Failure
TDA	–	Tired Derived Aggregate

TE	–	Thermal Exposure
TEM	–	Transmission Electron Microscopy
Temp. Diff.	–	Temperature Differential
TG	–	Thermogravimetry
TMA	–	Thermomechanical Analysis
Tnp	–	Test not Performed; the Sample Size did not Allow
TOC	–	Total Organic Carbon
UFSCAR	–	Federal University of São Carlos
US	–	The United States of America
USA	–	The United States of America
UV	–	Ultraviolet
UV-B	–	Ultraviolet B
1L	–	HDPE Geomembrane Sample with 1.0 mm of thickness
1.5L	–	HDPE Geomembrane Sample with 1.5 mm of thickness
2L	–	HDPE Geomembrane Sample with 2.0 mm of thickness

LIST OF SYMBOLS

Cl^-	Chloride Ion
cm	Centimeter
cc	Cubic Centimeter
δ	Delta
ºC	Celsius Degree
E”	Loss Module
g	Gram
h	Hour
hv	Photon Energy
J	Joule
kg	Kilogram
kN	Kilonewton
kPa	Kilopascal
L	Liter
MPa	Megapascal
m	Meter
min	Minute
mg	Milligram
mL	Milliliter
mm	Millimeter
mmmol	Millimole
µS	Millisecond
mW	Milli Watts
µm	Micrometer
nm	Nanometer
N	Newton
O_2	Oxygen
OH●	Reactive Free Radical
%	Percentage
ppm	Parts per Million
pH	Potential of Hydrogen
RH	Polyethylene Polymer Chain

R□	Reactive Free Radical
R●	Reactive Free Radical
ROO□	Hydroperoxid
RO●	Reactive Free Radical
ROO●	Hydroperoxid
ROOH	Hydroperoxy Radical
s	Second
S	South
ΔT	Temperature Variation
T_t	Transition Time
Δ	Variation
W	West
Fe^0	Zero-Valent Iron

SUMMARY

1 INTRODUCTION AND OBJECTIVES

1.1 Introduction

Geomembranes, or geosynthetics as barriers, are very low permeability coefficient polymeric sheets (typically 10^{-11} cm s^{-1} to 10^{-13} cm s^{-1}), manufactured by the industry, delivered in rolls and installed in the site. Geomembranes can be produced with smooth faces or textured ones and with different colors (ROLLIN and RIGO, 1991; ROWE, 2001; LOPES and LOPES, 2010; PALMEIRA, 2018; HOU *et al.*, 2021). To reduce pollution to a minimum, geocomposite barrier systems, that include geomembranes and CCLs and/or GCLs, are often used at the bottom of landfills liners (TOUZE-FOLTZ *et al.*, 2021).

Geomembranes started to be used in the 1930s, but became widespread in the 1940s. In the 1970s, geomembranes began to be specified for landfills. HDPE geomembranes started to be used first in Europe and South Africa, and then later on moved to North America. Initially, they were used in canals, and their applications then spread to Russia, Taiwan, Canada, and Europe. In the 1980s, HDPE geomembranes were famous for their high chemical resistance and for being thermally welded. The use of HDPE geomembranes in municipal landfills and the hazardous waste industry has advanced since 1985, mainly due to the high strength and low cost of the product. Nowadays, HDPE geomembranes are the most utilized component of the liner solutions in the world (ROLLIN AND RIGO, 1991; EITH and KOERNER, 1997; KOERNER, 2005; SCHEIRS, 2009; KOERNER *et al.*, 1999).

Although quite subjective, current geomembrane application areas can be observed in three categories: transportation, environmental, and geotechnical. Each category has a number of specific applications which have been reported in the literature (ROLLIN and RIGO, 1991).

Geomembranes are used in many situations and in different types of construction works and structures, such as (VILAR *et al.*, 2015):

- Solid waste landfills and industrial waste;
- Water ponds and liquid waste ponds;
- Waterproof liners with tunnels;
- Under highways;
- Farm ponds;

- Covers and subsoils of buildings;
- Raised or buried water tanks;
- Adduction and irrigation canals;
- Pools and artificial beaches;
- Vertical walls for contaminated areas;
- Rehabilitate old concrete dams (TOUZE, 2021);
- Construction of new concrete dams (TOUZE, 2021).

Based on information from a domestic manufacturer, in Brazil about a hundred million square meters of high-density polyethylene (HDPE) geomembranes have been installed over 20 years, initially in landfills and mining facilities. However, over the last decade, they have been more widely used for water ponds and liquid waste ponds, aquaculture ponds and irrigation canals.

Geomembranes in general are exposed to different aging mechanisms, including UV degradation, extraction degradation, thermal degradation, swelling, oxidative degradation, and biological degradation. These mechanisms can influence the material properties and even decrease their durability (ROWE AND SANGAM, 2002; KAY *et al.*, 2004).

High density polyethylene geomembranes are formulated with 96-97.5 % polyethylene, 2-3 % UV protection, generally carbon black, and 0.5-1.0 % antioxidants and thermostabilizers (HSUAN AND KOERNER, 1995; LODI and BUENO, 2012; EWAIS *et al.*, 2014; LODI *et al.*, 2013; ROWE and EWAIS, 2015). This product exposed to aging can experience property changes due to molecular chain scission, crosslinking and bond breaking (HSUAN and KOERNER, 1995; PERKINS, 2007).

The polymer polyethylene (PE) can be defined as polyolefin which has the hydrocarbon group containing carbon and hydrogen atoms in the chemical structure. When the co-monomer increases, the density of PE decreases. The density of polyethylene influences the physical and mechanical properties. There is a relationship between density and different PE properties, as shown in Figure 1. In general, the MDPE is more useful for liners, because it presents better chemical resistance, high strength, and low permeability when compared to LLDPE. However, HDPE, which is a semi-crystalline structure polymer, is susceptible to stress cracking. The HDPE geomembrane is formed by MDPE resin added with carbon black and additives, making the density greater than 0.940 g cm^{-3} (SCHEIRS, 2009; HSUAN *et al.*, 2008; PEGGS and KANNINEN, 1995; GIROUD, 1994).

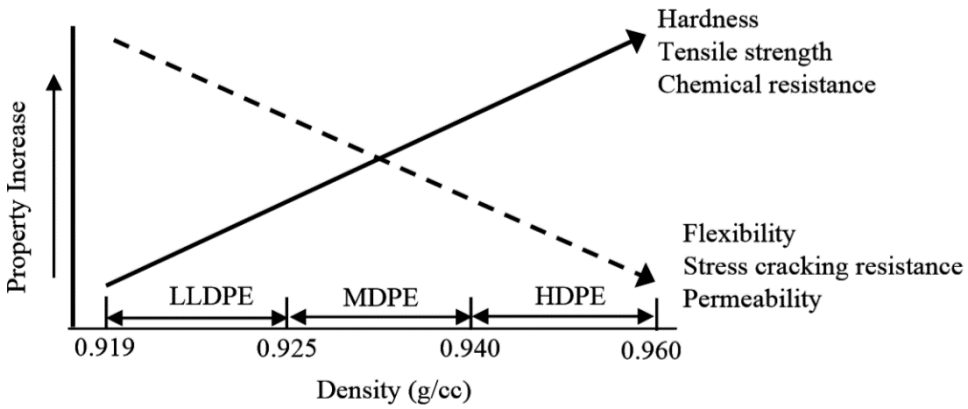

Figure 1. Material properties related to PE density (HSUAN *et al.*, 2008)

According to Lavoie *et al.* (2020), in addition to excellent resin, a suitable additive package, good industrial processability, good manufacturing quality control, satisfactory material specification for applications, a good installation practice must be specified and supervised in the field by the designer. The implications of bad installation procedures can lead to a short-term service life of high-density polyethylene geomembranes.

1.2 Research objectives

The general objective of this work was to analyze the durability of HDPE geomembranes through exhumation in constructions works and exposure in the laboratory, considering the classical analyzes and incorporating thermo-analytical analyzes, to assess the potential of these analyzes in the estimation of the durability.

The specific objectives of this research were:

1. To write a state-of-the-art about HDPE geomembranes durability;
2. To study the behavior of exhumed HDPE geomembrane samples in different applications with different times of exposures;
3. To analyze the performance of HDPE geomembrane samples conducted by laboratory exposure to UV radiation (UV weathering test chamber and xenon arc weatherometer);
4. To analyze the performance of HDPE geomembrane samples conducted by thermal aging (air-oven with forced circulation);

5. To analyze the performance of HDPE geomembrane samples conducted by a synergic exposure to UV radiation and thermal aging;
6. To compare the properties results among exhumed and exposed samples.

1.3 Dissertation structure

This dissertation is divided into five chapters. Chapter 1 presents the introduction and the research objectives of this work. Chapter 2 provides the literature review concerning the durability of the high-density polyethylene geomembranes. This chapter shows the types of degradation, the service life prediction of high-density polyethylene geomembranes, the laboratory studies of high-density polyethylene geomembrane durability, the field studies of HDPE geomembrane durability, the laboratory studies of exhumed HDPE geomembrane durability, and finally, high-density polyethylene geomembrane with nanoparticles. Chapter 3 presents the materials used in this research, detailing the virgin and exhumed high-density polyethylene geomembrane samples collected for this work. This chapter still detailed the laboratory aged exposure performed, the physical tests, and the thermal and complementary analyses realized. Chapter 4 provides the results and discussion of this dissertation, including the virgin, exhumed, and the exposed samples performed by physical, thermal, synergic exposure to UV radiation and thermal aging, and complementary analyses. Chapter 5 shows the current conclusion of this work and recommendations for future studies.

2 LITERATURE REVIEW

2.1 Types of degradation

The main mechanisms of high-density polyethylene geomembrane degradation are ultraviolet degradation, thermal degradation, oxidative degradation and the synergic effects of these mechanisms occurring simultaneously.

2.1.1 Oxidative degradation

Polyolefins including polyethylene (PE) degrade by oxidation, in which there is a reaction between the polymer and the oxygen molecule. The whole process of oxidation in solid state polymers is so complex and heterogeneous that its nature and kinetics still raise many open questions (GREENWOOD *et al.*, 2012).

The main process for HDPE oxidation is a free radical chain mechanism. Figure 2 shows the oxidation mechanism involving two-cycle processes. Cycle (A) is a chain reaction of alkyl/alkylperoxyl and the second one (B) is the formation of new radicals by chain reaction (homolysis of hydroperoxides). The oxidation can be stopped if all the links are foreclosed (ROWE and SANGAM, 2002; KELEN, 1983; GRASSIE and SCOTT, 1985).

To prevent the oxidation of the polymers, antioxidants are included in the HDPE resin. Two different types of antioxidants are used: the primary and secondary. The good efficiency of antioxidants depends on the amount and types, and the field temperature. Primary antioxidants work to prevent free radical formation, while secondary antioxidants work to decrease the formation of active hydroperoxides in inactive alcohols (CHIRINOS-PADRÓN and ALLEN, 1992; FAY and KING, 1994).

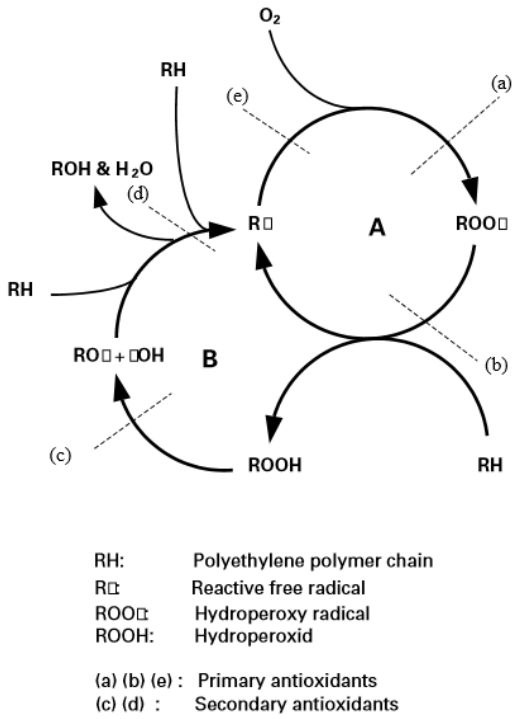

Figure 2. Oxidation cycle in polyethylene (ROWE and SANGAM, 2002)

The oxidation of HDPE geomembranes can be evaluated through three different stages, which is shown in Figure 3. Stage (A), the first one, is relative to antioxidant depletion. The quantity of antioxidants is measured by the oxidative induction time (OIT) test. In the second stage (B), the chain reaction begins, and changes in the molecular composition start. The third stage (C) represents significant changes in the molecular composition with the formation of free radicals, and cross-linking occurs in the free radicals. The result of these changes is a totally changed molecular structure, decreased in strength properties, the appearance of cracks, and there is an increase in the stress cracking susceptibility, culminating at the end of service life (ROWE and SANGAM, 2002; PERKINS, 2007; TISINGER and GIROUD, 1993; TIAN et al., 2018; EWAIS *et al.*, 2018; ABDELAAL *et al.*, 2019; ROWE *et al.*, 2013).

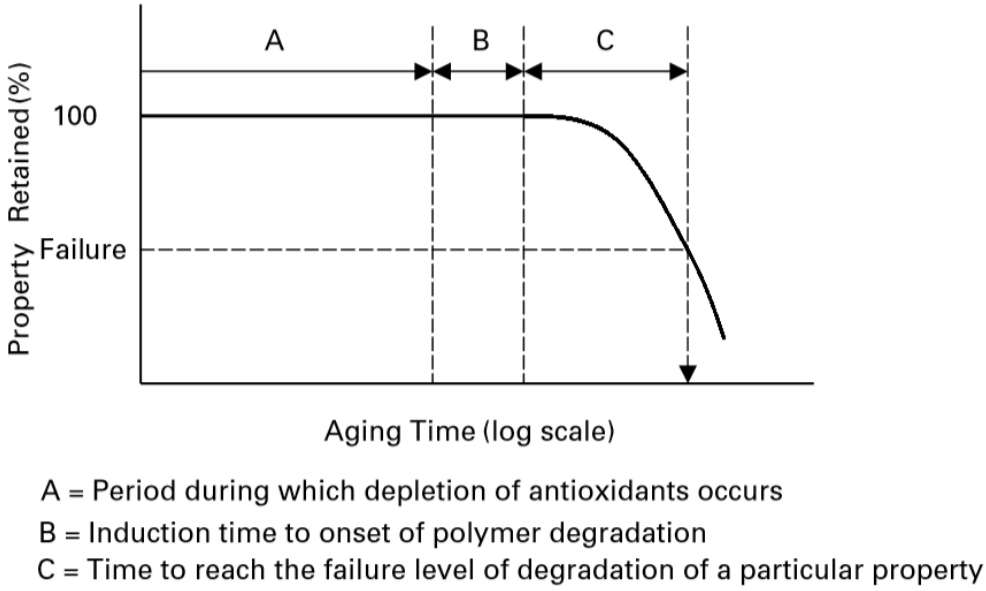

Figure 3. The concept of HDPE geomembrane oxidative degradation (ROWE and SANGAM, 2002)

High-density polyethylene geomembranes have several different degradation mechanisms, but, for base liner applications, oxidative degradation can be considered the most harmful (HSUAN and KOERNER, 1995; ROWE *et al.*, 2013).

2.1.2 Photo-degradation

The lifetime of geomembranes is led by ultraviolet (UV) radiation, or a combination of thermal and UV exposure. For this reason, carbon black is added to the blend to protect the HDPE, normally 2 % to 3 % (ROLLIN and RIGO, 1991; VAN SANTVOORT, 1994; LODI *et al.*, 2008; ISLAM *et al.*, 2011; SHARMA and LEWIS, 1994).

The sun's radiation wavelength prolongs from the infrared, through the visible spectrum into the ultraviolet. The infrared is bigger than 700 nm, the visible spectrum is between 400–700 nm and ultraviolet radiation is at 400 nm. Polymer chain scission and degradation of polymer properties can occur when the UV radiation reaches the geomembrane surface.

In exposed geomembrane applications, polyethylene (PE) is in contact with UV radiation, and the degradation is led by photo-oxidation with several free radical reactions (Expression 1) (SUITS and HSUAN, 2003; TIAN *et al.*, 2017).

$$RH + O_2 + hv \Rightarrow R\bullet + ROO\bullet + RO\bullet + OH\bullet \quad (1)$$

The R●, ROO●, RO● and OH● are the free radicals, RH is the polymer chain, hv is the photon energy with h and v representing Planck's constant and wavelength (SUITS and HSUAN, 2003).

There are different methods to study the behavior of plastics facing UV radiation. The natural solar radiation is used to evaluate sunlight degradation, but it requires a long-term evaluation. Laboratory methods to evaluate the effects of UV radiation are weatherometers, such as xenon-arc and ultraviolet-fluorescent. The correlation between sunlight exposure and weatherometers is controversial because there are several factors involving both types of exposure (SUITS and HSUAN, 2003).

2.1.3 Thermal degradation

A geomembrane may be submitted to higher temperatures than normal prior to installation, during installation, and during service. Thermoplastic geomembranes, if exposed to heat such as rolled or folded panels prior to installation, such as left in the sun, can block or stick together; afterward, when unfolded, a coated geomembrane may split or an unreinforced geomembrane may tear and become unserviceable (ROLLIN and RIGO, 1991).

The black geomembrane surface temperature, which was installed uncovered and exposed to solar radiation, reached over 70 °C (TAKE *et al.*, 2015). High temperatures can hasten UV and oxidative degradations, causing changes in physical, chemical and mechanical properties. In HDPE geomembranes, temperatures in the range of 80 °C to 90 °C are suggested as the maximum. Temperatures around 105 °C or higher should be avoided because the melting point of polyethylene is 125 ºC (KOERNER, 2005; ISLAM *et al.*, 2011; KOERNER *et al.*, 2007; ABDELAAL *et al.*, 2015).

Many authors reported field temperatures for HDPE geomembranes. In a landfill liner, the temperature might reach 80 °C to 90 °C. For nickel heap leach pads, the liner temperature may reach 70 °C. Some leachate temperatures above 143 °C are reported in a landfill with aluminum industry waste (ROWE, 2012; TELLES *et al.*, 1984).

The DSC (differential scanning calorimetry) analysis can show the changes in polymer morphology through high temperatures, such as annealing and chemical degradation. The peak associated with the recrystallization of the molten material after cooling to ambient temperature, even the peak associated with recrystallization of the molten

material during annealing and the endothermic peak representing the melting can be seen by the DSC curve (ROWE, 2012).

2.1.4 Chemical degradation

When in service, geomembranes are subjected to various chemical attacks. The general chemical resistance of different geomembranes to well defined chemicals is usually known. The problem arises when the chemical is not a single component material: in this case, possible synergistic effects, that are not completely known, can be originated (ROLLIN and RIGO, 1991).

It is important to observe what kind of chemical substances are directly in contact with a geomembrane in a design. Manufacturers need to evaluate the chemical resistance of geomembranes because the good behavior of geomembranes must be guaranteed at least during the useful life (KOERNER, 2005).

A structure modification of high-density polyethylene caused by chemical aging can culminate in chain scission or cross-linking. The chain scission reduces the molecular weight of the polymer, influencing the mechanical properties and the material becomes brittle. The cross-linking changes the mechanical behavior, increasing the stiffness (KAY *et al.*, 2004).

2.1.5 Environmental stress cracking

Stress cracking of polymers is a phenomenon caused by tensile stresses less than mechanical strength which promotes internal or external cracks. These cracks should be accelerated by the environment. The stress crack resistance of HDPE geomembranes is of great interest because the high crystallinity of HDPE puts the occurrence of this phenomenon at risk. The notched constant load (NCTL) test assesses the stress cracking resistance of HDPE geomembranes using a dogbone specimen that is notched in its central region with 20 % of the total thickness. Different percentages of tensile load are applied while being immersed in a solution with 10 % of Igepal CO-630 (surfactant) and 90 % of water at 50 °C (HSUAN and KOERNER, 1995; TELLES *et al.*, 1984; PEGGS and CARLSON, 1989; HALSE *et al.*, 1989; HALSE *et al.*, 1990; DIX and BURKINSHAW, 1991; LAVOIE *et al.*, 2014).

The melt flow index test (MFI) can provide a parameter on stress cracking. An HDPE geomembrane with a low melt flow index exhibits good stress cracking environmental resistance less than 1.0 g 10 min^{-1} (190 ºC–2.16 kg). Any change in the MFI should be related to the degradation of the geomembrane (TELLES *et al.*, 1984; MUÑOZ GÓMEZ, 2016).

The NCTL test can provide the transition time of the geomembranes because the failure times of the test specimens at various stresses are recorded and then plotted. The transition point between the two differently sloped portions is called transition time T_t and represents the transition from ductile behavior to brittle behavior of the polymer. The response of the curves resulting can be a "knee" (bi-linear curve), "nose" (overshoot curve) and "step" (tri-linear curve). A geomembrane which provides a high T_t value will exhibit a better stress cracking resistance than one with a lower T_t value (MUÑOZ GÓMEZ, 2016).

The first occurrences reported about stress cracks in geomembranes were observed along the seams. There have been several field reported incidents of stress cracking. All have been on polyethylene geomembranes exposed to the environment. Thus, ultraviolet light and oxidation are involved, as well as expansion and contraction to the extent that the geomembrane surface varies in temperature. All of the cracks occurred, or at least started, at field seams, according to different authors. In 1981 in the southwest of the US, a 2.0 mm thick HDPE geomembrane in contact with sludge for 7 years presented severity cracks along the seams caused by thermal stress. In 1989 in Canada, a 2.0 mm thick HDPE geomembrane in contact with black liquor with 2 years of service presented a large cracked area spreading throughout sheets and seams. In 1989 in Italy, a 2.0 mm thick HDPE geomembrane for the cover liner with 4 years of service presented small cracks at the seams and long cracks in the sheet (ROLLIN AND RIGO, 1991; PEGGS and KANNINEN, 1995; HSUAN, 2000).

2.1.6 Service life prediction of HDPE geomembranes

Long-term performance of HDPE geomembranes depends on several aspects, such as field temperature, exposure conditions, field stresses, covered or protected conditions, kind of liner layers, and resin and additive formulations. Evaluation of the performance and the lifetime assessment of the geomembranes is important from a managerial point of view (CAZZUFFI and GIOFFRÈ, 2020). The service life of geomembranes can be predicted based on accelerated tests in the laboratory using Arrhenius modeling, which makes a time-temperature prediction and can be estimated from a few years to 1000 years (ROWE and

SANGAM, 2002; ROWE, 2005; ZHANG, 2018; KOERNER and KOERNER, 2006; KOERNER *et al.*, 1992).

Several authors have used oxidative-induction time (OIT) and Arrhenius modeling to estimate the service life of HDPE geomembranes through the antioxidant's depletion. The OIT value is an index parameter related to the amount of antioxidant in the sample and is very useful for monitoring the antioxidant depletion in the HDPE geomembranes. The OIT value of the GM decreases as antioxidants are depleted with time (ROWE and SANGAM, 2002; RIMAL and ROWE, 2009; HSUAN and KOERNER, 1998; GULEC *et al.*, 2004). The determination of the OIT value from a standard test is shown in Figure 4. Initially, the specimen is conducted in a nitrogen gas environment at 200 °C until the melting reaction (endothermic reaction), followed by the oxygen gas environment until the oxidative reaction. The time to induct the oxidative reaction is measured.

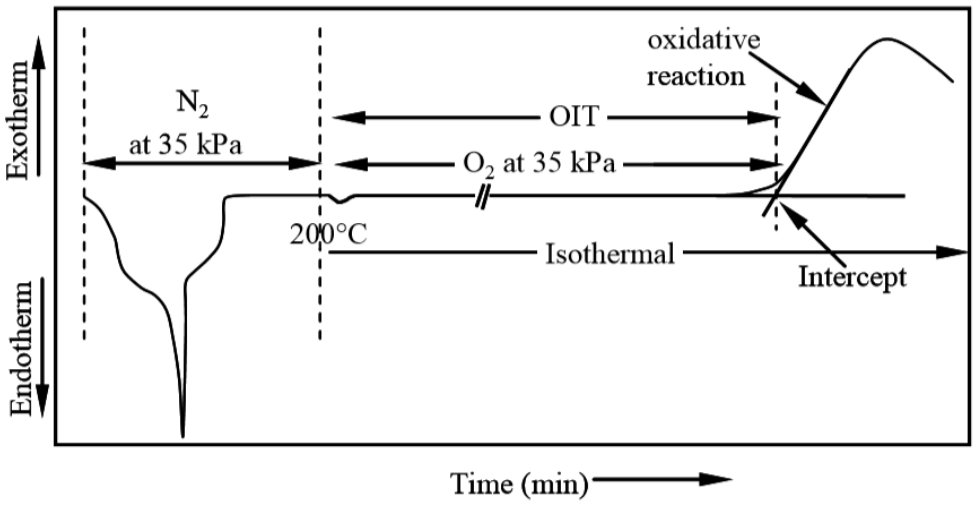

Figure 4. DSC thermogram from a standard OIT test (HSUAN *et al.*, 2008)

Jessberger and Heibrock (1997) estimated the service life of an HDPE geomembrane to be over 300 years under constant oxygen supply and 20 °C, but at 40 °C, under the same conditions, the service life was estimated to be approximately 45 years. Koerner (2005) estimated the service life of the backfilled HDPE geomembrane at 550 years under 20 °C, but at 40 °C the estimated service life was 90 years (ROWE AND SANGAM, 2002; GRASSIE and SCOTT, 1985; RIMAL and ROWE, 2009; HSUAN and KOERNER, 1998). According to Rowe and Ewais (2015), there is a need for more data related to the properties of geomembranes in the field after their useful life.

2.2 Studies of HDPE geomembrane durability

Many studies on HDPE geomembranes have been conducted in different parts of the world for over thirty years. Laboratory tests were carried out using virgin samples to simulate the field conditions. Exhumed samples of HDPE geomembranes were tested in the laboratory to understand the behavior of geomembranes after real exposures. Finally, field studies were performed to verify the service boundary conditions of the geomembranes.

2.2.1 Laboratory studies of HDPE geomembrane durability

Mitchell (1985) studied two compatibility tests with synthetic leachate from a uranium mill, one of them with a two-sided exposure sample and another one simulating a uranium tailing pond with a one-side exposure sample. The tests were conducted through columns at 18, 47, and 76 °C using a 1.0 mm thick high-density geomembrane. Moreover, destructive tests were performed after 1, 7, 30 and 120 days. The differential infrared transmission analysis results did not show oxidation products in the aged material. Changes in crystallinity were noted by differential scanning calorimetry (DSC). The virgin sample crystallinity was 52.3 %, while crystallinity for exposed samples at 18, 47 and 76 °C was 51.5, 53.4 and 55.7 %, respectively. According to the authors, the elevated exposure temperature presumably accelerates degradation; however, the correlation between temperature and degree of acceleration has not been made. Therefore, service life has not been predicted by these tests.

Schoenbeck (1990) tested seam samples with several methods to seam chlorosulfonated polyethylene (CSPE) geomembranes, such as dielectric seaming factory seams, by hot air and with a bodied solvent as well as a field seam made with a bodied solvent. The xenon arc weatherometer was used to conduct aging tests in hot air at 63 °C and 100 °C. Test results showed a significant increase in shear strength after 3000 hours.

Dix and Burkinshaw (1991) conducted DSC and melt flow index tests to evaluate the density of HDPE resins. The results showed that there is a tendency for density to decrease in lower heat of fusion and lower melting points.

Hsuan and Koerner (1995) conducted acceleration stress cracking tests for HDPE geomembrane 1 at 75 °C and slow stress cracking tests for HDPE geomembrane 2 at 40 °C and 25 °C. The acceleration test is used for high-stress crack resistance geomembrane and

slow stress cracking test for low stress crack resistance geomembrane. The results showed transition time values of 600 h at 50 °C and 40 h at 75 °C for HDPE geomembrane 1, and 6 h at 50 °C, 12 h at 40 °C, and 70 h at 25 °C for HDPE geomembrane 2. It is not recommended to use temperatures higher than 85 °C for HDPE as they cause material property changes.

Different organic liquids were used to evaluate the chemical compatibility with a 1.5 mm thick HDPE geomembrane by Aminabhavi and Naik (1998) at 25, 50 and 70 °C, including acetone, benzene, toluene, 1-chloronaphthalene, methyl ethyl ketone, methyl iso-butyl ketone, cyclohexanone, butyraldehyde, and others. The results showed that the sample has a high resistivity to these liquids and the diffusive transport of liquids depends on the temperature and concentration.

Mendes *et al.* (2003) analyzed HDPE samples with and without additives exposed to weathering in Rio de Janeiro, Brazil, up to 4000 h. The additives utilized were a phenol type antioxidant and two HALS-type light stabilizers. The authors used FTIR analysis, DSC analysis to determine the crystallinity, mechanical tests, and the variation of the sample's molecular weight was evaluated by gel permeation chromatography. The results showed decreased elongation at break for the sample without additives, demonstrating the almost total loss in ductility. The increase in crystallinity and reduction of molecular weight for the sample without additives was still verified. The sample stabilized with the additives remained its properties constant for the exposure time, especially for the impact resistance, elongation at break, molecular weight and crystallinity, demonstrating the additives' effectiveness.

Results from a laboratory exposure program were presented by Gulec *et al.* (2004) using a 1.5 mm HDPE geomembrane in contact with acidic mine drainage that came from a metallic mine waste facility. They used synthetic acidic mine drainage, acidic water, and deionized water at 20, 40, and 60 °C for a 22-month period. Results of the melt flow index (MFI) test, Fourier transform infrared spectroscopy (FTIR), and oxidative-induction time (OIT) demonstrated that MFI seems to increase gradually, the antioxidant depletion time was approximately from 46 to 426 years. It should be mentioned that no changes were observed in the polymer structure.

Merry *et al.* (2005) used an axisymmetric tension test apparatus that can perform constant-stress creep tests to compare the creep response of new and old HDPE geomembranes. Thirty-six-hour constant-stress creep tests were performed on new (about one year old) HDPE using a temperature range of 2–53 °C and stresses ranging from 2 to 15

MPa. Excess material was then stored in a laboratory for an additional 7 years, after which time tests on old geomembranes were performed. The results showed that there was essentially no difference in the creep response of the old geomembranes (7 year-stored sample).

The study of the thickness influence on antioxidant depletion from nominal 1.5, 2.0, and 2.5 mm HDPE geomembranes was conducted by Islam and Rowe (2007). They immersed the samples in synthetic leachate at four temperatures (22, 55, 70, and 85 °C) and the standard oxidative-induction time test was used to evaluate the behavior of different thicknesses. The results showed that antioxidants depleted faster from the 1.5 mm sample than others. According to the authors, thicker geomembranes have longer service lives.

Bueno (2007) analyzed two HDPE geomembranes of 1.0 and 2.0 mm of thickness immersed in gasoline (pH=9.5), caustic soda diluted in water in the proportion of 50 % (pH=10.75), and alcohol diluted in water (97 %) for 24 months at ambient temperature. There were performed tensile tests and thermogravimetric analysis. After the immersion, the samples became stiffer for all of the solutions. In some cases, the exposed samples presented lower loss masses than the virgin samples for the thermogravimetric analysis.

Rowe *et al.* (2008) tested a 1.5 mm thick high-density geomembrane on different laboratory leachates at 85, 70, 55, 40, and 22 ºC. They used Arrhenius modeling to evaluate the depletion of antioxidants. The results showed that faster depletion occurred in acidic and basic leachates, and the pH varied from 4 to 10.

The results of the 28,000 hour-test of the laboratory weatherometer was presented by Koerner *et al.* (2008). The authors used HDPE and LLDPE geomembranes 1.5 mm thick, and 1.0 mm thick, respectively. The test results showed that both samples starting the degradation mechanisms due to the losses in tensile properties verified. The LLDPE sample showed more degradation than the HDPE sample. According to the authors, the geomembrane lifetime depends on exposure site conditions.

Rimal and Rowe (2009) studied the behavior of HDPE geomembranes called “conventional or untreated” and fluorinated HDPE geomembranes or f-HDPE using fluorine gas (F2) to create a barrier to hydrocarbons. They immersed the HDPE and f-HDPE geomembranes in Jet A-1 at 23 ºC and, later, they compared them at 23, 9 and -22 ºC and used 1.5 mm thick HDPE, 1.5 mm thick f-HDPE and 2.0 mm thick HDPE. The samples could be differentiated by Fourier transform infrared (FTIR) scans. The authors measured

the crystallinity of the samples, and no changes were observed. The antioxidant depletion rate of the f-HDPE was about 30 % of the conventional HDPE.

The tensile properties in these samples were measured by the authors. It was observed that there is a statistically significant difference in tensile yield properties between the “dry” and “wet” test conditions. Higher yield strain was obtained in the “wet” condition due to the softening effect of the jet fuel absorbed in the samples. On the other hand, the yield strength of the samples was lower in the “wet” condition. The tensile break results did not show a statistically significant difference (RIMAL and ROWE, 2009).

Rowe *et al.* (2009) tested a 2.0 mm thick high-density geomembrane exposed to water, leachate, and air for 8 to 10 years. Several tests were conducted, such as OIT, crystallinity, tensile strength, stress cracking, melt flow index and surface analysis. The results showed that the service life, according to Arrhenius modeling, can reach more than 700 years immersed in leachate at 20 ºC, it can reach about 300 years at 35 ºC, and more than 50 years at 50 ºC.

The temperature of the secondary geomembrane used in the landfill liners was estimated by Rowe and Hoor (2009). According to the authors, the liner thickness and configuration can affect the temperature. The temperature predictions showed which service life of the secondary geomembrane can reach 390 years at 50 ºC and 75 years at 50 ºC if the liner has a primary liner comprising the geomembrane, a geosynthetic clay liner and at least 1 m above of the foundation layer.

Lodi and Bueno (2012) tested HDPE virgin and exposed (leachate and weathering for 30 months) geomembrane samples (0.8 and 2.5 mm of thickness). They utilized a thermogravimetric (TG) analysis to understand the behavior of the samples. Table 1 shows the values of the mass loss after TG tests. Figures 5 and 6 show the results of these analyses. It can be observed that for the 0.8 mm virgin sample, the initial mass loss temperature was 420 ºC, while this value was 440 ºC to 480 ºC for the exposed samples. For HDPE polymers, it is supposed that the mass loss starts at 470 ºC. For 2.5 mm thick samples, this behavior is the same as 0.8 mm thick samples, and the values with the initial temperature mass loss were close.

Table 1. Values of the mass loss after TG tests (LODI and BUENO, 2012)

Condition	HDPE (mm)	Parameter A (%)	Parameter B (%)
Fresh	0.8	99.79	0.15
	2.5	99.41	0.17
Weathering	0.8	99.90	0.08
	2.5	98.30	1.12
Leachate	0.8	99.11	0.10
	2.5	97.91	1.72

A = Polymer; B = Residual mass (carbon black + ash).

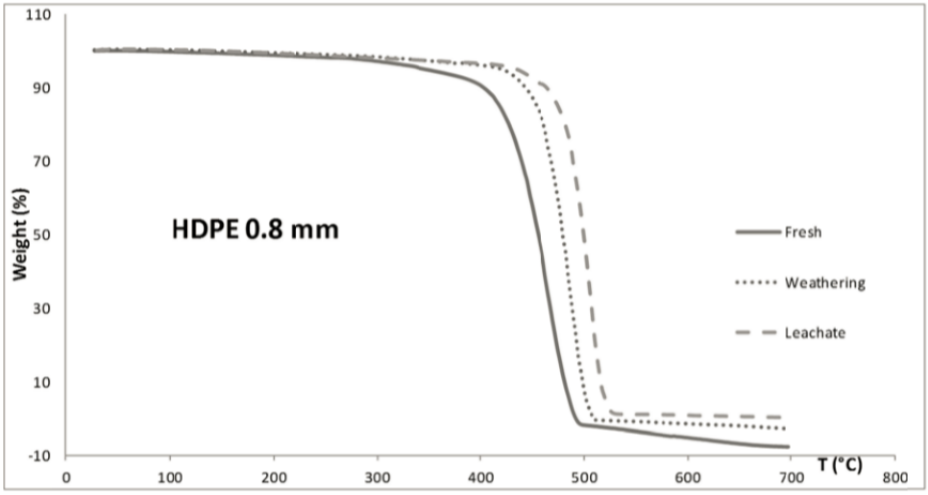

Figure 5. TG curves of 0.8 mm HDPE geomembrane sample (LODI and BUENO, 2012)

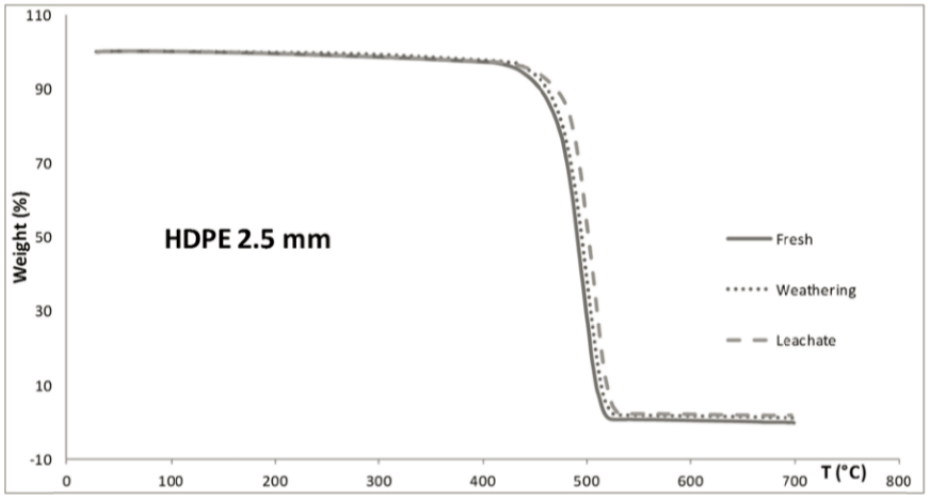

Figure 6. TG curves of 2.5 mm HDPE geomembrane sample (LODI and BUENO, 2012)

Lavoie *et al.* (2012) studied the stress cracking behavior of a high-density polyethylene geomembrane (2.0 mm thick). They tested the virgin sample by the notched constant tensile load test (NCTL) and the exposed samples by ultraviolet radiation (weatherometer) for 480 hours, thermal aging at 85 ºC (air oven) for 2,106 h, immersed in a solution with 10% in mass of sodium hydroxide at 50 ºC for 2,880 h. The authors commented that the exposed agents can accelerate the process of stress cracking because the exposed samples had a 50 % to 60 % of the reduction in the stress cracking resistance. Figure 7 presents the resulting curves of the applied stress versus respective failure times.

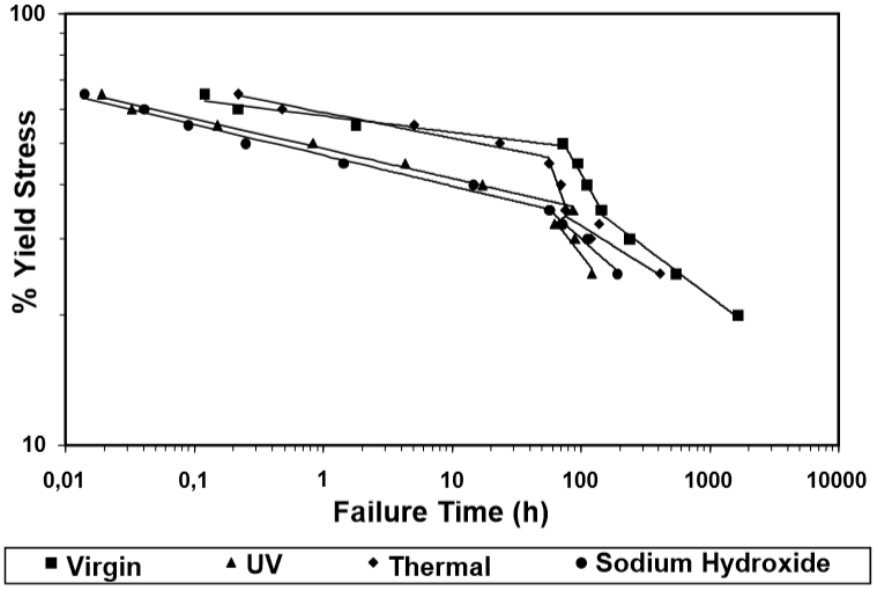

Figure 7. NCTL test curves (LAVOIE *et al.*, 2012)

A study provided by Abdelaal *et al.* (2012) evaluated the behavior of 1.5 mm thick HDPE and LLDPE geomembranes in acidic solutions with pH = 0.5 at 40, 50, and 60 ºC that represents the mining solutions for nickel, uranium, and copper heap leaching well with pH between 0.5 to 2.0. The research showed which depletion of the antioxidants for HDPE was faster than LLDPE resulting in 28 and 29 years at 40 ºC, 16 and 17 years at 50 ºC, and 9 and 11 years at 60 ºC, respectively for HDPE and LLDPE samples.

Lodi *et al.* (2013) evaluated the chemical compatibility of high-density polyethylene geomembranes with different thicknesses, 0.8 and 2.5 mm. The authors immersed the samples in a leachate and 60 % niobium solution for a maximum of 120 days at 23 and 50 ºC. Both samples presented an increase in tensile elongation. The results of melt flow index

tests showed a significant increase in the 2.5 mm sample, 52.7 % for niobium and 75.2 % for leachate. These increases indicate the chain scission mechanism.

Vinasse, an acid leachate from sugarcane, is commonly stored in HDPE geomembrane lined tanks. On the other hand, sodium hydroxide is widely used in the bauxite purification process and HDPE geomembrane is used as a pond liner. Lavoie *et al.* (2013) studied the chemical compatibility of a 2.0 mm HDPE geomembrane at 50 ºC for 120 days in a vinasse solution (acid solution) and also in a 10 % mass solution of sodium hydroxide (alkaline solution). The results of these immersions showed that thermogravimetric analysis did not show changes in thermal stabilities, but an average decrease was noted in the tensile yield strength of 34 % for the vinasse sample and an expressive tear strength loss of 40 % was verified in the sodium hydroxide sample.

Buaszczyk (2013) evaluated the effects of HDPE geomembranes (1.0 and 2.0 mm of thickness) immersed in hot and warm vinasse for 245 days, through physical, mechanical and thermal properties. Analyses by scanning electron microscopy (SEM) for the virgin 1.0 mm sample and 153 days of hot and warm exposure 1.0 mm sample were performed. It can be observed that both immersed samples presented flatter relief probably due to the effect of abrasion. Using Arrhenius modeling, the depletion of antioxidants was estimated in 4.3 years for the 1.0 mm thick geomembrane and 5 years for the 2.0 mm thick geomembrane. After 153 days of hot and warm exposure, thermo-oxidative degradation was observed preferably by branching into low molar mass fractions.

Abdelaal and Rowe (2014) evaluated a high-density polyethylene geomembrane with 1.5 mm of thickness without the presence of hindered amine light stabilizers (HALS) in the composition of the product, immersed in chlorinated water at different temperatures. The results showed that by using the Arrhenius modeling, the depletion of antioxidants varied from 0.5 to 23 years, respectively, at 20 ºC and 60 ºC.

HDPE geomembranes under high temperatures were evaluated by Abdelaal and Rowe (2014). Four samples of different geomembranes were incubated in leachate, water, and air at 95, 105 and 115 ºC. According to the authors, incubation in air at 115 ºC caused polymer degradation. High temperatures above 95 ºC should be used with caution. The degradation of geomembranes may occur before the complete depletion of antioxidants.

The accelerated notched tensile constant load test (NCTL) was evaluated by Lavoie *et al.* (2014) using a 2.0 mm thick high-density polyethylene geomembrane at 70 ºC and 50 ºC as a reference. The transition time by accelerated test (T_t = 18 h) decreased 87 %

compared to the reference test (T_t = 143 h). According to the authors, the behavior between both tests is different. The accelerated test provided a bi-linear curve, while the reference test provided a tri-linear curve.

Aging of the same geomembrane immersed in the same four synthetic municipal solid waste leachates tested by the research conducted by Rowe *et al.* (2008) for 2.65 years was continued by Abdelaal *et al.* (2014) for another 6.5 years. In summary, the results showed that the salts contained in leachates 1 and 3 changed the stress crack resistance, and even the mechanical properties of the sample.

Ewais *et al.* (2014) examined HDPE geomembranes, 1.5 mm thick, and manufactured them with different resins and additives. They immersed the samples in an artificial landfill leachate at 85 ºC and used the high-pressure oxidative-induction time (HP OIT) to evaluate the behavior of the samples. The largest HP OIT initial value was 960 min suggesting the presence of hindered amine light stabilizers (HALS) in the additive package, because traces of nitrogen were found. The lowest HP OIT initial value was 260 min and no traces of nitrogen were detected, which suggests no presence of HALS. According to the authors, when present, the depletion of HALS controlled the depletion of HP-OIT. However the nature and rate of depletion of HALS was very different for the type of HALS in two geomembrane samples analyzed in this study.

The changes in the structural properties of high-density polyethylene film exposed to UV-B radiation were studied by Martínez-Romo *et al.* (2015). The crystalline phase fraction of high-density polyethylene film increased further after 30 days of exposure to UV-B radiation, affecting the physical properties such as stiffness, dissolution resistance, and dimensional stability. The results showed which sample had a high oxidation degree.

Four different high-density polyethylene geomembranes, 1.5 mm thick, incubated in air at high temperatures were evaluated by Abdelaal *et al.* (2015). These aging samples were investigated by oxidative-induction time tests (standard and high-pressure), the melt flow index test, the stress cracking test (single point), and the morphological changes due to annealing, using the differential scanning calorimetry (DSC). The results of DSC curves for sample GMB1 aged at 115 and 105 ºC showed changes in melt behavior of aged samples by the increase of the temperatures' incubation. The melting point was 127 ºC for virgin samples and increased to 131.6 ºC for 4.2 months of incubation. For times higher than 4.2 months, the melting point increased to 140 ºC.

Aged samples experienced losses in stress crack resistance and melt flow index, showing changes in polymer morphology. It was observed, especially at high temperatures, that both mechanisms of degradation (cross-linking and chain scission) occurred at the same time (ABDELAAL *et al.*, 2015).

Finally, the authors concluded that morphological changes associated with annealing occurred for samples incubated in air at temperatures higher than 85 ºC, and the samples had different thermal behaviors due to high temperatures (ABDELAAL *et al.*, 2015).

Morsy and Rowe (2016) evaluated the depletion of antioxidants from different geomembranes immersed in chlorinated water at 85 °C. Chlorine is a strong agent of oxidation. The geomembranes tested were 1.5 mm thick, two from HDPE and one from LLDPE. After 20 days of exposure, the HDPE samples presented higher rates of antioxidant depletion than LLDPE samples. According to the authors, while a high initial Std OIT is usually preferred, the type of antioxidant and thus its resistance to chlorinated water may govern the time to antioxidant depletion.

Ewais *et al.* (2016) evaluated the rupture time to an HDPE geomembrane (1.5 mm of thickness) under 250 kPa of pressure, at 85 ºC in a composite liner configuration in 0.6-m-diameter geosynthetic liner longevity simulator cells. The tests were performed not replacing the gravel and replacing the gravel and using a nonwoven geotextile as a protective layer. The differences in the times to rupture in these different scenarios were attributed to the observed deterioration of the gravel above the geomembrane. For the conditions examined in the study with a geotextile as a protection layer, the gravel deterioration observed in this study was important in terms of protecting the geomembranes from rupturing. The authors concluded that the physically/chemically induced deterioration of the gravel can prolong the time HDPE geomembranes would take to rupture. The increase in the time to rupture would depend on the degree of the gravel deterioration.

Several polymers of polyethylene have been studied by Muñoz Gómez (2016) concerning crystallinity, melt flow index and stress cracking resistance. According to the author, each of the polymers analyzed was transformed into a polyethylene sheet following this general formulation with a base polymer, carbon black, antioxidants and ultraviolet stabilizers. Manufacturing was completed by a flat-die cast co-extrusion system. In all cases, the geomembrane was 7.5 m wide and 1.5 mm thick. The stress cracking resistance values were improved for higher densities but wider weight distribution. Samples with narrow molecular weight, but with lower density could improve their stress cracking resistance. The

best situation was noted for a low-density sample with wider molecular weight distribution. Density, crystallinity, and melt flow index results are shown in Table 2.

Table 2. Density, crystallinity, and melt flow index (MFI) of the polymers used (MUÑOZ GÓMEZ, 2016)

Polymer	**Density ($g\ cm^{-3}$)**	**Crystallinity (%)**	**MFI g 10 min^{-1} (190 ºC/2.16 kg)**	**MFI g 10 min^{-1} (190 ºC/5.0 kg)**	**MFI g 10 min^{-1} (190 ºC/21.6 kg)**
PE-1	0.932	51.2	0.78	2.19	19.76
PE-2	0.934	49.9	0.15	0.63	16.59
PE-3	0.936	56.8	0.93	2.65	23.54
PE-4	0.937	53.4	0.23	0.95	19.84
PE-5	0.938	54.5	0.23	1.0	18.95
PE-6	0.940	59.0	0.95	2.78	25.92
PE-7	0.941	49.4	0.12	0.57	11.67

The estimated half-life of an HDPE geomembrane with 1.5 mm of thickness in the covered or nonexposed condition was determined by Koerner *et al.* (2017). They incubated the sample in a device simulating a liner situated under 50 m of solid waste at 55, 65, 75 and 85 ºC and determined the half-life when the values of strength or elongation reached 50 %. The extrapolation of half-life made for 20 ºC resulted in about 450 years.

Four HDPE geomembranes with 1.5 mm of thickness were immersed in a brine solution (pH = 8.7) at 40, 65, 75, and 85 ºC for 4 years and evaluated by Rowe and Shoaib (2017). The half-life was less than 4 years of exposure at temperatures above 40 ºC for the whole samples. Otherwise, the estimated lifetime using the stress cracking resistance test result values for one of the samples was more than 20 years at temperatures below 75 ºC.

Coelho and Lavoie (2017) evaluated the behavior of two samples of HDPE geomembranes (0.8 mm and 2.0 mm of thickness) submitted to accelerated aging of up to 15,000 hours. The results of the tests performed on an accelerated aging chamber showed average losses in tensile elongation at break at around 20 % after 5,000 test hours, and less significant mean losses after 15,000 test hours, ranging from 11 % for the geomembrane of 0.8 mm and 3 % for the 2.0 mm sample. Therefore, it was observed that even after the accelerated weather exposure equivalent to 15 years, the product still retains more than 50 % of its tensile elongation property and it is still suitable for its intended application.

However, there is a tendency to reduce the mechanical properties after 15,000 hours of exposure to aging and it is, therefore, necessary to evaluate the material for longer periods.

Rowe and Shoaib (2017) investigated the heat-affected zone around the weld, the weld and the welded zone of an HDPE geomembrane (1.5 mm thick), utilizing dual wedge welding equipment with the samples immersed in synthetic leachate at different temperatures (40, 65 75, and 85 ºC). As a result, failures did not occur in the weld, but the slowest depletion of the antioxidants occurred in the weld, and the fastest depletion of the antioxidants occurred in the adjacent zone of the weld.

There is a lack of information on textured HDPE geomembranes in the literature. To the best of our knowledge, there is only one study carried out by Benson *et al.* (2010) who studied the behavior of LLDPE geomembrane seams. For this reason, Morsy and Rowe (2017) studied the textured HDPE geomembrane, 1.5 mm of total thickness and 0.43 mm of asperity thickness, and a smooth 1.5 mm thick HDPE geomembrane as a reference. Both samples were immersed at 75 and 85 ºC in synthetic leachate. The results showed 15 % less antioxidant depletion time than a smooth sample.

Tian *et al.* (2017) compared the depletion of antioxidants of a 2.0 mm thick high-density polyethylene geomembrane immersed in radioactive leachate and nonradioactive leachate, both synthetic, at 25, 50, 70, and 90 ºC. The results showed that after 12 months of immersion at 90 ºC, the antioxidant depletion of the sample for both leachate samples was complete. The results of the melt flow index, after 15 months of exposure, decreased in values, demonstrating the occurrence of crosslinking. Finally, they concluded that the total service life of the sample after immersion in radioactive synthetic leachate was estimated at 1975 years.

Zhang *et al.* (2018) tested an immersed HDPE geomembrane (1.5 mm thick) in a very low pH solution (pH=0.5) at 85, 75, and 65 ºC for approximately 1.6 years. The authors concluded that there is no evidence of polymer degradation up to 19 months of exposure. The estimate of oxidative depletion time for 50 ºC was 11 years, but for 20 ºC it was 250 years, both for the standard tests.

Valentin *et al.* (2018) used thermal analysis to analyze HDPE geomembranes manufactured in Brazil by different suppliers. They tested four geomembranes with nominal thicknesses of 2.0 mm (A and B), 1.5 mm (C) and 0.8 mm (D). The samples presented different behaviors in the thermogravimetric analysis. Figures 8 and 9 present, respectively, the DSC curves for heating and cooling at 20 ºC min^{-1} of rate. In this study, several rates

were used. The samples had overlapping reactions in the melting point, at about 133 ºC. The melting point in the second heating widened compared to the first heating. The exothermic reaction can be observed on the cooling curve (at 115 ºC), showing polymer recrystallization. For the DMA tests, the authors concluded that there were no significant changes among the curves' behavior.

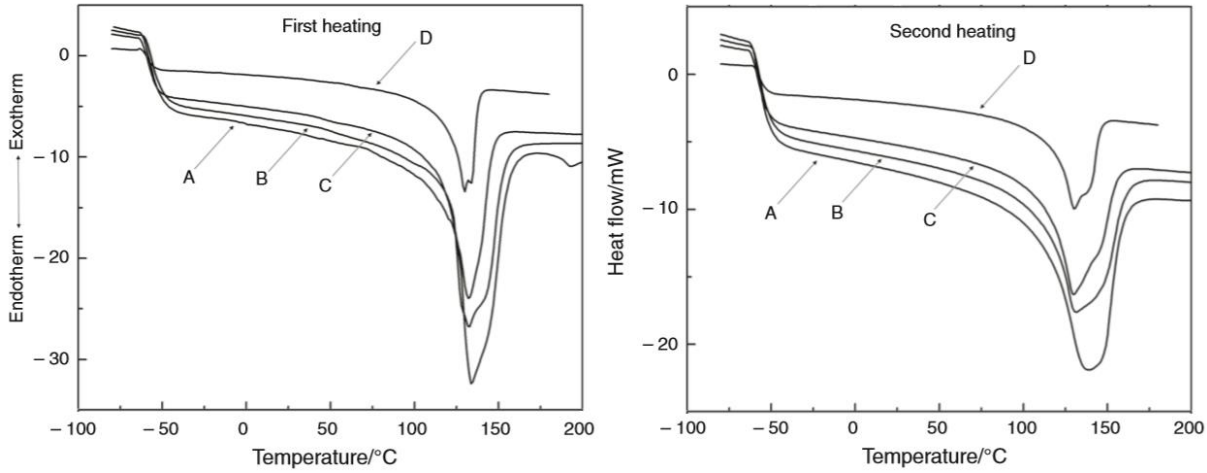

Figure 8. Differential scanning calorimetry heating curves of HDPE geomembrane samples under nitrogen gas purge (VALENTIN *et al.*, 2018)

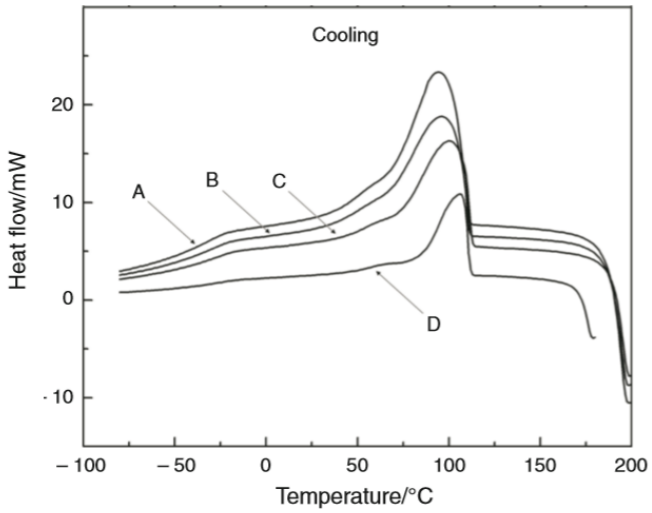

Figure 9. Differential scanning calorimetry cooling curve of HDPE geomembrane samples under nitrogen gas purge (VALENTIN *et al.*, 2018)

A long study over 17 years with HDPE geomembranes immersed in air, water, and leachate at 85, 70 and 55 ºC was conducted by Ewais *et al.* (2018). According to the authors, the oxidative degradation was clear by the loss in tensile properties, even loss in stress

cracking resistance, especially for the sample immersed in water and leachate at 70 ºC. Finally, the service life was estimated at about 13 years for leachate at 60 ºC and 660 years at 20 ºC.

Abdelaal and Rowe (2019) studied a 3-year-old HDPE geomembrane without HALS (hindered amine stabilizer) immersed in solutions with chlorinated water at various concentrations at different temperatures. According to the authors, the depletion in the antioxidants and the stress cracking resistance were faster compared to other solutions, such as synthetic leachate and tap water. In general, the results showed the capacity of the chlorinated water at high temperatures in polymer degradation.

Abdelaal *et al.* (2019) conducted oxidative-induction time tests, stress cracking tests, tensile tests and melt flow index tests to evaluate the behavior of an HDPE geomembrane with HALS under free chlorinated solutions in different conditions of temperature for about 70 months. Considering the increase in the solution concentration, the authors noted that fast degradation occurred. The estimated time to reach the service life of the product for free chlorinated water (0.5 ppm) at 85 ºC was 5 years.

Sahu *et al.* (2019) evaluated the influence of ultraviolet light on the thermal properties of HDPE for different carbon black concentrations from 1 to 3 %. The authors used an ultraviolet fluorescent weatherometer for a cycle of 192 h. The Fourier transform infrared spectroscopy (FTIR) and differential scanning calorimetry (DSC) were used to analyze the HDPE behavior before and after UV exposure. The analysis confirms that the carbon black was evenly dispersed without degradation in the HDPE matrix.

Jiang *et al.* (2019) investigated an HDPE resin after 800 h of exposure in a xenon arc lamp device. Antioxidants and a UV absorber were added to understand their influences on ultraviolet resistance. The authors performed FTIR, DSC, and TG analyses and the mechanical test. The results showed which UV absorbers presented better results than the antioxidants. The samples with UV absorbers added maintained their mechanical properties even after 600 h of exposure.

Rowe *et al.* (2019) examined the effect of physical aging on stress crack resistance (SCR) reduction before the initiation of oxidative degradation of eleven HDPE geomembranes. The authors used the notched constant load test (NCTL) to understand the effect of physical aging on the reduction of SCR. The samples were incubated in six different leachates for 116 months. A stress crack resistance value reduction was noted for a 1.5 mm-thick HDPE geomembrane after 3 months of incubation and stabilized until 116 months.

According to the authors, there was no evidence of oxidative degradation after 3 months of incubation for ten out of eleven evaluated HDPE geomembrane samples. The mean SCR reduction noted in this research for HDPE geomembranes immersed in leachate fluid was 37 %.

Vahidi *et al.* (2020) studied antioxidant depletion of high-density polyethylene coupons along the different layers of the thickness. The authors used a laboratory xenon light weatherometer to expose the coupons and still exposed coupons to sunlight in Florida, US. Oxidative-induction time (OIT) tests were run to evaluate the antioxidant depletion. The results presented the most antioxidant depletion for the surface layer of the samples. The study proved the reciprocity law for three irradiance levels at the surface layer. The intensity of the irradiation increased the antioxidant depletion for the surface layer. The core layer presented a slower decrease in the antioxidant depletion.

Marcotte and Fleming (2020) analyzed smooth HDPE geomembranes in a cylinder test to simulate loading in the liner using nonwoven geotextiles, a woven geotextile, and a geocomposite as potential protection from tire derived aggregate (TDA) wires. According to the authors, TDA is a risk of puncture, even when heavy nonwoven geotextile protection layers exceeding 1628 g m^{-2} are used. Thicker geomembranes were found the reduce the number of punctures, but a 2.0 mm geomembrane with a 1628 g m^{-2} protection layer still resulted in punctures from TDA.

2.2.2 Field studies of HDPE geomembrane durability

Outdoor weathering exposure was conducted by Qureshi *et al.* (1989) at Dhahran, Saudi Arabia using 3.0 mm thick linear low-density polyethylene (LLDPE). The sample was produced without an ultraviolet stabilizer. The location of the exposure has similar solar radiation to solar radiation in Arizona, USA (hot and humid). In three months of exposure, the sample showed a decrease of 50 % in tensile strength and elongation at break. According to the authors, photochemical degradation was verified due to chain scission and cross-linking reactions.

The investigation of 1.0 mm thick HDPE geomembrane seam failures was proceeded by Calabria and Peggs (1997) in the closure of an eastern Pennsylvania landfill in the US. The authors divided the area into two sections to facilitate the investigation. Fusion and extrusion seams were made in this construction site. In conclusion, the landfill gas did not

influence these failures and the cause of these failures was dirt within the seams during the installation.

Koerner *et al.* (1999) evaluated the effects of waves in an exhumed HDPE geomembrane of 1.5 mm. The material was installed for 8 years in a municipal landfill. According to the authors, they found three different types of waves, “prayer” wave, “s” wave and “mushroom” wave in the field. The laboratory investigation was conducted on flat, as well as waved geomembrane test specimens to evaluate the tensile strength properties, and stress cracking properties. As a result of the tests conducted, the tensile strength appears not to be significantly compromised. The geomembrane used at this site is a very high-quality stress cracking resistant material with failure times more than 1823 h. There appears to be a decrease in stress cracking resistance of waved versus non-waved geomembrane test specimens. There is a tendency for the stress cracking resistance to decrease, but it is still well above current specification values for this particular property.

Koerner and Koerner (2006) monitored the in-situ temperature of HDPE geomembranes used in a solid waste landfill liner and cover. The sensor called “dry cell” measured a non-liquid area, and the sensor called “wet cell” measured the high moisture area. Over 10.5 years of monitoring the “dry cell” and 3.7 years of monitoring the “wet cell”, the temperature for the “dry cell” was, on average, 20 °C, and the temperature for the “wet cell” temperature started at 25 °C and increased to 41–46 °C.

Lodi *et al.* (2013) exposed HDPE geomembranes to weathering (0.8 mm and 2.5 mm thick) for 6, 12, 18, and 30 months. The location of this research was in the southwest of Brazil (20º 22’ S and 51º 22’ W). They verified the physical, mechanical and thermal properties of these samples. The melt flow index results indicated the beginning of the degradation. The 0.8 mm sample showed an increase in melt flow index results, probably caused by chain scissioning.

Richgels (2016) evaluated field ultraviolet exposure and its effects. Field measurements of total and UV solar irradiation and temperature were available near Phoenix, Arizona and Miami, Florida in the US, from the Atlas Weathering Services Group. Using Arrhenius modeling, a half-life of exposed high-density polyethylene geomembrane was estimated in Miami in approximately 250 years. The projected line from the assumed stage of polymer degradation field data shows estimated half-life at approximately 220 years in Arizona. According to the author, after the sun has passed its daily peak irradiation time, the

thermal oxidation continues to occur in the geomembrane. Thermal energy will continue the polymer oxidation process of polyolefin resins.

Reis *et al.* (2017) evaluated five high-density geomembranes (HDPE), 2.0 mm thick, exposed to climate conditions over 12 years in 8 different regions of Portugal with different ultraviolet indexes. The samples, covered with geotextile and uncovered, were evaluated regarding their influence of protection for geomembranes. Many properties were evaluated, such as density, melt flow index, tensile strength, carbon black content, and oxidative-induction time (OIT). The results show that the properties of the geomembranes exposed to climatic conditions present some deterioration, especially regarding the OIT and density. As for the geomembranes exposed in locations with different UV indexes, it suggests that an increase of this index impacts the tensile properties and OIT. Finally, it was found which covered and exposed samples presented similar results.

2.2.3 Laboratory studies of exhumed HDPE geomembrane durability

The municipal waste landfill double liner system was exhumed by Eith and Koerner (1997) in the Mid-Atlantic Region of the US. Two layers of primary and secondary HDPE geomembranes of 1.5 mm thick were installed and they were exposed to leachate, methane, and stresses for 8 years. Physical, mechanical and endurance properties were evaluated, and no degradation was detected.

Hsuan (2000) and Hsuan *et al.* (1993) carried out NCTL tests in 18 commercially new HDPE geomembranes and seven field HDPE geomembranes. The test results reveal a wide range of transition times (T_t). It can be observed that the transition time is key to comparing the behavior of the different samples tested. High transition time means good stress cracking resistance. The highest transition time value of the seven field geomembranes was 97 h and the second highest value was 55 h. Regarding the new geomembranes tested, a half of those presented transition times less than 100 h.

Benson *et al.* (2010) exhumed different types of geosynthetics from a liner cover of a landfill in Wisconsin, the US, including a textured low linear density polyethylene (LLDPE) geomembrane, 1.0 mm thick. The geosynthetics had about 5 years of service. Both the melt flow index and the oxidative-induction time did not show any changes compared to the tests under manufacturing quality control (MQC) at construction time. The tensile yield

strength decreased 1.2 times compared to the MQC results, but it is not possible to affirm that there was chemical degradation due to this.

Seven-year-old exhumed fluorinated HDPE geomembranes from the Canadian Arctic were evaluated by Rowe *et al.* (2010). Geomembranes with thicknesses of 1.0 mm, 1.5 mm and 2.0 mm were exhumed by a hydrocarbon spill backfill liner system. Melt flow index, oxidative-induction time, crystallinity and tensile strength were used to study these samples. There were no changes detected in the melt flow index, crystallinity and tensile strength. According to Arrhenius modeling, the antioxidant depletion of a 1.5 mm thick sample was about 140 years for standard oxidative-induction time and over 200 years for high-pressure oxidative-induction time.

High-density geomembranes with 1.5 mm of thickness were exhumed by Safari *et al.* (2011) after 25 years of service from hazardous waste landfill liners (bottom and cover liners) at London Ontario, Canada. Using the Arrhenius modeling and oxidative-induction time method, the authors concluded that the total time remaining for the antioxidant depletion is, on average, 60 years. Table 3 shows OIT results and the ratio of HP OIT/Std. OIT for exhumed samples.

Table 3. OIT results and the ratio of HP OIT/Std. OIT for exhumed geomembranes (SAFARI *et al.*, 2011)

Geomembrane	**Age (year)**	**Std. OIT (min)**	**HP OIT (min)**	**HP OIT/Std. OIT**
Cover Cell 1	25	15 (±1.6)	114 (±10)	7.6
Cover Cell 2	24	24 (±1.5)	155 (±7)	6.5
Cover Cell 3	23	27 (±4.6)	163 (±15)	6.0
Cover Cell 4-1	22	25 (±1.9)	193 (±5)	7.5
Cover Cell 4-2	22	9 (±1.2)	121 (±13)	14
Bottom Liner Cell 3-1	23	7 (±0.8)	68 (±3.4)	9.2
Bottom Liner Cell 3-2	23	8 (±1)	64 (±3.7)	8.0
Bottom Liner Cell 4-1	22	53 (±1)	143 (±26)	2.7
Bottom Liner Cell 4-2	22	52 (±0.5)	162 (±16)	3.1
Sidewall Cell 3-1	23	62 (±0.7)	188 (±21)	3.0
Sidewall Cell 3-2	23	60 (±0.9)	197 (±9.7)	3.3

Standard deviations are between brackets.

The standard OIT test results were considerably lower than those of typical modern-day geomembranes. The high-pressure OIT test results of the cover geomembranes were also lower than typical high-pressure OIT values of the virgin geomembranes of today. The ratio of HP OIT/Std. OIT was similar for four of the five locations (SAFARI *et al.*, 2011).

The behavior of a 1.5 mm thick exhumed HDPE geomembrane, used as a liner in the San Isidro reservoir located on the Canary Islands, Spain, was evaluated by Noval *et al.* (2014). The authors used samples from the north and south slopes with 138, 162 and 174 months of age. The scanning electron microscopy results can be seen in Figure 10. After 138 months, the north slope sample showed the presence of grooves by manipulation (Figure 10a). After 162 months of exposure, the north slope sample presented cracks (Figure 10c). Figure 10b and 10d present the south slope sample after 174 months. A crack can be seen in Figure 10d.

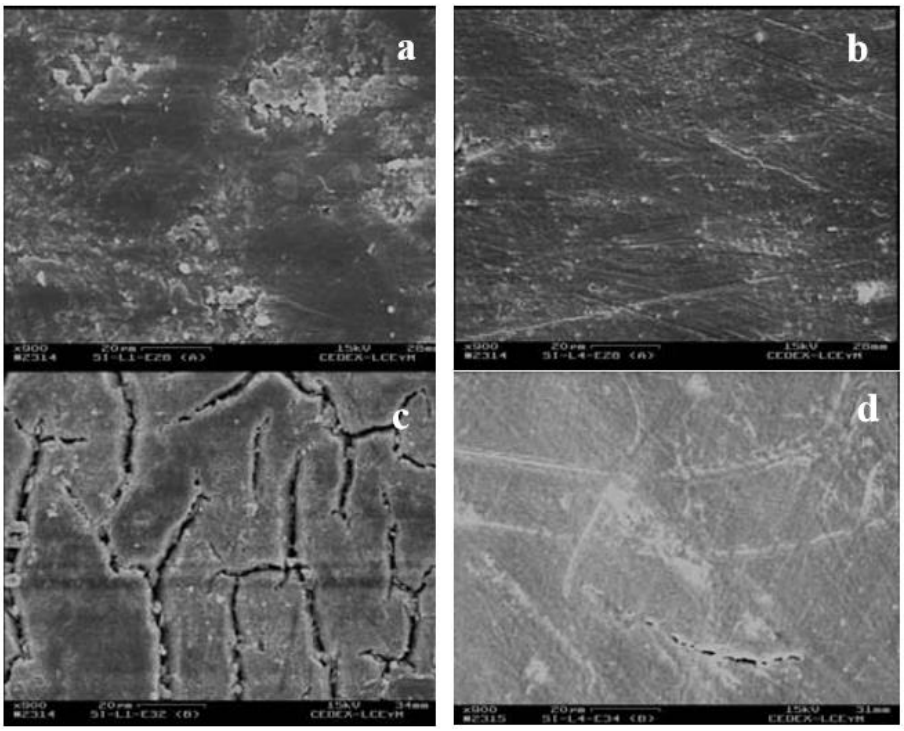

Figure 10. Scanning electron microscopy of the exhumed HDPE samples (NOVAL *et al.*, 2014)

Tensile strength properties were evaluated over 20 years of exposure, the variation in tensile properties is shown in Figure 11. The values had a huge variation and the elongation at break decreased less than 50 % of the original value in approximately 8 years. The depletion of antioxidants was estimated at 47 years for the northern slope sample and

58 years for the southern slope sample. Finally, the authors concluded that the geomembrane performed well as a liner (NOVAL *et al.*, 2014).

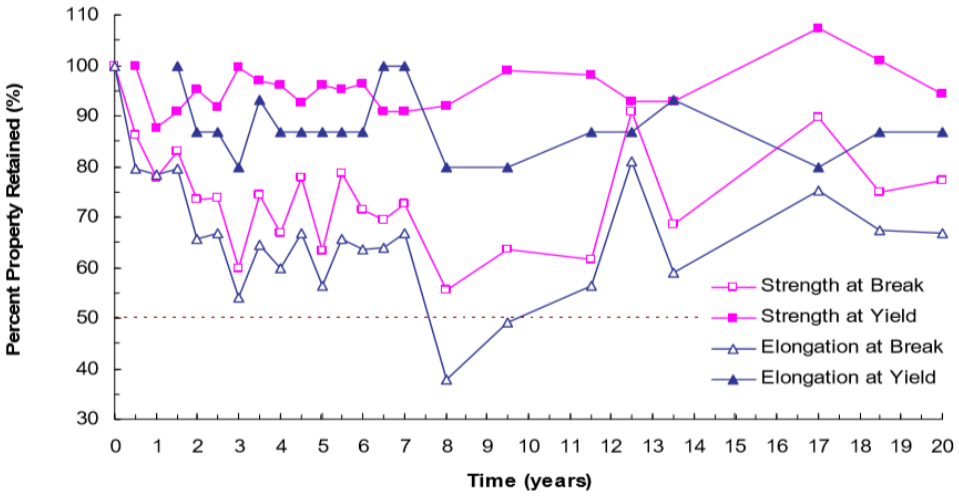

Figure 11. The variation in tensile properties over 20 years (NOVAL *et al.*, 2014)

Rowe and Ewais (2015) evaluated two exhumed samples of 1.5 mm high-density polyethylene geomembranes in different places. They proceeded the exhumation of a 16-year-old geomembrane in a mining facility in Argentina, and a 6-year-old geomembrane in the research site of Queen's University, Canada. The results showed the time nominal failure was reached in stress cracking resistance for the mine facility sample. For the Canadian sample, the depletion of antioxidants was faster in the slope than the bottom.

Santos (2014) and Santos and Gardoni (2016) studied a 1.5 mm thick HDPE geomembrane, used in a Brazilian tailing dam from 2006 to 2010. The tests were run on the virgin sample, laboratory aged sample and sample directly exhumed from the dam, thus comparing the durability and concluding the degree of aging and loss of durability. Chemical and mechanical durability tests, thermogravimetric tests, scanning electron microscopy (SEM) analysis, tensile tests on virgin and aged geomembranes were performed. The aging equipment was designed to reproduce field conditions such as the effects of solar radiation on the ultraviolet and infrared spectrum, as well as to simulate samples of immersion in the contaminated fluid for the study of aging on laboratory exposure of the samples to ultraviolet radiation, infrared radiation (40 ºC) and immersing the samples in fluid cyanide. Durability tests were performed on the geomembranes immersed in the fluid barrier and the temperature and UV exposure conditions were simulated. The SEM results showed that the exhumed samples show degradation, with some cracking process underway, cavities and the surface

with some degree of roughness were also observed. According to the authors, the exhumed sample presented a significant degree of degradation on its surface. The samples submitted to thermogravimetric analysis showed values of mass loss compatible with the one found in the literature and other research. The samples showed no significant loss of mass when comparing virgin, exhumed and aged samples.

The geomembranes generally are welded in the field. The seam is considered a critical point for possible injuries and future leaks in the barrier system. Rollin *et al.* (1999) advised which the total geomembranes injuries occurred in landfills, ponds and basins, 55 % of these injuries were at seams. Stark *et al.* (2020) evaluated seams made by industry and in the field of a polyolefin geomembrane (polypropylene) for a water reservoir project. According to the authors, the seams made by industry can minimize dirt and moisture in the seam, ambient temperature changes and wind. After good statistical data work, the results of this research showed that the seams made by industry were 9 % stronger than field seams for peel strength and 10 % stronger for shear strength. Beyond that, the seams by industry data presented less variability.

2.2.4 HDPE geomembrane with nanoparticles

To increase the thermal, mechanical and barrier properties of high-density polyethylene geomembranes, the incorporation of nanocomposites in the polymer blend is used as a new method. For instance, nanoclays are utilized with organic groups. The nanoparticles need to be properly dispersed in the polymer matrix. Besides that, polar compatibilizing agents are included in the formulation to refine the dispersion. However, the ideal conditions to improve the nanoparticle dispersion in the polymer matrix is still a challenge (DOLEZ *et al.*, 2017).

Shimotori *et al.* (2006) developed an HDPE geomembrane containing zero-valent iron (Fe^0) nanoparticles to apply as a reactive barrier. The nanoparticles of Fe^0 (zero-valent iron) were produced by an anaerobic chamber with sodium borohydride and ferric chloride. The polymer was mixed with the nanoparticles using a batch mixer. The partitioning coefficient and diffusion coefficient were calculated from breakthrough curves and the calculation estimates that only of 2.0-3.0 % of the Fe^0 nanoparticles reacted before the breakthrough of carbon tetrachloride.

The diffusion evaluation of multiwall carbon nanotubes through a 0.5 mm thick high-density polyethylene geomembrane was presented by Taghizadeh-Saheli *et al.* (2013). The carbon nanotube concentration was measured by a TOC analyser. The results have shown no significant partitioning of multiwall carbon nanotubes from source to geomembrane or diffusion throughout the 1 month of test. According to the authors, the production of carbon nanotubes is increasing because of the increasing demand and these kinds of nanoparticles will be used in landfill barrier systems.

The reduction of thermal expansion in high-density polyethylene geomembranes using nanoclay particles was studied by Dolez *et al.* (2016). The authors prepared several ratios of nanoclay particles from 0.5 to 50 % dispersed in an HDPE geomembrane and used a series of olefin-based polar compatibilizing agents with 5 and 10 %. They used a dynamic mechanic analyser (DMA) to evaluate the coefficient of linear thermal expansion and the transmission electron microscopy (TEM) to evaluate the nanoclay particles' degree exfoliation. The reduction in thermal expansion in comparison with a condition without a compatibilizing agent was noted only for one of the agents used in this study.

Dolez *et al.* (2017) analyzed HDPE geomembranes with nanocomposites through mechanical properties. The nanocomposite samples were prepared by a twin-screw extruder utilizing LLDPE, HDPE, various percentages of an organic-modified nanoclay, and four compatibilizing agents. The results indicate better compatibility of the nanoclay with a LLDPE masterbatch than the HDPE one. The decrease in tensile properties was observed for nanoclay concentrations over 5 %, probably due to imperfect bonding between the nanoclay and polymer matrix.

Saheli *et al.* (2017) studied the diffusion of multiwall carbon nanotubes (MWCNTs) dispersed in an aqueous media through an HDPE geomembrane. The permeation coefficient was approximated in 5.1×10^{-15} m^2 s^{-1} by laboratory tests and six different blend combinations. The low permeation coefficient value shows an HDPE geomembrane's effective diffuse barrier using nanotubes.

3 EXPERIMENTAL PROGRAM

This section presents the high-density polyethylene geomembrane samples used, the laboratory aged tests, the samples' characterization and the thermal analyses carried out in this research.

3.1 Materials

3.1.1 Virgin samples

This work utilized three high-density polyethylene smooth geomembrane virgin samples with nominal thicknesses of 1.0 (1L sample), 1.5 (1.5L sample), and 2.0 mm (2L sample). Different Brazilian manufacturers provided the samples. The virgin samples are described in Table 4. The materials were produced by the extrusion-blown film process and formulated with 96–97.5 % of medium-density polyethylene (density ≥ 0.940 g cm^{-3}), 2–3 % of carbon black and 0.5–1.0 % of antioxidants and thermostabilizers (LODI et al., 2013).

Table 4. HDPE geomembrane virgin samples used in this research

Sample	Nominal Thickness (mm)	Surface
1L	1.0	Smooth - both sides
1.5L	1.5	Smooth - both sides
2L	2.0	Smooth - both sides

3.1.2 Exhumed samples

The HDPE exhumed samples collected in the field and evaluated in this work are described in Table 5. The samples were collected in different Brazilian construction works in many applications.

Table 5. HDPE geomembrane exhumed samples used in this research

Sample	Nominal Thickness (mm)	Application	Exposure Time (years)
CLIQ	1.0	Industrial Water Pond	2.25
LTE	1.0	Sewage Treatment Aeration Pond	2.75
LCH	2.0	Municipal Landfill Leachate Pond	5.17
MIN	1.0	Pond for Water Use for the Iron Ore Process	7.92
MIN2	1.0	Spillway Channel of a Ferronickel Tailing Dam	10.08
LDO	0.8	Biodegradable Waste Pond	15.17
CAM	0.8	Shrimp Farming Pond – Bottom Liner	8.25
CAM1	0.8	Shrimp Farming Pond – Slope Liner	8.25
CAM2	0.8	Another Shrimp Farming Pond	3.0

The samples were collected directly from the construction works. The samples MIN, MIN2, LDO, CAM, CAM1 and CAM2 were stored in a covered place without contamination right after the collection until the transportation to the laboratory. Otherwise, the samples CLIQ and LCH were left uncovered in the field for 2 months before transportation to the laboratory. Finally, the sample LTE was left for 1 week uncovered in the field before the transportation to the laboratory.

3.1.2.1 CLIQ exhumed sample

CLIQ sample was exhumed by an industrial water pond with 2.25 years of exposure. Figure 12 shows the industrial water pond geomembrane before the exhumation, in service, with 1.0 mm of thickness. Figure 13 shows the industrial water pond after recuperation with

a new HDPE geomembrane. It was decided to recuperate it due to the lack of an adequate drainage system and the poor installation service, including the defects in the connection between the geomembrane and the concrete structures of the pond and the waves in the geomembrane panels.

Figure 12. The industrial water pond geomembrane before the exhumation, in service

Figure 13. The industrial water pond after being recuperated with a new HDPE geomembrane

3.1.2.2 LTE exhumed sample

LTE sample was exhumed from a sewage treatment aeration pond after 2.75 years of operation. This geomembrane was damaged during the operation, entailing the pond liner exchange. Table 6 presents the typical characteristics of the sewage. Figure 14 shows the sewage pond which presented an HDPE geomembrane with 1.0 mm of nominal thickness.

Table 6. Typical characteristics of the sewage (LEITE and LIGEIRO, 2017)

Characteristic	Unit	Result
Fixed Suspension Solids	mg L^{-1}	80
Volatile Suspended Solids	mg L^{-1}	320
Total Suspended Solids	mg L^{-1}	350
Fixed Dissolved Solids	mg L^{-1}	400
Volatile Dissolved Solids	mg L^{-1}	300
Total Dissolved Solids	mg L^{-1}	700
Sedimentable Solids	mg L^{-1}	15
Total solids	mg L^{-1}	1100
pH	-	6.5–7.5
BOD	mg L^{-1}	100–400

Figure 14. Sewage treatment aeration pond under operation

3.1.2.3 LCH exhumed sample

LCH sample was exhumed from a municipal landfill leachate pond after 5.17 years of operation. The exhumation of the geomembrane occurred because the site was used for the landfill expansion. Table 7 presents the chemical characteristics of the municipal landfill leachate. Figure 15 shows the landfill leachate pond that presented an HDPE geomembrane with 2.0 mm of nominal thickness.

Table 7. Chemical characteristics of the municipal landfill leachate
(QUÍMICA PURA LABORATÓRIO DE ANÁLISES QUÍMICAS, 2018)

Characteristic	**Unit**	**Result**
Total alkalinity	mg $CaCO_3$ L^{-1}	6912
Calcium	mg L^{-1}	366
Cadmium	mg L^{-1}	Not Detected
Lead	mg L^{-1}	Not Detected
Chloride	mg Cl^- L^{-1}	3502
Total Coliforms	MNP 100 mL^{-1}	8.3
Conductivity	µS cm^{-1}	23,210
BOD	mg O_2 L^{-1}	775
Iron	mg L^{-1}	11.4
Magnesium	mg L^{-1}	0.165
Mercury	mg L^{-1}	Not Detected
Nickel	mg L^{-1}	0.230
pH	-	8.19
Mineral Oils and Greases	mg L^{-1}	Not Detected

Figure 15. Municipal landfill leachate pond under demobilization

3.1.2.4 MIN exhumed sample

MIN sample was taken from a pond for water use for the iron ore process after 7.92 years of exposure. Table 8 presents, as a reference, the mining iron ore effluent's characterization parameters of mining in Minas Gerais, Brazil. The HDPE geomembrane presents 1.0 mm of nominal thickness.

Table 8. Parameters of iron mining effluent characteristics (FERREIRA et al., 2015)

Parameter	Average Value
Temperature	22 °C
pH	9.8
True color	66 mg Co L^{-1}
Turbidity	2133 NTU
Total solids	1229 mg L^{-1}
Dissolved solids	479 mg L^{-1}
Suspended solids	750 mg L^{-1}
Sedimentable solids	28 mg L^{-1}
Fixed solids	1159 mg L^{-1}
Volatile solids	70 mg L^{-1}
BOD	9.2 mg L^{-1}
Alkalinity	141.52 mg L^{-1} ($CaCO_3$)
Chloride	0.003 mg L^{-1}
Amine	2.1 mg L^{-1}

3.1.2.5 MIN2 exhumed sample

MIN2 sample was exhumed from a spillway channel of a ferronickel tailing dam after 10.08 years of service. Table 9 shows, as a reference, the chemical composition of a nickel waste disposed of in a tailing dam. The HDPE geomembrane presents 1.0 mm of nominal thickness.

Table 9. Nickel waste chemical composition (SOSA, 2016)

Chemical Compound	Composition (%)
CaO	0.532
MgO	4.260
TiO_2	0.183
Fe_2O_3	61.578
Al_2O_3	7.385
SiO_2	19.874
SrO	Not identified
BaO	Not identified
V_2O_3	0.120
Cr_2O_3	3.998
Mo_2O_3	0.025
MnO	0.516
CoO	0.112
NiO	0.662
CuO	0.031
ZnO	0.057
CdO	Not identified
P_2O_5	0.606
PbO	0.061

3.1.2.6 LDO exhumed sample

LDO sample presents 0.8 mm of nominal thickness and was exhumed from a biodegradable waste pond after 15.17 years of service. Table 10 presents the parameters of different biodegradable raw materials disposed of in the pond. Figure 16 shows the pond, with the LDO sample as a flow barrier system. The sample was collected from the pond's slope, which was in contact with the waste and the environmental conditions during the exposure time.

Table 10. Raw materials' parameters disposed of in the waste pond
(IBRA INSTITUTO BRASILEIRO DE ANÁLISES, 2019)

Parameter (%)	**Bagasse Bran**	**Boiler Ashes**	**Dry Boiler Ashes**	**Fruit Waste**	**Sludge**
Nitrogen	0.4	0.32	0.22	1.79	1.57
Total phosphorous	2.33	1.68	3.13	3.69	6.65
2 % Phosphorous citric acid solution	1.92	1.68	2.49	2.89	5.69
Potassium (HNO_3+$HClO_4$)	0.53	2.69	5.70	1.79	1.63
Calcium (HNO_3+$HClO_4$)	0.72	1.92	2.99	1.70	4.72
Magnesium (HNO_3+$HClO_4$)	0.17	0.80	1.92	0.28	0.52
Organic Material	91.85	13.55	16.0	81.5	47.65
Organic carbon	41.86	11.78	7.53	39.74	19.34
CEC (in mmolc kg^{-1})	400	225	300	575	700
Moisture content	80.95	58.85	2.47	0	79.25

Figure 16. Biodegradable waste pond using the LDO sample as a liner

3.1.2.7 CAM, CAM1 and CAM2 exhumed samples

Three HDPE geomembrane samples were exhumed from two different shrimp farming ponds in the northeast of Brazil with 0.8 mm of nominal thicknesses. The samples called "CAM" and "CAM1" represent the same geomembrane installed in a shrimp farming pond

and were collected after 8.25 years of field exposure. The CAM sample was exhumed from the bottom liner and had been in contact with the salinized water. The CAM1 sample was exhumed from the same pond of the CAM sample, but it was taken from the slope liner and had been in contact for 8.25 years with environmental conditions. The third sample (CAM2) was exhumed from another shrimp farming pond after 3.0 years of service. This pond has the particularity of being covered with an agricultural plastic film. Table 11 presents, as a reference, the salinized water parameters used for shrimp cultivation. Figures 17 and 18 show, respectively, the shrimp farming pond representing the CAM and CAM1 samples and the shrimp farming pond representing the CAM2 sample.

Table 11. Salinized water parameters used for shrimp cultivation (SPELTA, 2016)

Parameter	**Average Value (8 % of Salinization)**	**Average Value (16 % of Salinization)**
Dissolved Oxygen ($mg\ L^{-1}$)	5.81	5.49
Saturated Oxygen (%)	85.13	80.22
Water Temperature (°C)	27.81	27.54
pH	7.76	7.67
Total Alkalinity ($mg\ CaCO_3\ L^{-1}$)	93.69	120.06

Figure 17. Shrimp farming pond representing the CAM and CAM1 samples

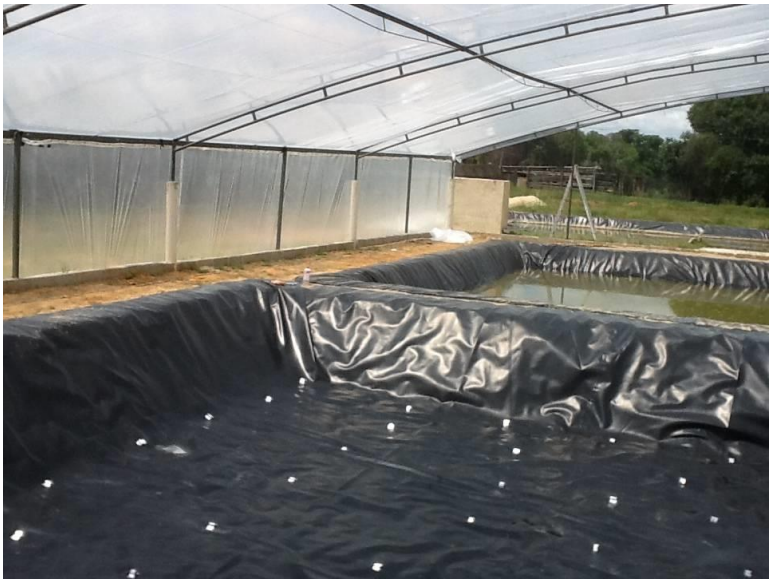

Figure 18. Shrimp farming pond representing the CAM2 sample

3.2 Laboratory aged exposures

3.2.1 Introduction

Virgin HDPE geomembranes were exposed by the laboratory to UV radiation, thermal aging, and synergy between UV radiation and thermal aging. The UV exposure was performed by the UV fluorescent device and xenon arc chamber. Table 12 shows the laboratory exposures performed, samples used, and exposure times.

Table 12. Laboratory exposures performed, samples used, and exposure times

Laboratory Exposure	Samples	Exposure Times (h)
UV fluorescent	1L and 1.5L	960, 4380 and 8760
Xenon Arc	1L	960, 1639 and 2160
Thermal Aging	1L, 1.5L and 2L	960, 4380 and 8760
Synergy: UV fluorescent – Thermal aging	1L and 1.5L	8760 of UV fluorescent and 4380 of Thermal aging

3.2.2 UV exposure

A UV-weathering chamber was used from Equilam at Diadema, Brazil, model EQUV, with fluorescent UVA-340 lamps, manufactured by Philips, programmed to work in

cycles of 20 ± 0.01 h of UV light at 75 ± 1 °C followed by 4 ± 0.01 h of condensation at 50 ± 0.01 °C for periods of 960, 4380, and 8760 ± 0.01 h. As a reference, the standard test method used was described by ASTM D7238. Figure 19 shows the UV-weathering chamber during the exposure.

Figure 19. UV-weathering chamber during the exposure (EESC-USP)

Moreover, the Xenon arc chamber used was from Q-Lab in Cleveland, USA, model Xe-3-HS, with UVA-340 fluorescent lamps, manufactured by Philips. The equipment was programmed to operate in 102 ± 0.01 min cycles with a black panel temperature of 60 ± 1 °C followed by 18 ± 0.01 min of light and water spray for periods of 960, 1639, and 2160 ± 0.01 h. As a reference, the standard test method used was described by ASTM G155. Figure 20 shows the xenon arc chamber used in this research.

Figure 20. Xenon arc chamber used in this research (IMT)

3.2.3 Thermal exposure

An air-oven was used from Quimis Aparelhos Científicos in Diadema, Brazil, model Q314M with forced circulation, programmed to work 24 hours at 85 ± 1 °C for periods of 960, 4380 and 8760 ± 0.01 h. As a reference, the standard test method described by ASTM D5721 and the specification described by GRI-GM13 were used. Figures 21 and 22 show, respectively, the air-oven used in this research and the air-oven during the exposure.

Figure 21. Air-oven used in this research (IMT)

Figure 22. Air-oven during the exposure (IMT)

3.2.4 Synergic exposure to UV radiation and thermal aging

The synergic effect between UV radiation (UV-weathering chamber) and thermal aging was evaluated for 1L and 1.5L samples exposed for 8760 ± 0.01 h by UV-weathering chamber and, after that, exposed by air-oven for more 4380 ± 0.01 h.

3.3 Physical tests

3.3.1 Introduction

The physical tests conducted to characterize the virgin and exhumed samples in this research are described in Table 13. The tests were performed in two laboratory facilities, in São Carlos School of Engineering, University of São Paulo (EESC-USP) at São Carlos, Brazil, and in Mauá Institute of Technology (IMT) at São Caetano do Sul, Brazil.

Table 13. Physical tests conducted to characterize the HDPE geomembrane samples

Property	Unit	Standard Test Method	Laboratory Facility
Thickness	mm	ASTM D5199	EESC-USP
Density	g cm^{-3}	ASTM D792	EESC-USP
Melt flow index (MFI)	g 10 min^{-1}	ASTM D1238	IMT
Carbon Black Content (CBC)	%	ASTM D4218	EESC-USP
Carbon Black Dispersion (CBD)	Category	ASTM D5596	EESC-USP
Tensile Resistance	kN m^{-1}	ASTM D6693	EESC-USP
Tensile Elongation	%		
Puncture Resistance	N	ASTM D4833	EESC-USP
Tear Resistance	N	ASTM D1004	EESC-USP
Stress Crack Resistance (SCR)	h	ASTM D5397	IMT
Oxidative Induction Time (OIT)	min	ASTM D3895 ASTM D5885	EESC-USP

The physical analyses of the laboratory aged samples were performed according to Table 14, which contains the relevant properties to understand the changes that occurred in the polymer.

Table 14. Physical analyses performed for the laboratory aged samples

Laboratory Exposure	Samples	Analyzed Properties
UV fluorescent	1L	MFI, Tensile Properties, and OIT
UV fluorescent	1.5L	MFI, Tensile Properties, OIT, and SCR
Xenon Arc	1L	MFI, and OIT
Thermal Aging	1L, 1.5L and 2L	MFI, Tensile Properties, OIT, and SCR
Synergy: UV fluorescent – Thermal aging	1L and 1.5L	MFI, Tensile Properties, OIT, and SCR

3.3.2 Thickness and density tests

The HDPE geomembrane's thickness is determined using the dead-weight loading gauge (200 ± 0.2 kPa) measuring the difference between the dead-weight loading gauge with and without the specimen with a precision of 0.001 mm.

The test performed to determine the HDPE geomembrane's density uses the Archimedes' principle measuring the immersed mass of the specimen (1.0 ± 0.1 g) in isopropyl alcohol at 21 ± 0.1 °C. The specimen's mass is determined using an analytical balance with a precision of 0.0001 g. The specimen is measured before and after the immersion in a vessel and beaker.

3.3.3 Melt flow index (MFI) test

The melt flow index (MFI) test was carried out using a plastometer manufactured by Instron at Norwood, USA, model CEAST MF20. The material was extruded through a smooth bore (2.095 ± 0.005 mm in diameter and 8000 ± 0.025 mm long) at 190 ± 0.08 °C with a 5.0 ± 0.01 kg of deadweight. After 10 min (with precision of 1 s) of the sample extrusion, the material mass was measured using an analytical balance with 0.0001 g of precision. Figure 23 shows the plastometer used in this research.

Figure 23. Plastometer used in this research (IMT)

3.3.4 Carbon black properties

The carbon black content (CBC) is determined measuring an HDPE geomembrane's specimen mass (1.0 ± 0.1 g) with a precision of 0.0001 g by an analytical balance before and after burning at 605 ± 5 °C in a muffle furnace.

The carbon black dispersion (CBD) is determined by a qualitative evaluation of carbon black agglomerates and other inclusions in HDPE geomembranes. This evaluation is

based on carbon black dispersion size calculated area within microscopic fields of view. Using a microtome, the sample is clamped in the sample holder, which can be raised or lowered precisely. A rigid knife is slid manually across the sample so that the specimens' range in thickness from 8 to 20 ± 1 µm. After the specimen's preparation, the microscopic manufactured by Bel Photonics in Milano, Italy, model STM Pro, is used to compare the specimen's view with a standard reference chart.

3.3.5 Mechanical properties

The mechanical tests were performed using a universal machine manufactured by EMIC in São José dos Pinhais, Brazil, model DL 3000 (Figure 24), with a 2-kN load cell. The tensile test was conducted with a test speed of 50 ± 1 mm min^{-1} and the type IV dog bone specimen. The tensile strength and tensile elongation were recorded for the material's machine direction. The tear and puncture tests were performed, respectively, with test speeds of 51 and 300 ± 1 mm min^{-1}. The tear strength was recorded for the material's machine direction.

Figure 24. Universal machine used to conduct the mechanical tests (EESC-USP)

3.3.6 Stress crack resistance (SCR) test

The stress crack resistance (SCR) was determined using the deadweight load of 30 % of the yield tensile strength of the samples (precision of 10 g) and a notch of 20 % of the specimen thickness (precision of 0.001 mm). The test was performed using equipment

manufactured by WT Indústria at São Carlos, Brazil. The specimens were immersed in a solution with 10 ± 0.1 % of Igepal CO 630 and 90 ± 0.1 % of water at a constant temperature of 50 ± 1 °C. The results were reported using the mean rupture time of 5 specimens with precision of 1 s. Figure 25 shows the stress cracking equipment utilized in this research with the specimens before the immersion in the solution.

Figure 25. Stress cracking equipment utilized in this research (IMT)

3.3.7 Oxidative-induction time (OIT) tests

This study utilized two tests to determine the oxidative-induction time (OIT) of the HDPE geomembrane samples. The standard OIT (Std. OIT) and the high-pressure OIT (HP OIT) tests were performed. Both tests can search the different antioxidants in the material's blend. DSC (differential scanning calorimetry) equipment was used to perform the tests, model Q20 (Figure 26), manufactured by TA Instruments in New Castle, USA, using a sample mass of 5 ± 0.5 mg inside an aluminum crucible. The standard OIT test was performed at 200 ± 2 °C with an oxygen constant pressure of 140 ± 5 kPa, a heating rate of 20 ± 1 °C min^{-1} and a flow rate of 50 ± 5 mL min^{-1}. The high-pressure OIT test was conducted at 150 ± 0.5 °C with an oxygen constant pressure of 3.4 ± 0.06 MPa and a heating rate of 20 ± 1 °C min^{-1}. Figure 26 shows the DSC equipment utilized in this research to obtain the OIT values.

Figure 26. DSC equipment utilized in this research to obtain the OIT values (EESC-USP)

3.4 Thermal analyses

3.4.1 Introduction

The thermoanalytical evaluation was carried out by thermogravimetry (TG/DTG), differential thermal analysis (DTA), differential scanning calorimetry (DSC), thermomechanical analysis (TMA), and dynamic mechanic analysis (DMA). The analyses were realized in four laboratory facilities, in Chemical Institute, São Paulo State University (IQ-UNESP) at Araraquara, Brazil, in Mauá Institute of Technology (IMT) at São Caetano do Sul, Brazil, in São Carlos Chemical Institute, University of São Paulo (IQSC-USP) at São Carlos, Brazil, and in Material Characterization and Development Center, Federal University of São Carlos (CCDM-UFSCar) at São Carlos, Brazil. Table 15 shows the laboratory facilities in which each thermal analysis was conducted. Table 16 shows the analyzed samples by each thermal analysis utilized in this research.

Table 15. Laboratory facilities utilized for the thermal analyses

Thermal Analysis	Laboratory Facility
TG/DTG and DTA (simultaneously)	IQ-UNESP
TG/DTG	IMT
DSC	IQ-UNESP and IMT
TMA	IQ-UNESP
DMA	IQSC-USP and CCDM-UFSCar

Table 16. Analyzed samples by thermal analysis

Sample	Thermal Analysis
1L	TG/DTG and DTA, DSC, TMA, and DMA
1.5L	DSC and DMA
2L	DMA
CLIQ	TG/DTG and DTA, DSC, and TMA
LTE	TG/DTG and DTA, DSC, and DMA
LCH	TG/DTG and DTA, DSC, and DMA
MIN	TG/DTG and DTA, and DSC
MIN2	TG/DTG and DTA, and DSC
LDO	DSC and DMA
CAM	TG/DTG, DSC, and DMA
CAM1	TG/DTG, DSC, and DMA
CAM2	TG/DTG, DSC, and DMA
UV fluorescent Aged Samples: 1L and 1.5L	DSC
Xenon Arc Aged Samples: 1L	DSC
Thermal Aged Samples: 1L, 1.5L, and 2L	DMA
Synergic Aged Samples: 1L and 1.5L	DMA

3.4.2 Thermogravimetry (TG/DTG) and differential thermal analysis (DTA)

The TG/DTG and DTA were performed simultaneously, using SDT 2960 equipment, manufactured by TA Instruments at New Castle, USA, using an alumina crucible. Table 17 presents the utilized parameters for these analyses in each sample. Figure 27 shows the TG/DTG and DTA equipment used in this research.

Table 17. TG/DTG and DTA utilized parameters

Samples	Heating Rate (°C min^{-1})	Purge Gas	Flow (mL min^{-1})	Sample Mass (mg)
1L and CLIQ	5, 10, 20, and 30 ± 1	Synthetic Air and Carbonic Gas	110 ± 5	3.5 ± 0.5
LTE and LCH	5, 10, 20, and 30 ± 1	Synthetic Air and Carbonic Gas	100 ± 5	7.5 ± 0.5
MIN and MIN2	10 ± 1	Synthetic Air	100 ± 5	7.0 ± 0.5

Figure 27. TG/DTG and DTA equipment utilized in this research (UNESP-Araraquara)

3.4.3 Thermogravimetry (TG/DTG)

The thermogravimetric analysis (TG) was conducted using a heating rate of 10 ± 1 °C min^{-1} under nitrogen purge gas with a 90 ± 5 mL min^{-1} of flow, using an aluminum crucible. The equipment used in this analysis was the Q50, manufactured by TA Instruments, in New Castle, USA. Figure 28 shows the TG/DTG equipment used in this research.

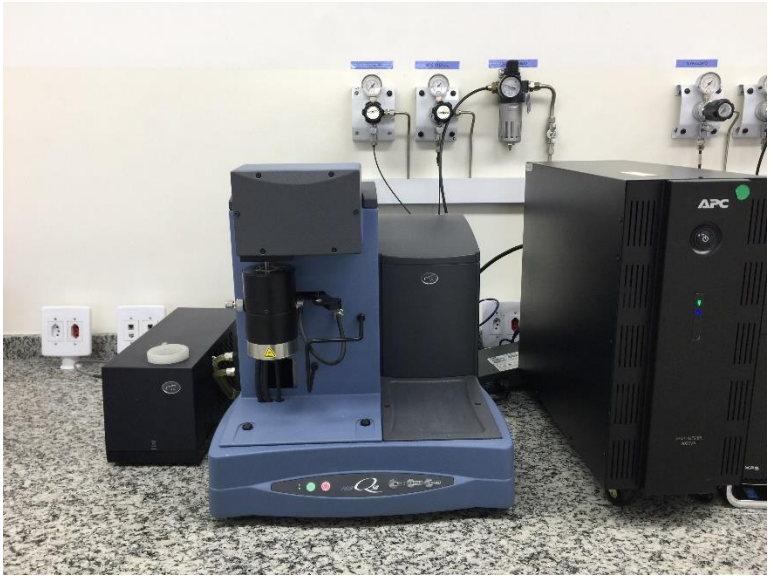

Figure 28. TG/DTG equipment utilized in this research (IMT)

3.4.4 Differential scanning calorimetry (DSC)

There was utilized DSC equipment at IQ-UNESP, manufactured by Mettler Toledo (DSC1 Stare model) at Columbus, USA. DSC analysis was performed using an alumina crucible with temperature ranges of -80 to 200 ± 2 °C and 200 to 25 ± 2 °C in a nitrogen gas environment with a flow of 50 ± 5 mL min^{-1}.

The DSC analysis was also performed using DSC equipment at IMT, manufactured by TA Instruments at New Castle, USA, model Q20. The analysis was conducted using a nitrogen gas purge with a 50 ± 5 mL min^{-1} flow and a temperature range of 25 to 200 ± 2 °C.

Table 18 presents the utilized parameters for these analyses in each sample. Figure 29 shows the DSC equipment used in this research.

Table 18. DSC utilized parameters

Samples	Heating Rate (°C min^{-1})	Crucible	Sample Mass (mg)	Laboratory Facility
1L and CLIQ	10 and 30 ± 1	Alumina	3.5 ± 0.5	IQ-UNESP
LTE	30 ± 1	Aluminum	7.5 ± 0.5	IQ-UNESP
LCH	30 ± 1	Aluminum	15.5 ± 0.5	IQ-UNESP
MIN and MIN2	10 ± 1	Aluminum	3.0 ± 0.5	IQ-UNESP
CAM, CAM1 and CAM2	10 ± 1	Aluminum	3.0 ± 0.5	IMT
LDO	10 ± 1	Aluminum	3.0 ± 0.5	IMT
1L	10 ± 1	Aluminum	5.0 ± 0.5	IMT
1.5L	10 ± 1	Aluminum	10.0 ± 0.5	IMT
UV fluorescent Aged Samples: 1L	10 ± 1	Aluminum	5.0 ± 0.5	IMT
UV fluorescent Aged Samples: 1.5L	10 ± 1	Aluminum	10.0 ± 0.5	IMT
Xenon Arc Aged Samples: 1L	10 ± 1	Aluminum	5.0 ± 0.5	IMT

Figure 29. DSC equipment utilized in this research at IMT

3.4.5 Thermomechanical analysis (TMA)

The Thermomechanical analysis (TMA) was performed using an equipment manufactured by TA Instruments, in New Castle, USA, SDT 2940 model. The samples were submitted to purge gases of synthetic air and nitrogen, with a flow of 50 ± 5 mL min^{-1}, and a heating rate of 5 ± 1 ºC min^{-1}. The specimen's dimensions were 5 ± 1 x 5 ± 1 mm, and there was used the standard expansion probe. Additionally, the TMA analyses were performed in an environment oven without purge gas flows. Figure 30 shows the TMA equipment used in this research.

Figure 30. TMA equipment utilized in this research (UNESP-Araraquara)

3.4.6 Dynamic mechanical analysis (DMA)

DMA equipment was used at IQSC-USP, model Q800, manufactured by TA Instruments at New Castle, USA. DMA analysis was conducted in the dual cantilever mode. The samples had a dimension of 35 × 13 ± 1 mm and were performed under a heating rate of 10 ± 1 °C min^{-1} with nitrogen purge gas (flow of 50 ± 5 mL min^{-1}). The oscillation amplitude of 20 µm was used, with a frequency of 1 Hz and a temperature range from −80 ± 2 °C to 125 ± 2 °C.

DMA analysis was also conducted using equipment at CCDM-UFSCar, manufactured by TA Instruments, at New Castle, USA, model Q800. The analysis was performed in the dual cantilever mode, with 10 ± 1 °C min^{-1} of heating rate, and heating from – 100 ± 2 °C to 130 ± 2 °C. The oscillation amplitude of 20 µm was used, with a frequency of 1 Hz. The specimen's dimensions were 35 x 13 ± 1 mm.

Table 19 shows the analyzed samples by each thermal analysis utilized in this research. Figure 31 shows the DMA equipment used in this research (CCDM-UFSCar).

Table 19. Laboratory facilities utilized for the DMA analysis

Sample	Laboratory Facility
LTE and LCH	IQSC-USP
LDO	CCDM-UFSCar
CAM, CAM1, and CAM2	CCDM-UFSCar
Virgin Samples: 1L, 1.5L, and 2L	CCDM-UFSCar
Thermal Aged Samples: 1L, 1.5L, and 2L	CCDM-UFSCar
Synergic Aged Samples: 1L and 1.5L	CCDM-UFSCar

Figure 31. DMA equipment utilized in this research (CCDM-UFSCar)

3.5 Complementary analysis

Some samples were complementarily evaluated for Fourier-transform infrared spectroscopy (FTIR). Table 20 shows the samples analyzed by FTIR. Figure 32 shows the FTIR equipment used in this research.

Table 20. Sample analyzed by FTIR

Laboratory Exposure	Sample Analyzed by FTIR
UV fluorescent	1L
Xenon arc	1L

Figure 32. FTIR equipment utilized in this research (IMT)

3.6 Research planning

Table 21 presents the research planning, including the analyzed samples, physical tests, thermal analyses and FTIR analyses conducted in this work. There were realized 165 physical tests, 150 thermal analyses and 7 FTIR analyses.

Table 21. Research planning

Sample	Physical tests	Thermal and FTIR analyses
CLIQ	T, D, MFI, CBC, CBD, Tens, Tear, P, SCR, Std. OIT and HP OIT	TG/DTG, DTA, DSC and TMA
LCH	T, D, MFI, CBC, CBD, Tens, Tear, P, SCR, Std. OIT and HP OIT	TG/DTG, DTA, DSC and DMA
LTE	T, D, MFI, CBC, CBD, Tens, Tear, SCR, Std. OIT and HP OIT	TG/DTG, DTA, DSC and DMA
MIN	T, D, MFI, CBC, CBD, Tens, Tear, SCR, Std. OIT and HP OIT	TG/DTG, DTA and DSC
MIN2	T, D, MFI, CBC, CBD, Tens, Tear, SCR, Std. OIT and HP OIT	TG/DTG, DTA and DSC
LDO	T, D, MFI, CBC, CBD, Tens, Tear, SCR, Std. OIT and HP OIT	DSC and DMA
CAM	T, D, MFI, CBC, CBD, Tens, Tear, P, SCR, Std. OIT and HP OIT	TG/DTG, DSC and DMA
CAM1	T, D, MFI, CBC, CBD, Tens, Tear, P, SCR, Std. OIT and HP OIT	TG/DTG, DSC and DMA
CAM2	T, D, MFI, CBC, CBD, Tens, Tear, P, SCR, Std. OIT and HP OIT	TG/DTG, DSC and DMA
1L	T, D, MFI, CBC, CBD, Tens, Tear, P, SCR, Std. OIT and HP OIT	TG/DTG, DTA, DSC, TMA, DMA and FTIR
1L UV fluorescent	MFI, Tens, Std. OIT and HP OIT	DSC and FTIR
1L Xenon arc	MFI, Std. OIT and HP OIT	DSC and FTIR
1L Thermal Exposure	MFI, Tens, SCR, Std. OIT and HP OIT	DMA
1L Synergic Effect	MFI, Tens, SCR, Std. OIT and HP OIT	DMA
1.5L	T, D, MFI, CBC, CBD, Tens, Tear, P, SCR, Std. OIT and HP OIT	DSC and DMA
1.5L UV fluorescent	MFI, Tens, SCR, Std. OIT and HP OIT	DSC
1.5L Thermal Exposure	MFI, Tens, SCR, Std. OIT and HP OIT	DMA
1.5L Synergic Effect	MFI, Tens, SCR, Std. OIT and HP OIT	DMA

2L	T, D, MFI, CBC, CBD, Tens, Tear, P, SCR, Std. OIT and HP OIT	DMA
2L Thermal Exposure	MFI, Tens, SCR, Std. OIT and HP OIT	DMA

D – Density

P – Puncture

T – Thickness

Tens – Tensile

4 RESULTS AND DISCUSSION

4.1 Physical test results

4.1.1 Virgin samples results

Table 22 shows the initial properties of the tested virgin samples.

Table 22. Initial properties' mean values of the HDPE geomembrane virgin samples

Property	Method	1L Sample	1.5L Sample	2L Sample
Thickness (mm)	ASTM D5199	1.040 (±0.079)	1.652 (±0.039)	1.984 (±0.061)
Density (g cm^{-3})	ASTM D792	0.958 (±0.002)	0.945 (±0.001)	0.948 (±0.001)
MFI (5 kg/190 °C) (g 10 min^{-1})	ASTM D1238	0.6800 (±0.0217)	0.5054 (±0.0102)	0.4406 (±0.0067)
CBC (%)	ASTM D4218	3.14 (±0.13)	2.92 (±0.12)	2.27 (±0.09)
CBD (Category)	ASTM D5593	Category I	Category I	Category I
Tensile break resistance (kN m^{-1})	ASTM D6693	28.52 (±1.55)	46.93 (±7.04)	59.68 (±4.59)
Tensile break elongation (%)		733.47 (±10.76)	704.67 (±101.30)	820.03 (±33.63)
Tear resistance (N)	ASTM D1004	169.17 (±8.76)	242.53 (±0.40)	296.27 (±8.14)
Puncture resistance (N)	ASTM D4833	434.17 (±18.19)	677.30 (±16.47)	788.37 (±5.99)
SCR (h)	ASTM D5397	16.47 (±2.66)	629.84 (±67.55)	319.73 (±31.25)
Std. OIT (min)	ASTM D3895	40.49 (±0.73)	199.78 (±4.03)	113.80 (±5.32)
HP OIT (min)	ASTM D5885	125.70 (±0.42)	287.25 (±1.06)	241.50 (±5.37)

Standard deviations are between brackets.

The GRI-GM13 is an American standard that prescribes the minimum values for the essential properties to analyze in manufacturing quality control of smooth and textured HDPE geomembranes.

The geomembrane thickness influences the mechanical properties and, according to Islam and Rowe (2007), the durability of the product. The thickness' mean values of 1L and 1.5L samples were higher than the nominal values. However, the 2L sample presented a thickness' mean value lower than the minimum prescribed by the GRI-GM13.

The density test results showed values higher than 0.940 g cm^{-3}, which is the minimum required value for GRI-GM13. Meanwhile, the 1L sample presented a high-density value, which is incompatible with a modern HDPE geomembrane.

The melt flow index (MFI) is a good parameter to compare virgin with exposed or exhumed samples. The increase or decrease in this index can provide an understanding of possible polymer degradation (TELLES *et al.*, 1984). All of the virgin samples presented lower values than 1.0 g 10 min^{-1}, with highlighted for the 1L sample, that showed the highest MFI value among the virgins samples analyzed.

The GRI-GM13 prescribes a range of 2–3 % of carbon black content in the product. The 1L sample presented a value slightly higher than 3 %, but the other samples showed carbon black content values in the range prescribed by the American standard. Samples with lower values than 2 % of carbon black could be prejudicial to the resin protection of weather exposure. All samples tested were classified as category I (diameter of particles less than 35 µm) for carbon black dispersion, representing an adequate dispersion. According to Sofri (2005), the carbon black dispersion quality for plastics is an important component of UV resistance. Carbon black particles with smaller diameters will have a higher superficial area for incident light contact, and, because of that, they will have better radiation absorption (SOFRI, 2005).

The tensile and tear tests were conducted only for the machine direction. The virgin samples are according to the GRI-GM13 about the minimum values of the mechanical properties (tensile, tear and puncture). The 1.5L sample showed high tensile elongations' standard deviation due to one specimen, which presented a value lower than 600 %. Figures 33, 34, and 35 show, respectively, the tensile test curves for the 1L, 1.5L, and 2L samples.

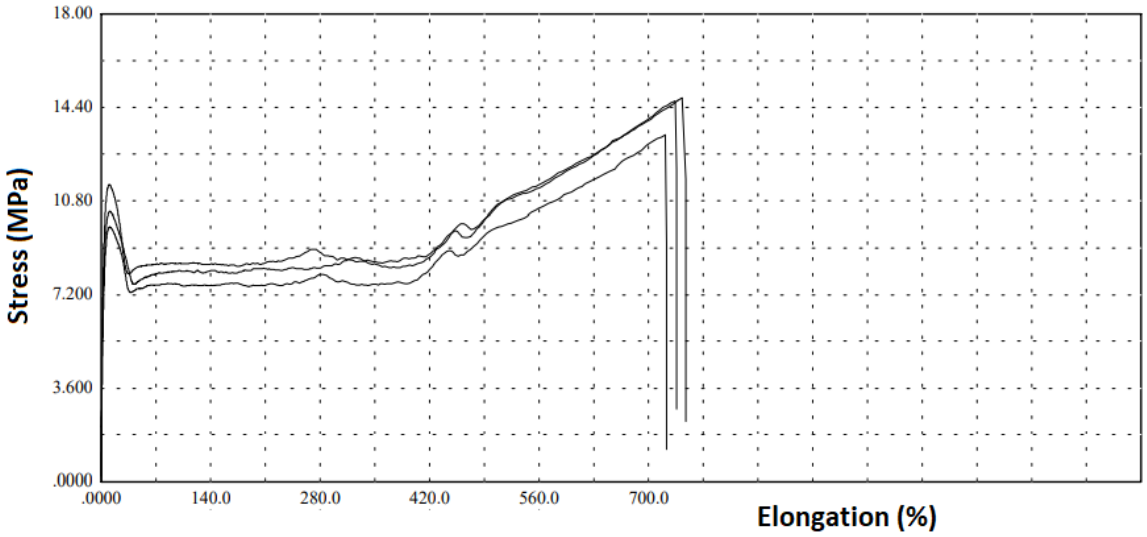

Figure 33. Tensile test curves for the 1L sample

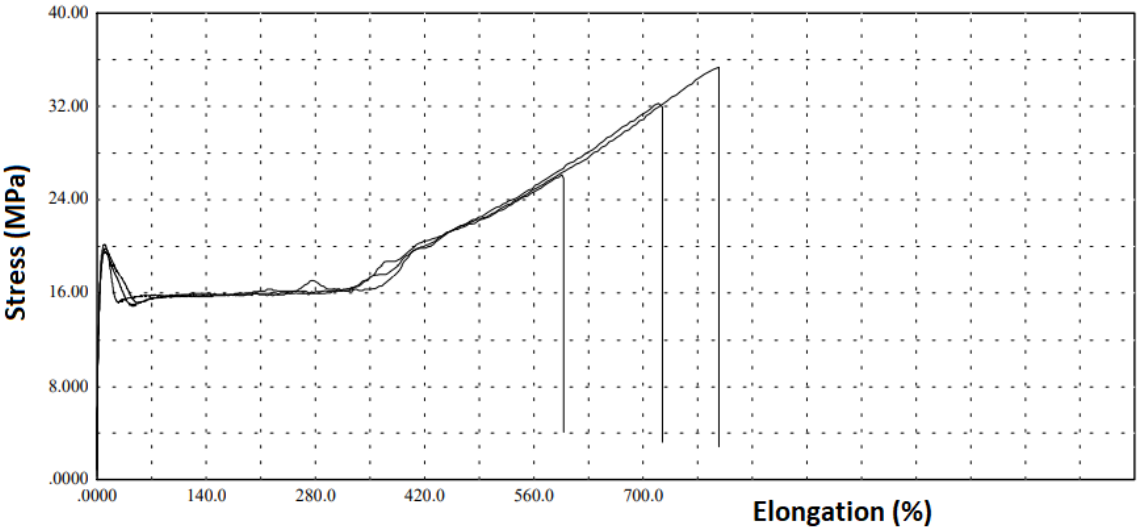

Figure 34. Tensile test curves for the 1.5L sample

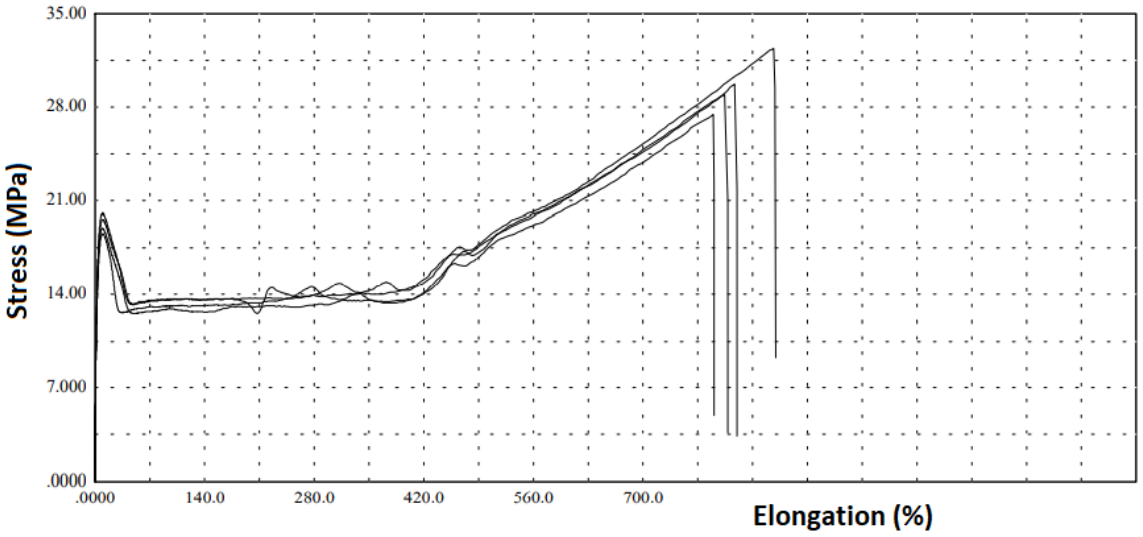

Figure 35. Tensile test curves for the 2L sample

According to the GRI-GM13, the minimum required value for the stress cracking test (NCTL-SP) is 500 h. Only the 1.5L sample presented the SCR value higher than 500 h. The 2L sample showed SCR about 60 % of the minimum required value, meanwhile the 1L sample obtained the lowest value, about 3 % of the minimum required value. The 1L sample behavior shows that this material can fail quickly in the field.

The minimum required value (GRI-GM13) for the standard OIT (Std. OIT) and high-pressure OIT (HP OIT) tests are, respectively, 100 and 400 min. According to Mueller and Jakob (2003), the main function of antioxidants is to prevent the initiation of oxidation chain reactions. Antioxidants are most effective over a certain range of temperature. For instance, phosphites are most effective at higher temperatures, whereas hindered amine light stabilizers (HALS) are effective at ambient temperature. Hindered phenols, however, are used as long-term stabilizers since they are effective over a wide range of temperature. The 1.5 L and 2L samples presented higher Std. OIT values than the minimum required value by the American standard. The 1L sample presented Std. OIT value 40 % of the minimum value required by the GRI-GM13, significantly reducing the material's lifetime. None of the tested samples presented HP OIT values equal to or higher than 400 min. The HP OIT results for 1.5L, 2L, and 1L samples were, respectively, about 70, 60, and 30 % of the minimum required value. The presence of HALS in the additive package increases the HP OIT results because this test is performed at 150 ºC, probably none of the virgin samples presented HALS in their additive package.

In Brazil, some geomembranes have polyethylene resins with low-stress crack resistance, additive packages without HALS (hindered amine light stabilizers) and sometimes off-grade resins. Such types of products can have a short-term life, causing environmental and financial losses (LAVOIE *et al.*, 2020-1).

4.1.2 Exhumed samples results

4.1.2.1 Industrial water pond: CLIQ and 1L samples

Table 23 shows the results from the physical properties for both analyzed samples, CLIQ sample, the reference sample (1L), and for the minimum values specified by GRI-GM13. Exhumed geomembranes with property values lower than this standard specification minimum values can support to understand changes in the polymer morphology.

Table 23. Physical properties of the high-density polyethylene geomembrane CLIQ and 1L samples

Property	Method	1L Sample	CLIQ Sample	GRI-GM13
Thickness (mm)	ASTM D5199	1.040 (±0.079)	0.998 (±0.095)	≥ 1.0
Density (g cm^{-3})	ASTM D792	0.958 (±0.002)	0.943 (±0.002)	≥ 0.940
MFI (5 kg/190 °C) (g 10 min^{-1})	ASTM D1238	0.6800 (±0.0217)	0.4256 (±0.0079)	-
CBC (%)	ASTM D4218	3.14 (±0.13)	1.24 (±0.17)	2.0–3.0
CBD (Category)	ASTM D5593	Category I	Category I	*
Tensile break resistance (kN m^{-1})	ASTM D6693	28.52 (±1.55)	21.98 (±6.82)	≥ 27.0
Tensile break elongation (%)		733.47 (±10.76)	482.63 (±329.65)	≥ 700.0
Tear resistance (N)	ASTM D1004	169.17 (±8.76)	145.50 (±3.29)	≥ 125.0
Puncture resistance (N)	ASTM D4833	434.17 (±18.19)	473.23 (±35.22)	≥ 320.0
SCR (h)	ASTM D5397	16.47 (±2.66)	709.45 (±78.63)	≥ 500.0
Std. OIT (min)	ASTM D3895	40.49 (±0.73)	53.27 (±10.86)	≥ 100.0
HP OIT (min)	ASTM D5885	125.70 (±0.42)	162.55 (±7.42)	≥ 400.0

Standard deviations are between brackets.

*10 different views: 9 in Categories I or II and 1 in Category III.

The nominal thickness of both samples is 1.0 mm, and the values obtained were close to the nominal value. The density values showed that the reference sample has a higher density than the exhumed sample. Both samples are in accordance with the GRI-GM13 criteria. According to Telles et al. (1984), low MFI values exhibit good stress cracking environmental resistance for HDPE geomembranes. The melt flow index results showed a lower value for the exhumed sample (CLIQ) than the reference sample. This result follows the stress crack resistance results because the exhumed sample presented a higher SCR value than the GRI-GM13 minimum required value. Otherwise, the reference sample presented a low SCR value.

The tensile test values of the samples showed a better behavior for the reference sample than the exhumed sample. There was not in accordance with the GRI-GM13 criteria for the exhumed sample. Figure 36 shows the tensile test curves for the exhumed sample. The reference sample shows a typical HDPE behavior. The exhumed sample exhibits brittle behavior for one of the test specimens tested without deformation prior to rupture. The GRI-GM13 criteria require a minimum of 700 % in the tensile break elongation and the average value of the exhumed sample was 482.63 % with a high standard deviation. Therefore, it was observed which exhumed sample had a change in the tensile behavior, probably caused by the weather conditions, as UV radiation and high temperatures. Following this behavior, it was noted that the exhumed sample had a low carbon black content, lower than the GRI-GM13 minimum required value, which can contribute to an inadequate polymers' UV protection. Still, the exhumed sample presented lower OIT test results than the GRI-GM13 minimum required values.

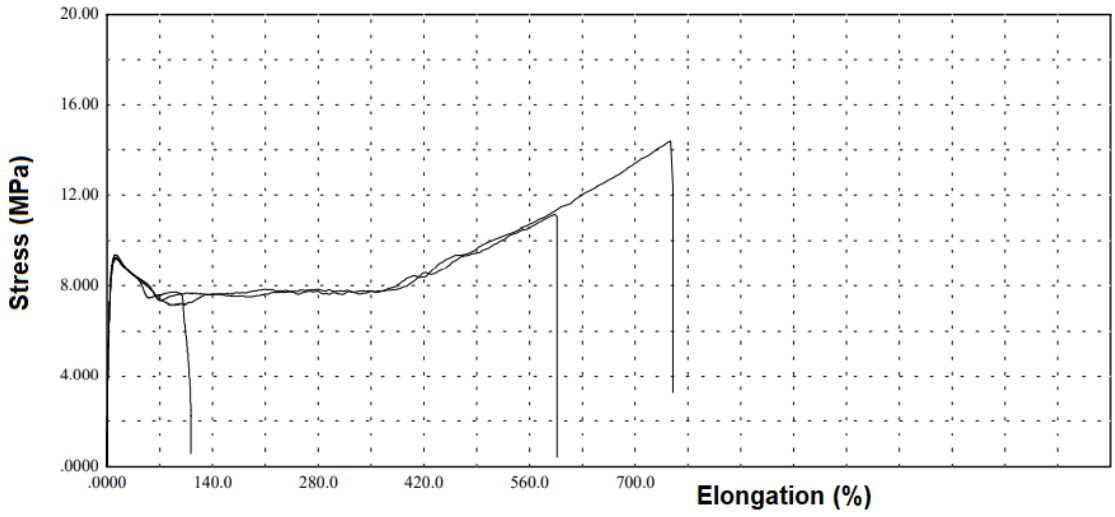

Figure 36. Tensile test curves for the CLIQ sample

4.1.2.2 Sanitation ponds: LCH and LTE samples

Table 24 shows the results from the physical properties for both exhumed samples from the sanitation ponds (LCH and LTE).

Table 24. Physical properties of the high-density polyethylene geomembrane LCH and LTE samples

Property	Method	LCH Sample	LTE Sample
Thickness (mm)	ASTM D5199	2.075 (±0.036)	1.001 (±0.038)
Density (g cm^{-3})	ASTM D792	0.946 (±0.002)	0.959 (±0.001)
MFI (5 kg/190 °C) (g 10 min^{-1})	ASTM D1238	0.5008 (±0.0072)	0.4555 (±0.0061)
CBC (%)	ASTM D4218	2.36 (±0.11)	2.49 (±0.47)
CBD (Category)	ASTM D5593	Category I	Category I
Tensile break resistance (kN m^{-1})	ASTM D6693	60.40 (±7.66)	27.12 (±1.30)
Tensile break elongation (%)		752.60 (±81.38)	679.33 (±27.53)
Tear resistance (N)	ASTM D1004	321.80 (±8.92)	170.13 (±2.05)
Puncture resistance (N)	ASTM D4833	815.77 (±12.70)	Tnp
SCR (h)	ASTM D5397	542.15 (±508.17)	30.89 (±12.31)
Std. OIT (min)	ASTM D3895	110.70 (±1.56)	60.69 (±0.21)
HP OIT (min)	ASTM D5885	231.50 (±2.12)	180.0 (±1.41)

Standard deviations are between brackets.

Tnp – Test not performed; the sample size did not allow.

The average values of the thickness are following the minimum values of the GRI-GM13. The carbon black content values obtained are also according to the GRI-GM13, which determines values between 2–3%. The obtained density values follow the GRI-GM13, which requires a minimum density value of 0.940 g cm^{-3}. The LTE sample presented a high-density value. The obtained results showed low MFI values for both tested samples.

The mechanical tests were conducted only for the machine direction. The samples' results are according to the GRI-GM13 concerning the minimum values of the tensile break (27 kN m^{-1} for 1.0 mm of thickness and 53 kN m^{-1} for 2.0 mm of thickness) and tear resistance (125 N for 1.0 mm of thickness and 249 N for 2.0 mm of thickness). For the

analyzed samples, only the LCH sample presented tensile elongation at breaks higher than 700%, which is the minimum value prescribed by GRI-GM13.

According to the GRI-GM13, the minimum required value for the stress cracking test (NCTL-SP) is 500 h. The LCH sample performed an average value higher than 500 h but presented a high variation in each specimen value tested, two of the five specimens tested obtained values higher than 1000 h, but the other two of the five specimens obtained values less than 200 h. The mean stress cracking value is in agreement with the tensile behavior of this sample. For the other exhumed sample tested, the results showed a low value of stress crack resistance. The LTE sample, despite having good tensile behavior and an adequate melt flow index, presented unexpected stress cracking results.

The minimum required values for the Std. and HP OIT tests, according to the GRI-GM13 are, respectively, 100 and 400 min. LTE sample presented Std. OIT value lower than 100 min. None of the samples presented OIT-HP values equal to or higher than 400 min. Probably none of the samples presented HALS in the additive package. The LCH sample obtained the highest OIT-HP value of the exhumed samples tested.

4.1.2.3 Mining facility constructions: MIN and MIN2 samples

Table 25 shows the results from the physical properties for MIN and MIN2 exhumed samples from the mining facility constructions.

Table 25. Physical properties of the high-density polyethylene geomembrane MIN and MIN2 samples

Property	Method	MIN Sample	MIN2 Sample	GRI-GM13
Thickness (mm)	ASTM D5199	0.896 (±0.003)	0.942 (±0.024)	≥ 1.0
Density (g cm^{-3})	ASTM D792	0.947 (±0.001)	0.949 (±0.001)	≥ 0.940
MFI (5 kg/190 °C) (g 10 min^{-1})	ASTM D1238	0.4016 (±0.0052)	0.8635 (±0.0229)	-
CBC (%)	ASTM D4218	2.02 (±0.47)	2.81 (±0.04)	2.0–3.0
CBD (Category)	ASTM D5593	Category I	Category I	*
Tensile break resistance (kN m^{-1})	ASTM D6693	22.11 (±4.05)	24.14 (±4.30)	≥ 27.0
Tensile break elongation (%)		301.15 (±397.19)	495.52 (±445.38)	≥ 700.0
Tear resistance (N)	ASTM D1004	162.73 (±3.05)	153.60 (±2.10)	≥ 125.0
Puncture resistance (N)	ASTM D4833	Tnp	Tnp	≥ 320.0
SCR (h)	ASTM D5397	45.25 (±34.13)	20.22 (±7.04)	≥ 500.0
Std. OIT (min)	ASTM D3895	29.55 (±4.70)	10.86 (±5.60)	≥ 100.0
HP OIT (min)	ASTM D5885	110.45 (±5.87)	113.25 (±12.37)	≥ 400.0

Standard deviations are between brackets.

*10 different views: 9 in Categories I or II and 1 in Category III.

Tnp – Test not performed; the sample size did not allow.

During the exposure period, the geomembrane samples were able to experience the exposure of environmental agents in the field, such as ultraviolet radiation and thermal variations. Moreover, chemical contact occurred between the samples with the effluents. These agents can change the samples' properties, modifying the materials' performance as an environmental protection liner.

The thickness mean values of both exhumed samples were lower than the nominal value (1.0 mm). The MIN sample presented a thickness mean value 10 % lower than the nominal value, whereas the MIN2 sample showed a thickness value 6 % lower than 1.0 mm. This non-compliance of the minimum thickness mean value required by the manufacturer can prematurely decrease the material's properties and, consequently, decrease the product's lifetime.

The density test results showed values higher than 0.940 g cm^{-3}, which is the minimum required value for GRI-GM13. The density of polyethylene influences the

physical and mechanical properties. In general, medium-density polyethylene (MDPE) is more useful for liners, because it presents better chemical resistance, high strength, and low permeability when compared to linear low-density polyethylene (LLDPE). However, HDPE, which is a semi-crystalline structure polymer, is susceptible to stress cracking. The HDPE geomembrane is formed by MDPE resin added with carbon black and additives, making the density higher than 0.940 g cm^{-3} (SCHEIRS, 2009; HSUAN *et al.*, 2008). The test results demonstrate the use of adequate resin of MDPE in the blend of both geomembrane samples.

The exhumed samples tested presented lower MFI values than 1.0 g 10 min^{-1}. However, the MIN2 sample obtained the highest MFI value of the samples studied, which was the double value of the MIN sample value. According to Muñoz Gómez (2016), high MFI values are related to the low molecular weights of HDPE geomembranes. A polymer with a wide molecular weight distribution presents a low viscosity and good stress crack resistance. Comparing both tested samples, the MIN sample showed a lower MFI value and higher stress crack resistance, demonstrating the same effect noted by Muñoz Gómez (2016).

Both samples tested presented low values of Std. OIT, lower than 100 min. It is possible to understand that the amount of antioxidants has almost ended for antioxidants that work in the temperature range of 200 °C. Sample MIN2 presented the lowest Std. OIT. The OIT results may have been influenced due to the longer exposure time of this sample. None of the tested samples presented HP OIT values equal to or higher than 400 min. The presence of HALS (hindered amine light stabilizer) in the additive package increases the HP OIT results because this test is performed at 150 °C. Probably none of the tested samples presented HALS in their blend. Three different stages can evaluate the HDPE geomembrane's oxidation. The first stage is related to antioxidant depletion. The chain reaction and the molecular composition changes start at the second stage. The third stage is related to the free radical formations, and cross-linking occurs in the free radicals with high changes in the molecular composition. Therefore, the mechanical and stress cracking properties are decreased, increasing the susceptibility of the polymer to the degradation effects (ROWE and SANGAM, 2002; KOERNER *et al.*, 2007; ABDELAAL *et al.*, 2019). It can be observed that the samples are still in the first stage of oxidation.

Lavoie *et al.* (2020-1) tested a virgin HDPE geomembrane with 1.0 mm of nominal thickness and obtained an expected ductile tensile behavior for all specimens tested. Otherwise, the MIN and MIN2 samples exhibited brittle tensile behavior for some of the specimens tested, demonstrating a variation among the specimens. The MIN sample

presented specimens 1, 3, and 4 with elongations lower than 700 %, otherwise specimens 2 and 5 presented elongations higher than 700 %. MIN2 sample showed brittle behavior for specimens 2 and 5, while specimens 1, 3, and 4 presented elongations higher than 700 %. This heterogeneity in the tensile elongation among the specimens for both samples analyzed demonstrates that changes occurred in the samples due to field exposition. Figures 37 and 38 show the samples' tensile curves. Both samples presented tensile resistance values lower than the minimum required value for the American standard. The MIN sample presented the lowest value between the samples, probably influenced by the lower thickness. The tensile elongation values demonstrated, for both samples, lower values than the minimum required value for the GRI-GM13. The MIN sample presented the lowest average tensile elongation value, lower than 350 %, which is less than 50 % of the minimum required for the GRI-GM13 for the tensile elongation value. It is interesting to note that, despite the consumption of antioxidants still being noticed (the first oxidation stage of the HDPE geomembrane), changes occurred in the tensile properties of the samples.

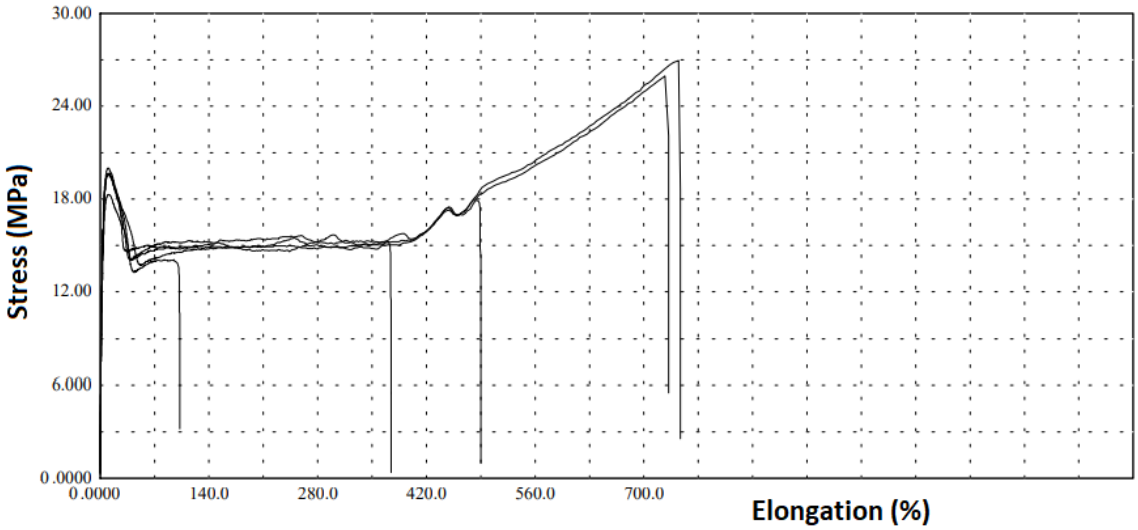

Figure 37. MIN sample's tensile test curves, demonstrating the elongation's variations among the tested specimens

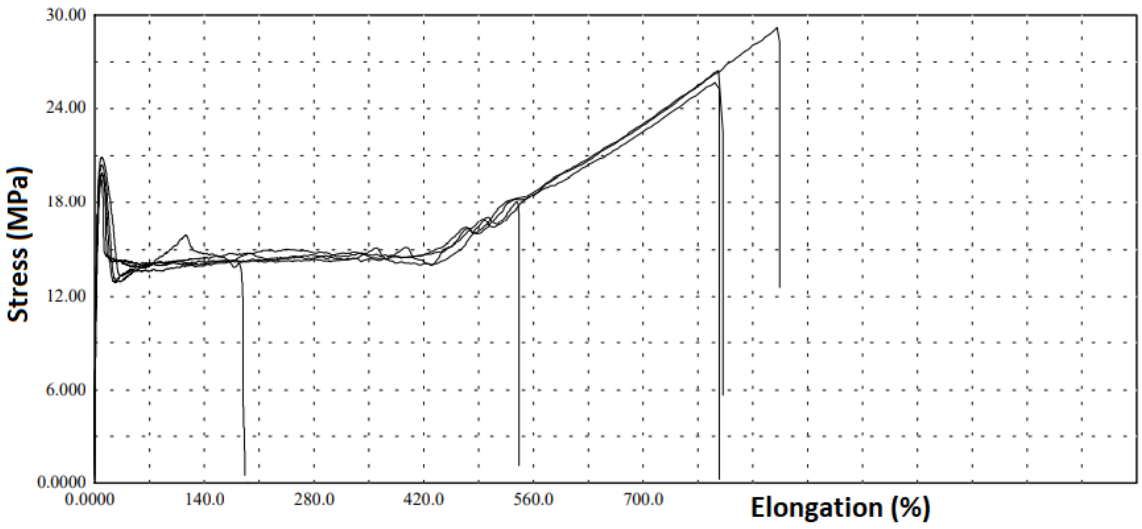

Figure 38. MIN2 sample's tensile test curves, demonstrating the elongation's variations among the tested specimens

Stress cracking of polymers is a phenomenon caused by tensile stresses lower than mechanical strength, which promotes internal or external cracks. These cracks can be accelerated by the environment (TELLES *et al.*, 1984). Both samples presented stress crack resistance values lower than the minimum required value by the American standard, especially for the MIN2 sample, which presented the highest MFI value and the lowest stress crack resistance between the samples. The MIN and MIN2 samples presented similar behaviors between stress cracking and tensile parameters, with low tensile elongation values and low-stress crack resistance.

4.1.2.4 Biodegradable waste pond: LDO sample

Table 26 shows the exhumed sample's physical tests results and the American standard's minimum properties values as a reference.

Table 26. Physical properties of the high-density polyethylene geomembrane LDO sample

Property	Method	LDO Sample	GRI-GM13
Thickness (mm)	ASTM D5199	0.843 (±0.028)	≥ 0.80
Density (g cm^{-3})	ASTM D792	0.965 (±0.0007)	≥ 0.940
MFI (5 kg/190 °C) (g 10 min^{-1})	ASTM D1238	0.7375 (±0.0225)	-
CBC (%)	ASTM D4218	2.60 (±0.66)	2.0–3.0
CBD (Category)	ASTM D5593	Category I	*
Tensile break resistance (kN m^{-1})	ASTM D6693	20.35 (±0.98)	≥ 22.0
Tensile break elongation (%)		259.24 (±342.71)	≥ 700.0
Tear resistance (N)	ASTM D1004	142.93 (±7.82)	≥ 100.0
Puncture resistance (N)	ASTM D4833	Tnp	≥ 256.0
SCR (h)	ASTM D5397	8.89 (±4.12)	≥ 500.0
Std. OIT (min)	ASTM D3895	6.94 (±1.04)	≥ 100.0
HP OIT (min)	ASTM D5885	106.45 (±5.87)	≥ 400.0

Standard deviations are between brackets.

*10 different views: 9 in Categories I or II and 1 in Category III.

Tnp – Test not performed; the sample size did not allow.

The sample analyzed presented an average thickness value higher than the nominal thickness. The sample's density showed a value higher than the minimum specified, and it is related to high crystallinity. The sample density value is considered high for a modern HDPE geomembrane. A high-density polyethylene geomembrane with a high crystallinity tends to present low-stress crack resistance values (HSUAN, 2000). The sample's MFI result presented a high value, near 1.0 g 10 min^{-1}. According to Hsuan (2000), the stress crack resistance is closely related to the polymer's density and MFI. An HDPE with a low MFI value can indicate a high molecular weight, which exhibits a higher SCR than a polymer that presents a high MFI value. The sample's carbon black content result is according to the range prescribed by the GRI-GM13.

The LDO sample presented average tensile resistance lower than the minimum value required by the American standard and average tensile elongation value lower than 350 % (less than 50 % of the minimum required for the GRI-GM13, with a high standard deviation. The LDO sample presented a low-stress crack resistance result, showing brittle behavior,

according to the high crystallinity of the polymer, high MFI value of the geomembrane, and the low average tensile elongation value obtained.

The Std. OIT result demonstrated that the antioxidant depletion in the test temperature range of 200 °C is almost done. The HP OIT result showed a value lower than the minimum required by GRI-GM13, but an amount of antioxidants remained in the sample to deplete.

4.1.2.5 Shrimp farming ponds: CAM, CAM1 and CAM2 samples

Tables 27 shows the physical results of the HDPE geomembranes exhumed samples from the Brazilian shrimp farming ponds.

Table 27. Physical properties of the high-density polyethylene geomembrane CAM, CAM1 and CAM2 samples

Property	Method	CAM Sample	CAM1 Sample	CAM2 Sample
Thickness (mm)	ASTM D5199	0.800 (±0.014)	0.769 (±0.011)	0.772 (±0.038)
Density (g cm^{-3})	ASTM D792	0.937 (±0.002)	0.941 (±0.004)	0.952 (±0.002)
MFI (5 kg/190 °C) (g 10 min^{-1})	ASTM D1238	1.4191 (±0.0325)	3.9939* (±0.2188)	0.5831 (±0.1380)
CBC (%)	ASTM D4218	3.03 (±0.27)	3.14 (±0.45)	2.75 (±0.52)
CBD (Category)	ASTM D5593	Category I	Category I	Category I
Tensile break resistance (kN m^{-1})	ASTM D6693	19.23 (±3.11)	16.12 (±2.09)	16.37 (±2.15)
Tensile break elongation (%)		684.63 (±96.46)	627.07 (±63.27)	312.74 (±335.42)
Tear resistance (N)	ASTM D1004	111.03 (±6.49)	99.60 (±5.74)	106.90 (±7.77)
Puncture resistance (N)	ASTM D4833	354.25 (±6.51)	346.03 (±8.78)	309.97 (±11.96)
SCR (h)	ASTM D5397	1151.98 (±44.64)	4.25 (±1.52)	90.41 (±17.01)
Std. OIT (min)	ASTM D3895	6.36 (±0.52)	9.65 (±0.70)	67.61 (±5.13)
HP OIT (min)	ASTM D5885	60.60 (±4.81)	0 (±0)	166.05 (±15.06)

Standard deviations are between brackets.

*Test carried out at 160 °C.

CAM1 and CAM2 samples presented mean thickness values lower than the nominal value. The samples of the shrimp farming pond after 8.25 years obtained density values near

0.940 g cm^{-3}. However, the CAM2 exhumed sample for another shrimp farming pond presented a higher density value of 0.952 g cm^{-3} than the minimum value of the GRI-GM13. This density value is considered high for a modern HDPE geomembrane. The carbon black content measured of the three samples was satisfactory, although the CAM1 sample presented a higher value than 3.0 %.

The melt flow index test results showed an atypical behavior for the CAM1 sample, in which it was impossible to perform the test with the standard temperature (190 °C), as the material melted quickly. The test then was carried out at 160 ºC, and the obtained melt flow index was high (3.9939 g 10 min^{-1}). Different polymer molecular changes occurred between the samples from the shrimp farming pond after 8.25 years of exposure, considering that the CAM and CAM1 samples represent the same geomembrane; the first sample exhumed from the bottom liner and the other sample exhumed from the slope liner. The CAM2 sample presented a typical melt flow index test result.

The CAM and CAM1 samples showed a tendency to decrease the ductile tensile, although the tensile resistance at the break mean value and the tensile elongation at the break mean value were lower than the minimum required values prescribed by the GRI-GM13. The CAM2 sample presented a brittle behavior. The average tensile elongation value of this sample was lower than 350 %. It means less than 50 % of the minimum required for the GRI-GM13 for the tensile elongation value.

The difference between the stress crack resistance results of CAM and CAM1 samples was evident. The CAM sample (exhumed from the pond's bottom liner) presented a high-stress crack resistance, higher than the minimum required value by GRI-GM13. Moreover, the CAM1 sample (exhumed from the pond's slope liner) presented a low-stress crack resistance near zero. An HDPE geomembrane with a low melt flow index value can denote a polymer with a high molecular weight that provides a high SCR (HSUAN, 2000). It can be observed which CAM1 sample presented a high MFI test result and a low SCR test result. CAM2 sample presented a lower value than the minimum required value by GRI-GM13.

The antioxidant depletion was measured using the Std. OIT and the HP OIT tests, including the analyses of different antioxidant groups. The results of the CAM1 sample showed the total antioxidant depletion for the HP OIT test and the almost total antioxidant depletion for the Std. OIT test, demonstrating unprotection from the additives to the polymer against the thermo-oxidative degradation. The CAM sample still presented some antioxidant

amount for the HP OIT test but presented a low Std. OIT value. CAM2 sample presented OIT values lower than the minimum required values by the GRI-GM13.

4.1.2.6 Overall exhumed samples results

The MFI is a good parameter to compare virgin with exposed or exhumed samples. The increase or decrease in this index can explain possible polymer degradation (TELLES *et al.*, 1984). Figure 39 presents the exhumed samples MFI results versus exposure time (log scale), including the tendency line of the results. Some samples tested (LDO, MIN2, CAM, and CAM1) presented near or higher values than 1.0 g 10 min^{-1}. The highlight was for the CAM1 sample, which obtained the highest MFI value. The tendency line indicates the MFI's increase during the exposure time.

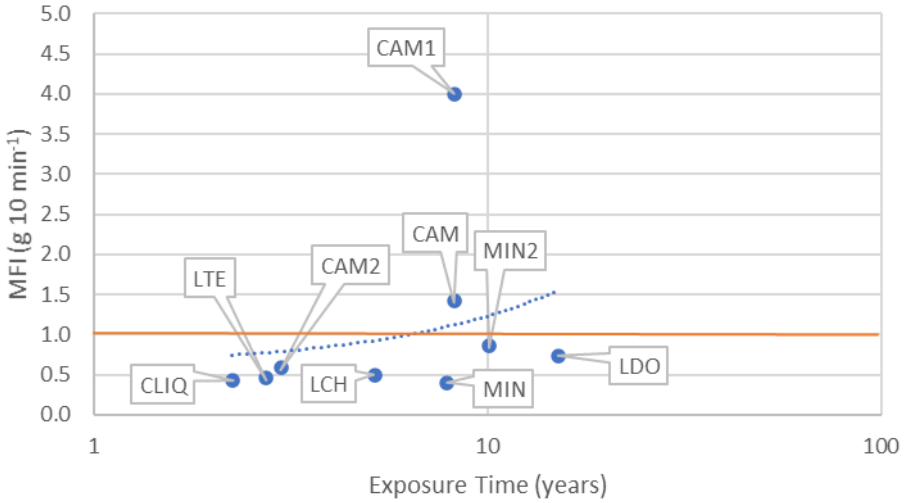

Figure 39. MFI results *versus* exposure time for the exhumed samples

Figures 40 and 41 show, respectively, the tensile resistance *versus* exposure time (log scale) and the tensile elongation *versus* exposure time for the exhumed samples, including the tendency lines of the results. Figure 40, the 100 % representing the minimum value required for the GRI-GM13 for each thickness. Only the LCH and LTE samples presented higher tensile resistance than the minimum tensile resistance value prescribed by GRI-GM13. The tendency line presents a constant behavior close to 90 % of the retained tensile resistance. For the tensile elongation results (Figure 41), only the LCH sample presented a value higher than 700 %. It is important to note that the LCH sample was the thickest

exhumed sample, presenting the best mechanical behavior. Samples CLIQ, MIN, MIN2, LDO, and CAM2 exhibited fragile behavior for some test specimens tested. Three samples (CAM2, MIN, and LDO) presented average tensile elongation values lower than 350 % it means less than 50 % of the minimum required for the GRI-GM13 for the tensile elongation value. The worst tensile behavior was verified for the LDO sample. The tendency line indicates the tensile elongation's decrease during the exposure time.

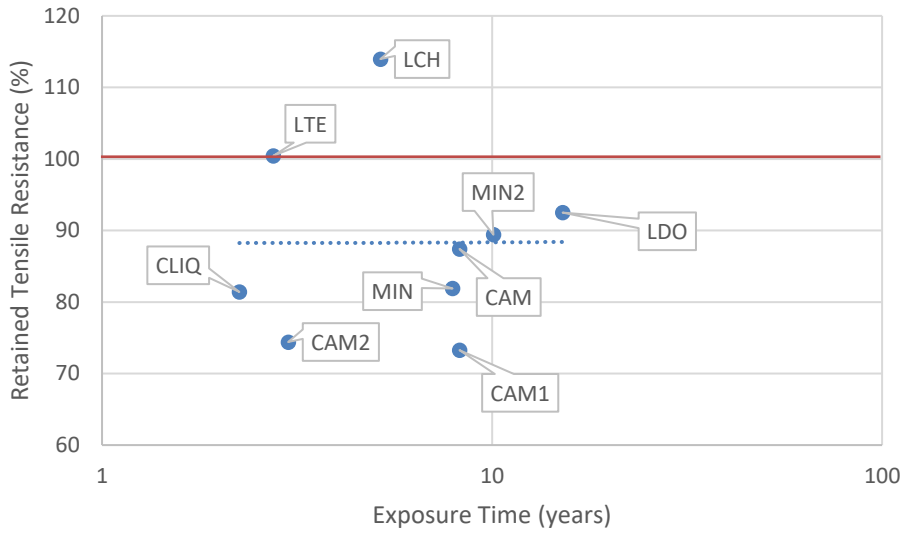

Figure 40. Tensile resistance results *versus* exposure time for the exhumed samples

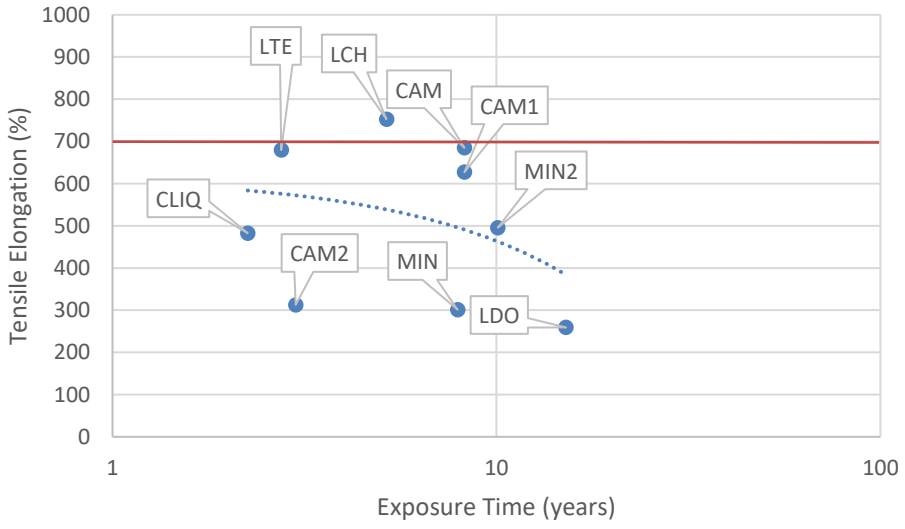

Figure 41. Tensile elongation results *versus* exposure time for the exhumed samples

Figure 42 shows the stress crack resistance results versus exposure time (log scale) for the exhumed samples, including the tendency line of the results. The minimum SCR value required by GRI-GM13 is 500 h. CAM, CLIQ, and LCH samples presented SCR values higher than the minimum value prescribed by the American standard. The other samples obtained SCR values lower than 100 h, especially LDO and CAM1 samples, which exhibited very low SCR values. The tendency line indicates the stress crack resistance's decrease during the exposure time, reaching 100 h for 15 years.

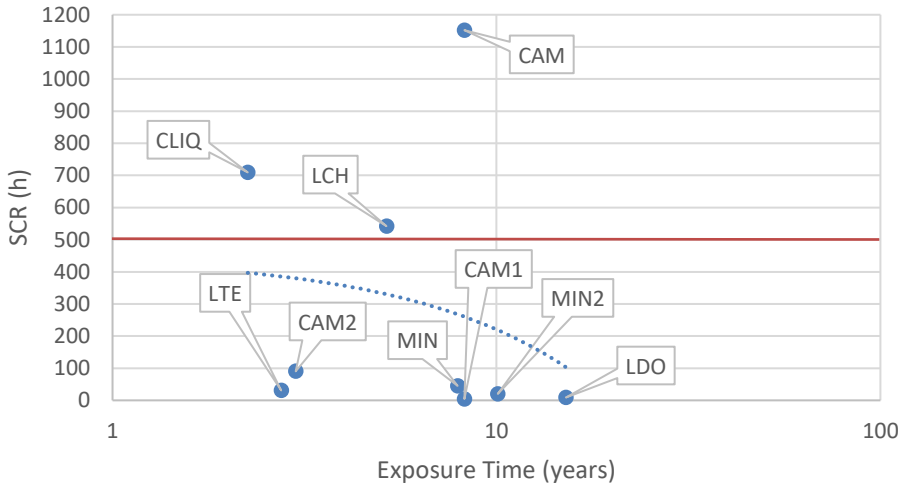

Figure 42. SCR results *versus* exposure time for the exhumed samples

Figure 43 shows the Std. OIT results versus exposure time (log scale) for the exhumed samples, including the tendency line of the results. The minimum Std. OIT value required by GRI-GM13 is 100 min. LCH sample was the only exhumed geomembrane that presented Std. OIT value is higher than 100 min. CAM2, LTE, and CLIQ samples presented Std. OIT values higher than the 50 min (50 % of the minimum required value by GRI-GM13). Nonetheless, LDO, CAM, and CAM1 samples presented Std. OIT values lower than the 10 min (10 % of the minimum required value by GRI-GM13), representing the antioxidants' depletion. The tendency line indicates the Std. OIT's decrease during the exposure time, reaching the total antioxidant consumption before 15 years.

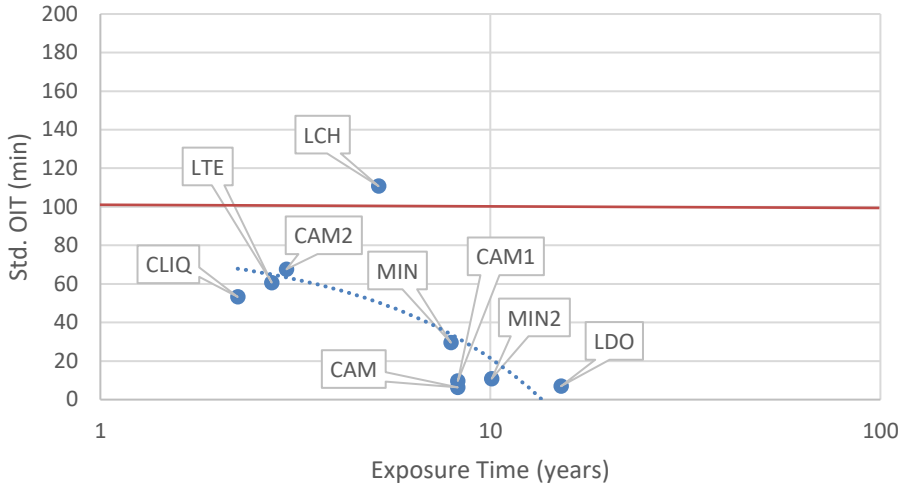

Figure 43. Std. OIT results *versus* exposure time for the exhumed samples

Figure 44 shows the HP OIT results versus exposure time (log scale) for the exhumed samples, including the tendency line of the results. The minimum HP OIT value required by GRI-GM13 is 400 min. None of the tested samples presented OIT-HP values equal to or higher than 400 min, including the virgin samples. The presence of HALS in the additive package increases the OIT-HP results because this test is performed at 150 ºC, probably none of the virgin samples presented HALS in their additive package. The best performance was for the thicker sample (LCH). CLIQ, LTE, and CAM2 samples presented HP OIT values higher than 150 min (37.5 % of the minimum required value by GRI-GM13). MIN, MIN2, and LDO samples presented HP OIT values higher than 100 min (25 % of the minimum required value by GRI-GM13). Otherwise, CAM and CAM1 samples, representing the same shrimp farming pond liner, presented different results. The CAM1, which was exhumed from the slope liner, presented oxidation directly after the oxidation process started in the test, that is, the antioxidant content was completely depleted. This result is according to the exposure of the CAM1 sample, which had weather exposure during the 8.25 years. The tendency line indicates the HP OIT's decrease during the exposure time, reaching 50 min for 15 years.

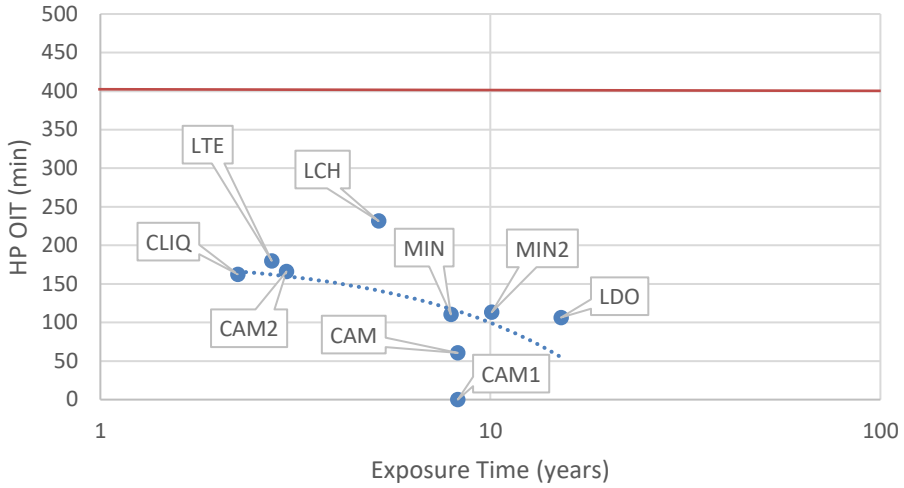

Figure 44. HP OIT results *versus* exposure time for the exhumed samples

4.1.3 UV exposure results

4.1.3.1 UV fluorescent and xenon arc exposures: 1L sample

Table 28 presents the results of the MFI tests after ultraviolet exposure in the laboratory. Figure 45 shows the behavior of the samples in percent for the two laboratory exposure devices retained from the property. It can be observed that for the exposure in the xenon arc chamber, the sample showed continuous growth in the melt flow index during the exposure times. On the other hand, the sample under exposure by the UV fluorescent device showed variations in the results of the MFI tests during the exposure times.

Table 28. MFI test results after UV laboratory exposures

Sample	Exposure Time (h)	MFI (g 10 min^{-1})	MFI (%)
Virgin	0	0.6800 (±0.0217)	100.0
UV fluorescent	960	0.7094 (±0.0460)	104.33
UV fluorescent	4380	0.6275 (±0.0369)	92.29
UV fluorescent	8760	0.6991 (±0.0594)	102.81
Xenon arc	960	0.6958 (±0.0161)	102.33
Xenon arc	1639	0.7437 (±0.0514)	109.36
Xenon arc	2160	0.7677 (±0.0453)	112.89

Standard deviations are between brackets.

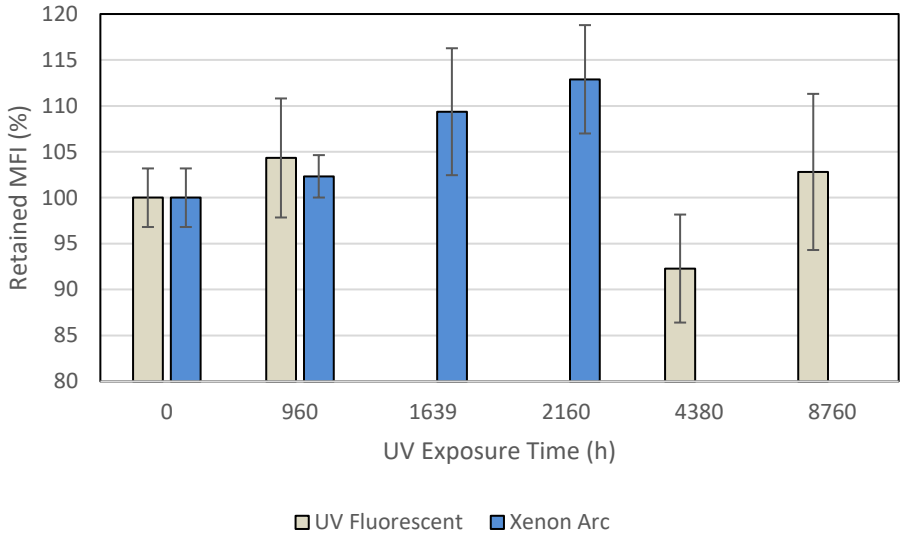

Figure 45. MFI test results showing behavior of the samples after UV exposures

Many authors (LODI *et al.*, 2013; HSUAN and KOERNER, 1998; ROWE *et al.*, 2008) described an understanding of the melt flow index result behavior. Generally, a decrease in MFI test results can indicate an increase in molecular weight by cross-linking reactions; whereas, an increase in MFI can indicate a decrease in molecular weight due to chain scission reactions. The MFI is a qualitative test to assess the polymer's molecular weight. If the MFI value does not change after exposure, this method is not sufficient to understand the material behavior. In this case, both reactions (cross-linking and chain scission) could occur at the same time. Lodi *et al.* (2013) evaluated the MFI test results of high-density polyethylene geomembranes after 30 months of weathering exposure in Brazil. The results showed an increase of up to 50 % for the 2.5 mm-thick sample and decreased to 15 % for the 0.8 mm-thick sample. According to the authors, the melt flow index results for the 2.5 mm-thick geomembrane indicates chain scission.

The sample in the xenon arc exposure chamber showed increases of 2, 9, and 13 %, respectively, for 960, 1639 and 2160 h of exposure. The increasing trend can indicate changes in the polymer morphology. However, it was noted that the sample exposed in the UV fluorescent device showed variations between the virgin samples of 4, -8, and 3 %, respectively, for 960, 4380, and 8760 h of exposure. In this case, there is no tendency to explain the behavior of the material. These variations are probably related to variation in the material's properties due to the manufacturing process and variation in exposure to the UV fluorescent device. The standard test method ASTM D7238 prescribes the rotation of the samples in the UV fluorescent device every week to minimize variations among the samples.

Table 29 presents the tensile test results at break for the UV fluorescent device exposure. Figure 46 shows the tensile behavior of the sample as a percentage retained from the property. The same behavior was noted for the resistance and elongation properties during the exposure time. The sample exhibited a tendency to lose ductility, without showing brittle behavior.

Table 29. Tensile at break test results after UV fluorescent device exposure

Exposure Time (h)	**Tensile Resist. (kN m^{-1})**	**Tensile Resist. (%)**	**Tensile Elong. (%)**	**Tensile Elong. (%)**
0	28.52 (±1.55)	100.0	733.47 (±10.76)	100.0
960	20.87 (±1.12)	73.18	511.47 (±13.67)	69.73
4380	20.09 (±1.64)	70.45	509.67 (±16.20)	69.49
8760	20.00 (±1.54)	77.15	558.70 (±12.47)	76.17

Standard deviations are between brackets.

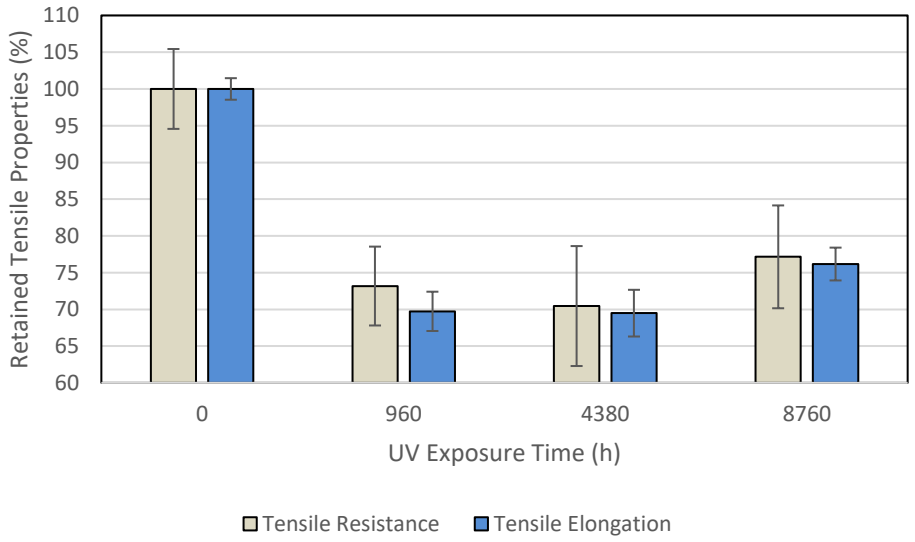

Figure 46. Tensile behavior of the samples after UV fluorescent device exposure

Tensile properties were evaluated by Noval *et al.* (2014) for an HDPE geomembrane with 1.5 mm of thickness during 20 years of weathering exposure in the San Isidro reservoir in Spain. The resistance and elongation presented the same trend during the examined time. The lowest values found were after 8 years of exposure, with decreases of around 45 and 60 %, respectively, for tensile strength and tensile elongation. After 20 years of exposure, the

final evaluation showed decreases of about 25 and 35 %, respectively, for the tensile resistance and tensile elongation.

Lavoie *et al.* (2020-1) noted the tensile brittle behavior tendency for a high-density polyethylene geomembrane with 1.0 mm of thickness after 2.25 years of weathering exposure in an industrial water pond in Brazil (CLIQ sample).

The sample under UV fluorescent device exposure presented decreases for the tensile resistance of 27, 30, and 23 %, respectively, for 960, 4380, and 8760 h of exposure. The sample presented decreases for the tensile elongation of 30, 31, and 24 %, respectively, for 960, 4380, and 8760 h of exposure. On average, the resistance and elongation decreased during the exposure times by around 30 %.

Table 30 presents the Std. OIT test results after the ultraviolet exposures at the laboratory. Figure 47 shows the behavior of the sample for both laboratory exposure devices in percent retained from the property. The antioxidant depletion for both exposures can be observed. The fastest antioxidant depletion occurred for the xenon arc exposure chamber considering that the exposure time was shorter than the exposure in the fluorescent UV device.

Table 30. Std. OIT test results after the UV laboratory exposures

Sample	**Exposure Time (h)**	**Std. OIT (min)**	**Std. OIT (%)**
Virgin	0	40.49 (±0.73)	100
UV fluorescent	960	37.63 (±3.30)	92.94
UV fluorescent	4380	28.32 (±2.11)	69.93
UV fluorescent	8760	11.30 ((±1.48)	27.91
Xenon arc	960	34.15 (±1.27)	84.33
Xenon arc	1639	28.40 (±0.93)	70.13
Xenon arc	2160	24.88 (±2.04)	61.45

Standard deviations are between brackets.

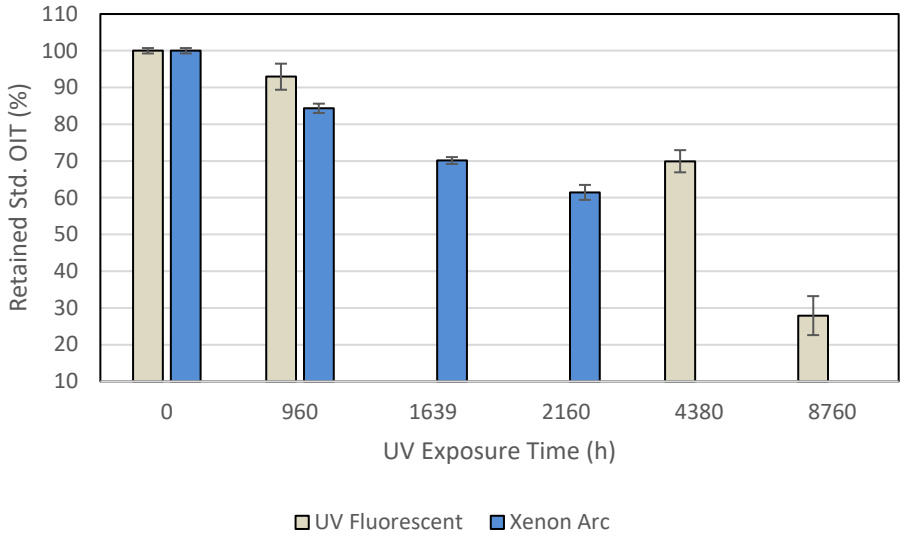

Figure 47. Std. OIT test results showing behavior of the samples after UV exposures

Reis *et al.* (2017) evaluated the Std. OIT results for two weathering exposure locations in Portugal. After 12 years of weathering exposure, the 2.0 mm-thick geomembrane samples exposed at Bigorne and Viana de Castelo showed decreases of about 40 and 50 %, respectively.

The sample under exposure in the xenon arc exposure chamber showed a decrease in OIT values of 16, 30, and 39 %, respectively, for 960, 1639, and 2160 h of exposure. The sample under UV fluorescent device exposure demonstrated decreases of 7, 30, and 72 %, respectively, for 960, 4380, and 8760 h of exposure. The comparison of the OIT values between the xenon arc exposure chamber in 1639 h and the fluorescent UV exposure device in 4380 h showed approximately the same consumption of antioxidants, demonstrating that the fastest depletion rate of antioxidants was for the xenon arc exposure chamber. The fast antioxidant depletion was noted for both exposure devices, demonstrating the ultraviolet radiation effect on the material's antioxidants.

Table 31 presents the HP OIT test results after the ultraviolet exposures in the laboratory. Figure 48 shows the behavior of the sample for the two laboratory exposure devices in percent retained from the property. Similar antioxidant depletion for both device exposures was noted.

Table 31. HP OIT test results after UV laboratory exposures

Sample	Exposure Time (h)	HP OIT (min)	HP OIT (%)
Virgin	0	125.70 (±0.42)	100
UV fluorescent	960	118.02 (±2.62)	93.89
UV fluorescent	4380	103.09 (±2.13)	82.01
UV fluorescent	8760	80.96 (±1.46)	64.40
Xenon arc	960	124.69 (±0.86)	99.20
Xenon arc	1639	119.17 (±2.10)	94.80
Xenon arc	2160	114.83 (±1.20)	91.35

Standard deviations are between brackets.

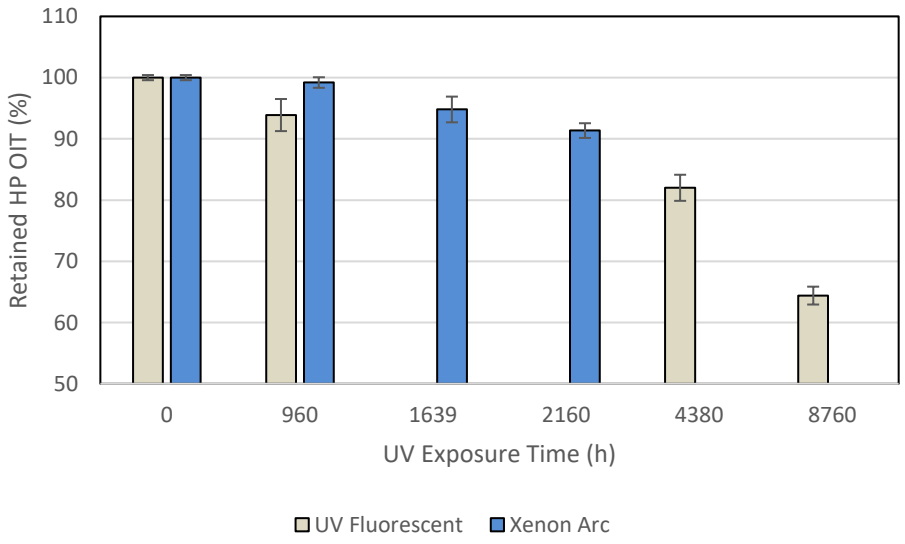

Figure 48. HP OIT test results showing behavior of the samples after UV exposures

According to Hsuan and Koerner (1998), the high-pressure OIT test can distinguish different types of antioxidants, and the test operation's temperature promotes a good relation to the service conditions.

The sample in the Xenon arc exposure chamber demonstrated decreases of 0.8, 5, and 9 %, respectively, for 960, 1639, and 2160 h of exposure. The sample under UV fluorescent device exposure demonstrated decreases of 6, 18, and 36 %, respectively, for 960, 4380, and 8760 h of exposure. A lower antioxidant depletion compared with the Std. OIT test was noted for both exposures.

4.1.3.2 UV fluorescent exposure: 1.5L sample

Table 32 presents the MFI test results for the virgin and the exposure samples after 960 h, 4380 h, and 8760 h by UV fluorescent. Figure 49 shows the samples' behavior after the exposure, presented in retained MFI results.

Table 32. MFI test results after UV fluorescent exposure

Exposure Time (h)	MFI (g 10 min^{-1})	MFI (%)
0	0.5054 (±0.0102)	100.0
960	0.5088 (±0.0132)	100.68
4380	0.5045 (±0.0225)	99.82
8760	0.4978 (±0.0109)	98.49

Standard deviations are between brackets.

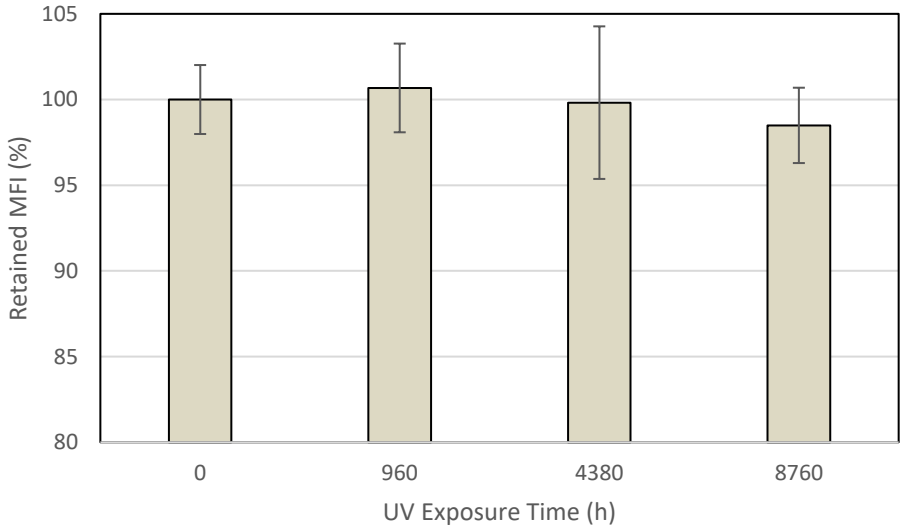

Figure 49. MFI test results demonstrating samples' behavior after the UV fluorescent exposure

According to Gulec *et al.* (2004), the MFI test is commonly used as a molecular weight index for chemical compatibility studies, and it is a simple method to assess the polymer's molecular weight. It is possible to note minor variations of MFI test results among the exposure samples. After 960 h of exposure, the MFI test result increased 0.68 %. Although, after 4380 and 8760 h of exposure, the MFI test results decreased 0.18 and 1.51 %. The obtained variations after exposure are lower than the virgin sample's standard

deviation. Thus, the obtained variations after exposure can be understood as a manufacturing process' variation.

The evaluated tensile properties were resistance and elongation at break. Table 33 shows the tensile resistance and elongation test results for the virgin and the exposure samples after 960 h, 4380 h, and 8760 h by UV fluorescent. Figure 50 shows the samples' behavior after the exposure, presented in retained tensile properties.

Table 33. Tensile test results after UV fluorescent exposure

Exposure Time (h)	**Tensile Resist. (kN m^{-1})**	**Tensile Resist. (%)**	**Tensile Elong. (%)**	**Tensile Elong. (%)**
0	46.93 (±7.04)	100.0	704.67 (±101.30)	100.0
960	44.36 (±0.48)	94.52	659.30 (±5.83)	93.56
4380	40.37 (±1.47)	86.03	642.30 (±17.46)	91.15
8760	41.48 (±3.47)	88.40	653.90 (±61.35)	92.80

Standard deviations are between brackets.

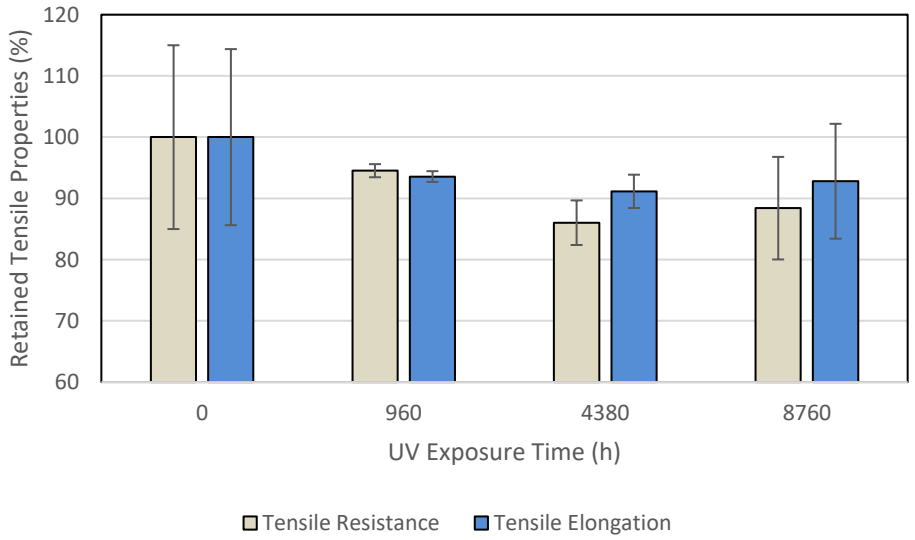

Figure 50. Tensile test results demonstrating samples' behavior after the UV fluorescent exposure

Firstly, it is possible to note that the virgin sample showed a high standard deviation due to one specimen, which presented a tensile resistance at break value of 39.25 kN m^{-1} and a tensile elongation at break value of 596.50 %.

Koerner *et al.* (2008) exposed for 28,000 h a 1.5 mm thick HDPE geomembrane using a UV fluorescent weatherometer. The sample presented a decrease of about 20 % in the tensile properties (resistance and elongation).

The tensile resistance at break test results decreased 5.48 %, 13.97 %, and 11.60 %, respectively, for 960 h, 4380 h, and 8760 h of UV exposure, compared to the virgin sample result. On the other hand, the tensile elongation at break test result decreased 6.44 %, 8.85 %, and 7.20 %, respectively, for 960 h, 4380 h, and 8760 h of UV exposure compared to the virgin sample result. The slight increase in the tensile properties' values between the 4380 h and 8760 h can be attributed to the variation in the manufacturing process.

Lavoie *et al.* (2021) analyzed a 1.0 mm-thick HDPE geomembrane after 8760 h of UV fluorescent exposure (1L sample). The authors obtained a decrease in the resistance and elongation tensile values by around 30 % during the exposure times. The HDPE geomembrane sample analyzed in this work presented lower decreases in tensile properties values after UV exposure than the sample analyzed by Lavoie *et al.* (2021), demonstrating that this sample presented a better behavior after the ultraviolet radiation exposure.

Table 34 shown the SCR test results for the virgin and the exposure samples after 960 h, 4380 h, and 8760 h by UV fluorescent. Figure 51 shows the samples' behavior after the exposure, presented in retained stress crack resistance.

Table 34. SCR test results after UV fluorescent exposure

Exposure Time (h)	**SCR (h)**	**SCR (%)**
0	629.84 (±67.55)	100.0
960	587.32 (±24.13)	93.25
4380	501.62 (±29.72)	79.64
8760	299.29 (±18.39)	47.52

Standard deviations are between brackets.

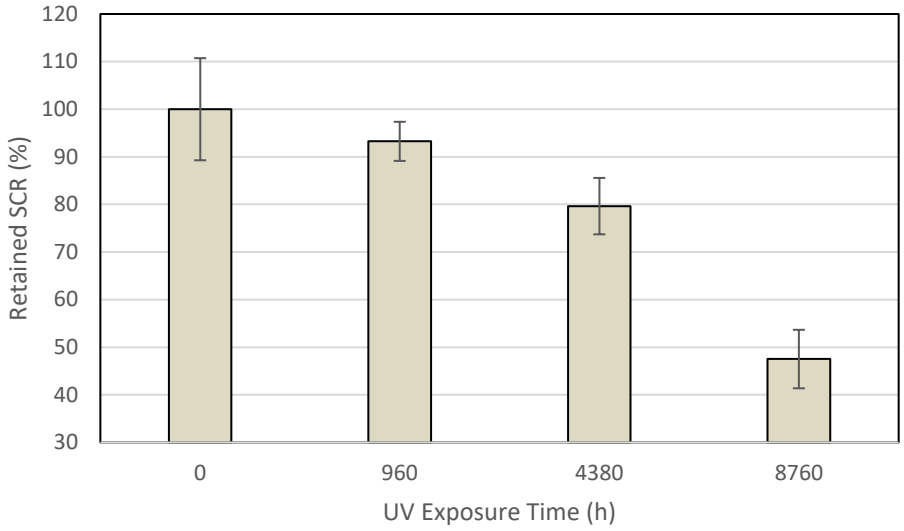

Figure 51. SCR test results demonstrating samples' behavior after the UV fluorescent exposure

The obtained stress crack resistance results after 960 h, 4380 h, and 8760 h of UV exposure decreased, were respectively, 6.75 %, 20.36 %, and 52.48 %, compared to the initial value. The SCR retained value after 1 year (8760 h) of laboratory UV exposure obtained in this work (47.52 %) compared with the SCR mean retained value showed by Rowe et al. 2019 for eleven HDPE geomembranes immersed in leachate (37 %) presents similarities. The authors suggest that the SCR value can stabilize after 3 months of leachate incubation.

Table 35 shows the standard (Std.) and high-pressure (HP) OIT tests results for the virgin and the exposure samples after 960 h, 4380 h, and 8760 h by UV fluorescent. Figure 52 shows the samples' behavior after the exposure, presented in retained OIT values.

Table 35. OIT tests results after UV fluorescent exposure

Exposure Time (h)	**Std. OIT (min)**	**Std. OIT (%)**	**HP OIT (min)**	**HP OIT (%)**
0	199.78 (±4.03)	100.0	287.25 (±1.06)	100.0
960	166.85 (±3.94)	83.52	268.52 (±3.04)	93.48
4380	143.87 (±1.98)	72.01	201.81 (±2.53)	70.26
8760	21.59 (±1.01)	10.81	134.57 (±3.67)	46.85

Standard deviations are between brackets.

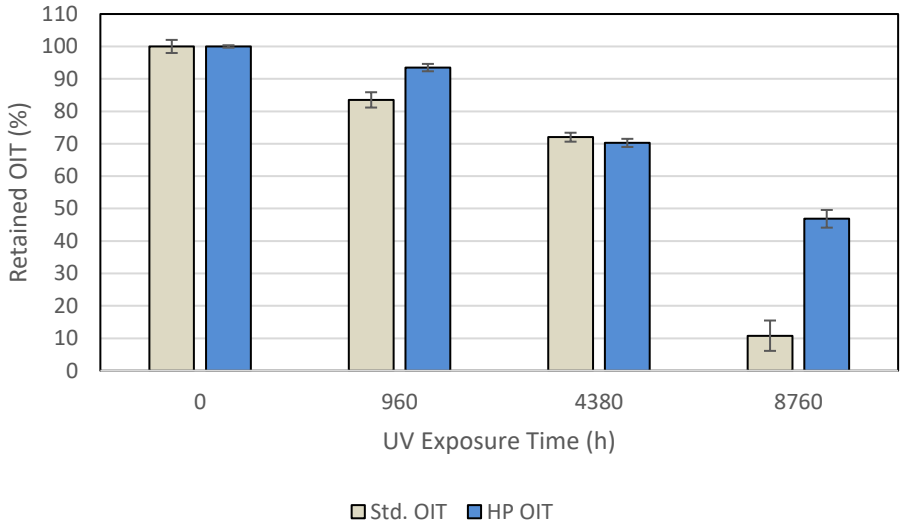

Figure 52. OIT tests results demonstrating samples' behavior after the UV fluorescent exposure

The Std. OIT test results decreased 16.48 %, 27.99 %, and 89.19 %, respectively, for 960 h, 4380 h, and 8760 h of UV exposure, compared to the virgin sample result. There was noted a considerable decrease in Std. OIT results between the 4380 h and 8760 h of UV exposure. After 1 year of exposure, the depletion of the antioxidants was almost complete, and the chain reaction and the molecular composition can start. Lavoie *et al.* (2021-1) evaluated two exhumed HDPE geomembranes of 1.0 mm of thickness applied in mining facility constructions in Brazil. Both samples presented low Std. OIT values, brittle tensile behavior, and low SCR values.

Nonetheless, the HP OIT test results decreased 6.52 %, 29.74 %, and 53.15 %, respectively, for 960 h, 4380 h, and 8760 h of UV exposure compared to the initial value. Lavoie *et al.* (2021) obtained a decrease of 35.6 % in HP OIT result after 1 year of laboratory UV fluorescent exposure for a 1.0 mm-thick HDPE geomembrane, demonstrating that the sample evaluated in this work presented a higher antioxidants' depletion.

4.1.4 Results of thermal exposure and synergic exposure to UV radiation and thermal aging

Table 36 presents the MFI test results for the thermal exposure samples and the synergic exposure to UV radiation and thermal aging samples. Figure 53 shows the samples' behavior after the exposures, presented in retained MFI results.

Table 36. MFI test results after thermal exposure and after the synergy exposure to UV radiation and thermal aging

Sample	Exposure Time (h)	MFI (g 10 min^{-1})	MFI (%)
1L	0	0.6800 (±0.0217)	100.0
1L	960	0.6856 (±0.0753)	100.82
1L	4380	0.6320 (±0.0232)	92.94
1L	8760	0.6098 (±0.0304)	89.68
1L	8760 UV – 4380 TE	0.5522 (±0.0370)	81.21
1.5L	0	0.5054 (±0.0102)	100.0
1.5L	960	0.4744 (±0.0116)	93.87
1.5L	4380	0.4241 (±0.0243)	83.91
1.5L	8760	0.4884 (±0.0251)	96.64
1.5L	8760 UV – 4380 TE	0.3674 (±0.0252)	72.69
2L	0	0.4406 (±0.0067)	100.0
2L	960	0.3696 (±0.0272)	83.89
2L	4380	0.4182 (±0.0339)	94.92
2L	8760	0.3925 (±0.0165)	89.08

Standard deviations are between brackets.

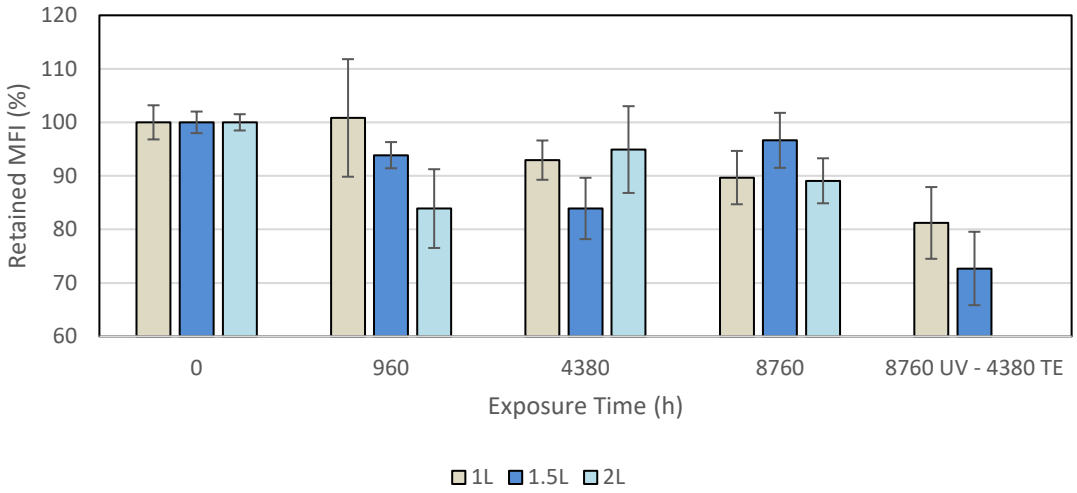

Figure 53. MFI test results demonstrating samples' behavior after the thermal exposure and after the synergy exposure to UV radiation and thermal aging

It is possible to note a tendency to decrease MFI results for all the tested samples after the exposure. 1L sample presented an MFI value decrease of 10.32 % after 1 year of thermal exposure. Lavoie *et al.* (2021) evaluated the same HDPE geomembrane sample

under UV fluorescent radiation. The authors obtained an increase of 2.81 % in the MFI results after 8760 h of UV exposure. The synergy exposure to UV radiation (8760 h) and thermal aging (4380 h) provided an MFI value decrease of 18.89 % for the 1L sample, comparing to the virgin sample's MFI value.

The MFI result of 1.5L sample after 4380 h of thermal exposure, compared to the virgin sample's MFI result, showed a decrease of 16.09 %. Otherwise, after 8760 h of thermal exposure, the sample presented 3.36 % of decrease. This variation was unexpected. The same sample after 8760 h of UV exposure obtained a decrease of 1.51 %. Although, after 8760 h of UV radiation and 4380 h of thermal exposure, this synergy provided an MFI value decrease of 27.31 %.

The behavior of the 2L sample after the thermal exposure showed decreases of 16.11 %, 5.08 %, and 10.92 %, respectively, for 960, 4380, and 8760 h. The MFI results presented variations along the exposure time. However, for all the obtained MFI values, it is possible to understand a decrease compared to the virgin MFI sample value.

The samples after laboratory thermal exposure and after the synergy exposure to UV radiation and thermal aging presented decreases in the MFI values, demonstrating the occurrence of cross-linking reactions (HSUAN and KOERNER, 1998; ROWE *et al.*, 2008; LODI *et al.*, 2013).

Table 37 presents the tensile resistance test results for the thermal exposure samples and the synergic exposure to UV radiation and thermal aging samples. Figure 54 shows the samples' behavior after the exposures, presented in retained tensile resistance results.

Table 37. Tensile resistance test results after thermal exposure and after the synergy exposure to UV radiation and thermal aging

Sample	Exposure Time (h)	Tensile Resist. (kN m^{-1})	Tensile Resist. (%)
1L	0	28.52 (±1.55)	100.0
1L	960	21.40 (±0.86)	75.04
1L	4380	22.54 (±0.20)	79.03
1L	8760	21.46 (±1.70)	75.25
1L	8760 UV – 4380 TE	22.81 (±3.34)	79.98
1.5L	0	46.93 (±7.04)	100.0
1.5L	960	40.89 (±5.52)	87.13
1.5L	4380	38.62 (±2.26)	82.29
1.5L	8760	41.43 (±1.45)	88.28
1.5L	8760 UV – 4380 TE	39.42 (±3.53)	84.0
2L	0	59.68 (±4.59)	100.0
2L	960	50.34 (±2.98)	84.35
2L	4380	49.97 (±1.69)	83.73
2L	8760	48.82 (±6.18)	81.80

Standard deviations are between brackets.

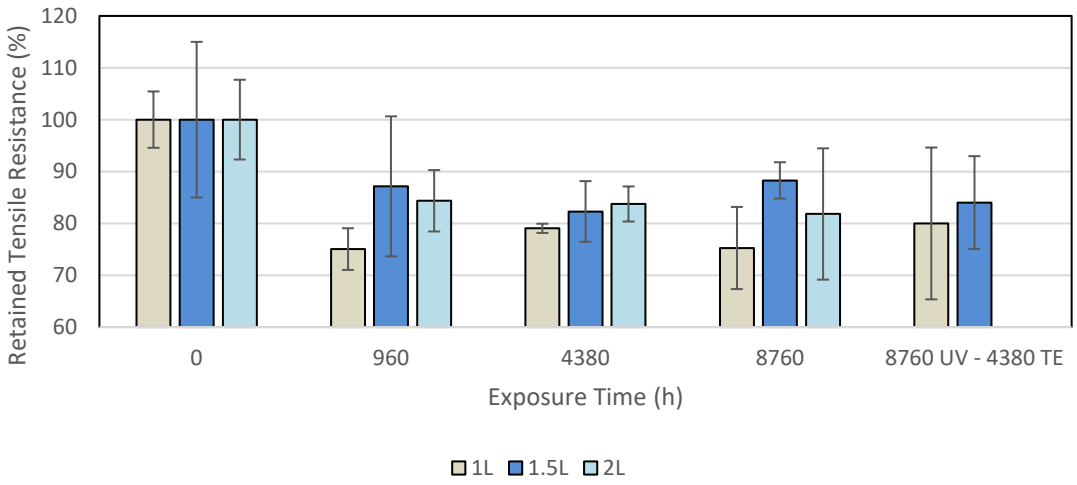

Figure 54. Tensile resistance test results demonstrating samples' behavior after the thermal exposure and after the synergy exposure to UV radiation and thermal aging

After 8760 h of thermal exposure, the evaluated samples presented tensile resistance result decreases between 10 and 25 %, demonstrating changes in this property due to the

exposure. The 1L sample presented the major decrease, of 24.75 %, compared to the tensile resistance test result of the virgin sample. The 1.5L sample showed a minor decrease of 11.72 %. It was noted for the 2L sample a decrease of 18.20 %.

After the synergy exposure to UV radiation (8760 h) and thermal aging (4380 h), the 1L sample presented a decrease of 20.02 %. According to Lavoie *et al.* (2021), the same sample showed a decrease of 22.85 % after 8760 h of UV exposure. That is, the thermal exposure seems not to change the tensile resistance of this sample. The 1.5L sample presented a decrease of 16 % after the synergic effect and showed a decrease of 11.6 % under the UV exposure after 8760 h. For this sample (1.5L), the synergic effect demonstrated losses in the tensile resistance.

Table 38 presents the tensile elongation test results for the thermal exposure samples and the synergic exposure to UV radiation and thermal aging samples. Figure 55 shows the samples' behavior after the exposures, presented in retained tensile elongation results.

Table 38. Tensile elongation test results after thermal exposure and after the synergy exposure to UV radiation and thermal aging

Sample	**Exposure Time (h)**	**Tensile Elong. (%)**	**Tensile Elong. (%)**
1L	0	733.47 (±10.76)	100.0
1L	960	519.13 (±122.21)	70.78
1L	4380	566.43 (±46.31)	77.23
1L	8760	506.67 (±116.43)	69.08
1L	8760 UV – 4380 TE	432.78 (±370.45)	59.0
1.5L	0	704.67 (±101.30)	100.0
1.5L	960	620.50 (±90.13)	88.06
1.5L	4380	583.33 (±34.20)	82.78
1.5L	8760	649.57 (±19.45)	92.18
1.5L	8760 UV – 4380 TE	604.93 (±62.32)	85.85
2L	0	820.03 (±33.63)	100.0
2L	960	698.87 (±38.83)	85.22
2L	4380	688.47 (±6.49)	83.96
2L	8760	585.77 (±282.70)	71.43

Standard deviations are between brackets.

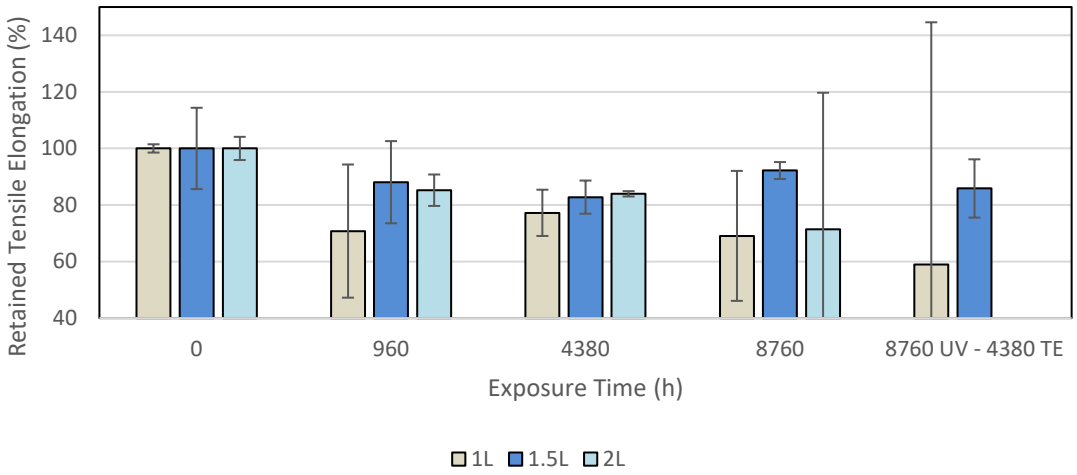

Figure 55. Tensile elongation test results demonstrating samples' behavior after the thermal exposure and after the synergy exposure to UV radiation and thermal aging

It is possible to note decreases in the tensile elongation values after 8760 h of thermal exposure for all the tested samples. There were observed decreases of 30.92 %, 7.82 %, and 28.57 %, respectively, for the 1L, 1.5L, and 2L samples. Some tensile elongation results demonstrated high standard deviations attributed to the properties changes due to the exposure.

The 1L and 1.5L samples presented, respectively, decreases of 41.0 % and 14.15 % in the tensile elongation values after the synergy exposure to UV radiation and thermal aging. Both samples demonstrated that the synergic effect decreased the elongation capacity because, after 8760 h of UV exposure, the 1L and 1.5L samples presented tensile elongation decreases of 23.83 % and 7.2 %. Figure 56 shows the tensile curves for the 1L sample after the synergy exposure to UV radiation and thermal aging, presenting one specimen with brittle behavior. It was noted that the 1.5L sample demonstrated the highest retained tensile elongation among the samples tested for both exposures (thermal and synergic). Otherwise, the 1L sample presented the lowest retained tensile elongation of the samples evaluated.

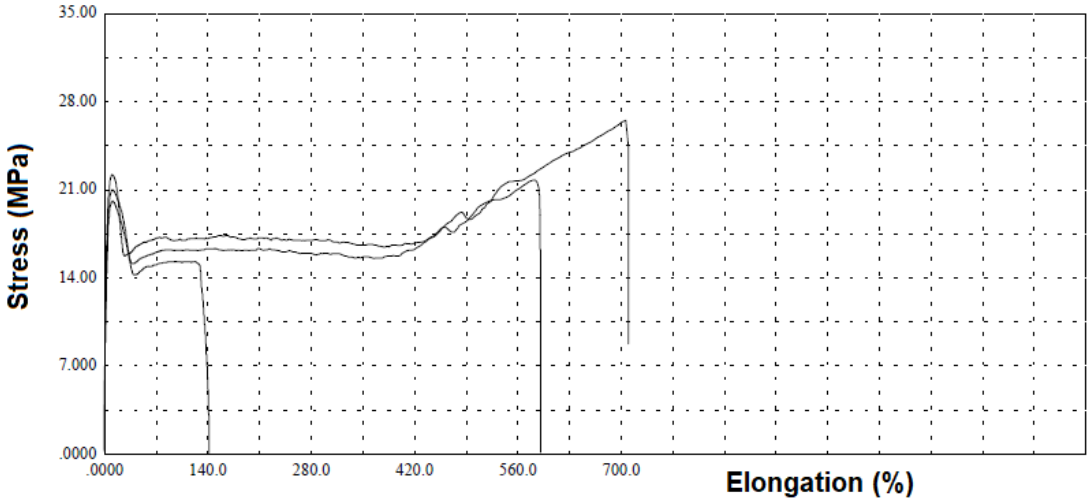

Figure 56. Tensile test curves for the 1L sample after the synergy exposure to UV radiation and thermal aging

Table 39 presents the SCR test results for the thermal exposure samples and the synergic exposure to UV radiation and thermal aging samples. Figure 57 shows the samples' behavior after the exposures, presented in retained SCR results.

Table 39. SCR test results after thermal exposure and after the synergy exposure to UV radiation and thermal aging

Sample	Exposure Time (h)	SCR (h)	SCR (%)
1L	0	16.47 (±2.66)	100.0
1L	960	16.07 (±0.38)	97.57
1L	4380	8.38 (±2.53)	50.88
1L	8760	5.0 (±1.40)	30.36
1L	8760 UV – 4380 TE	8.34 (±0.79)	50.64
1.5L	0	629.84 (±67.55)	100.0
1.5L	960	505.81 (±35.39)	80.31
1.5L	4380	356.74 (±1.05)	56.64
1.5L	8760	288.98 (±38.99)	45.88
1.5L	8760 UV – 4380 TE	48.03 (±18.24)	7.63
2L	0	319.73 (±31.25)	100.0
2L	960	109.84 (±40.70)	34.35
2L	4380	65.22 (±9.70)	20.40
2L	8760	44.70 (±5.94)	13.98

Standard deviations are between brackets.

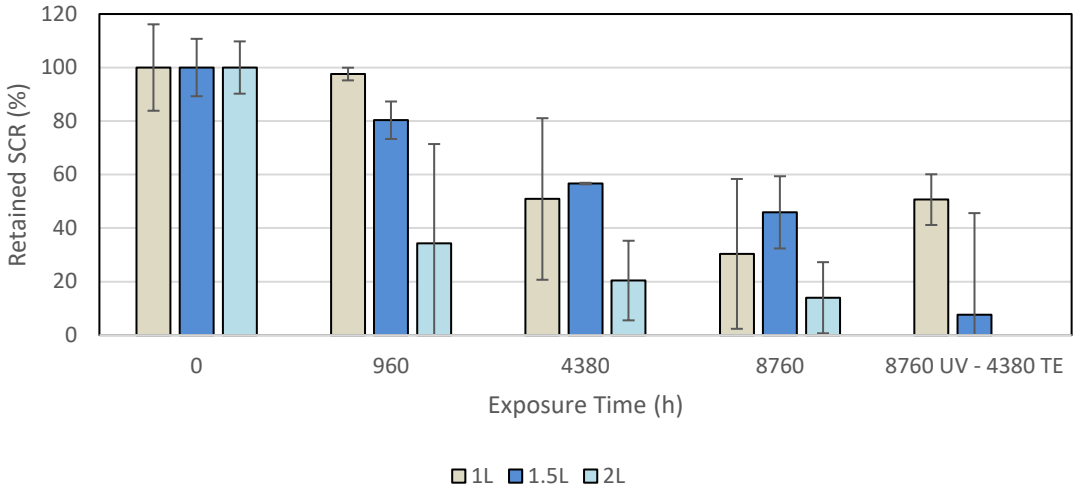

Figure 57. SCR test results demonstrating samples' behavior after the thermal exposure and after the synergy exposure to UV radiation and thermal aging

Abdelaal *et al.* (2015) incubated an HDPE geomembrane with 1.5 mm of thickness in the air at 85 °C, 95 °C, 105 °C, and 115 °C. The SCR value after 34 months at 85 °C presented a decrease of about 60 %. After 24 months at 95 °C, the sample showed an SCR value decrease of about 40 %. Meanwhile, at 105 °C and 115 °C, the geomembrane obtained 100 % of SCR value decrease after, respectively, 18 and 9 months, demonstrating morphological changes in the polymer.

After 8760 h of thermal exposure, the SCR test results presented decreases of 69.64 %, 54.12 %, and 86.02 %, respectively, for the 1L, 1.5L, and 2L samples. It was noted that all samples presented considerable changes in SCR behavior, highlighted for the 2L sample, which presented the highest SCR value decrease.

The result of SCR after the synergy exposure to UV radiation and thermal aging for the 1L sample demonstrated that UV exposure caused a lower SCR value decrease than the thermal exposure. However, the 1.5L sample, which presented the SCR value decrease of 52.48 % after 8760 h of UV exposure, showed an SCR value decrease of 92.37 % after the synergic effect of UV and thermal exposure. Both exposures (UV and thermal) after 8760 h caused approximately the same SCR value decrease for the 1.5L sample.

Table 40 presents the Std. OIT test results for the thermal exposure samples and the synergic exposure to UV radiation and thermal aging samples. Figure 58 shows the samples' behavior after the exposures, presented in retained Std. OIT results.

Table 40. Std. OIT test results after thermal exposure and after the synergy exposure to UV radiation and thermal aging

Sample	Exposure Time (h)	Std. OIT (min)	Std. OIT (%)
1L	0	40.49 (±0.73)	100.0
1L	960	37.73 (±1.39)	93.18
1L	4380	20.77 (±1.40)	51.30
1L	8760	8.90 (±1.47)	21.98
1L	8760 UV – 4380 TE	0.63 (±0.20)	1.56
1.5L	0	199.78 (±4.03)	100.0
1.5L	960	168.70 (±10.56)	84.44
1.5L	4380	111.39 (±7.54)	55.76
1.5L	8760	0.56 (±1.36)	35.32
1.5L	8760 UV – 4380 TE	53.88 (±0.24)	26.97
2L	0	113.80 (±5.32)	100.0
2L	960	108.0 (±0.04)	94.90
2L	4380	86.70 (±1.27)	76.19
2L	8760	55.67 (±3.66)	48.92

Standard deviations are between brackets.

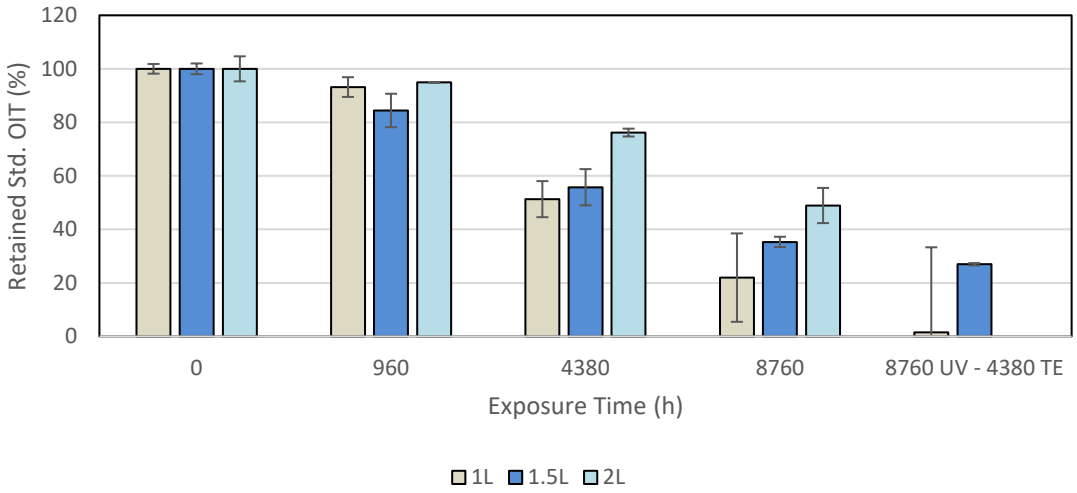

Figure 58. Std. OIT test results demonstrating samples' behavior after the thermal exposure and after the synergy exposure to UV radiation and thermal aging

The tested samples presented decreases in the Std. OIT values after 8760 h of thermal exposure of 78.02 %, 64.68 %, and 51.08 %, respectively, for the 1L, 1.5L, and 2L samples. The 1L sample showed the highest antioxidant depletion among the samples analyzed. The

thicker sample (2L) demonstrated the lowest antioxidant depletion after the thermal exposure.

According to Lavoie *et al.* (2021), the 1L sample obtained an Std. OIT value decrease by 72.09 % after 8760 h of UV exposure. The synergic effect between the UV (8760 h) and thermal (4380 h) exposures caused almost the total antioxidants' consumption (Std. OIT value decrease of 98.44 %).

The antioxidant depletion for the 1.5L was higher for the UV exposure (89.19 % of the Std. OIT value decrease) than the synergic exposure of UV and thermal exposures (73.03 % of the Std. OIT value decrease). This result is unexplainable because the synergic effect should cause a higher antioxidant depletion. The considerable difference between the Std. OIT results of 4380 h and 8760 h (UV exposure) can explain the obtained results.

Table 41 presents the HP OIT test results for the thermal exposure samples and the synergic exposure to UV radiation and thermal aging samples. Figure 59 shows the samples' behavior after the exposures, presented in retained HP OIT results.

Table 41. HP OIT test results after thermal exposure and after the synergy exposure to UV radiation and thermal aging

Sample	Exposure Time (h)	HP OIT (min)	HP OIT (%)
1L	0	125.70 (±0.42)	100.0
1L	960	127.50 (±0.42)	101.43
1L	4380	90.55 (±0.90)	72.04
1L	8760	69.51 (±2.66)	55.30
1L	8760 UV – 4380 TE	54.03 (±6.30)	42.98
1.5L	0	287.25 (±1.06)	100.0
1.5L	960	285.74 (±12.15)	99.47
1.5L	4380	236.27 (±7.71)	82.25
1.5L	8760	184.30 (±6.19)	64.16
1.5L	8760 UV – 4380 TE	162.65 (±10.08)	56.62
2L	0	241.50 (±5.37)	100.0
2L	960	228.32 (±1.06)	94.54
2L	4380	193.71 (±2.77)	80.21
2L	8760	145.71 (±4.01)	60.34

Standard deviations are between brackets.

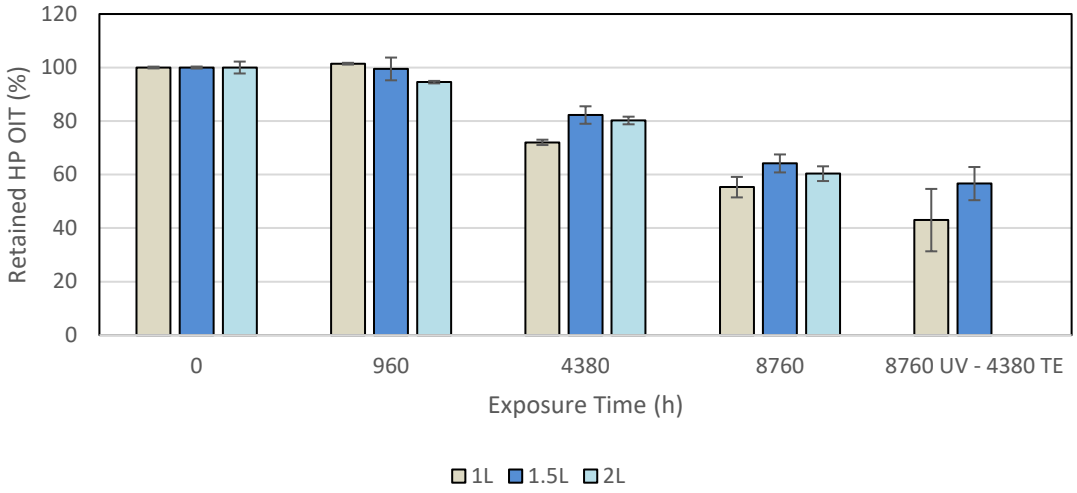

Figure 59. HP OIT test results demonstrating samples' behavior after the thermal exposure and after the synergy exposure to UV radiation and thermal aging

The decreases of HP OIT results compared to the virgin sample result were about 35 % to 45 % for the thermal exposure. The samples presented decreases of 44.7 %, 35.84 %, and 39.66 %, respectively, for 1L, 1.5L, and 2L.

After 8760 h of UV exposure, the 1L sample presented an HP OIT value decrease of 35.6 %. Otherwise, for the thermal exposure after 8760 h the same sample presented a higher HP OIT value decrease. The synergic effect between the UV and thermal exposure caused an HP OIT value decrease of 57.02 %.

For the 1.5L sample, the UV exposure caused a higher antioxidant depletion than the thermal exposure, both after 8760 h. The synergic effect between both exposures showed the same behavior noted in the Std. OIT, the highest HP OIT retention result for the synergic exposure than for the UV exposure.

4.2 Thermal analysis results

4.2.1 Industrial water pond: CLIQ and 1L samples

There were analyzed two HDPE geomembrane samples of 1.0 mm nominal thickness; one exhumed by an industrial water pond (CLIQ) with 2.25 years of exposure and, the other sample, a virgin geomembrane (1L) having similar characteristics to the exhumed sample, used as a reference.

Recently, Valentin *et al.* (2018) studied four HDPE geomembrane samples with different thicknesses, virgin samples (new samples), widely marketed in Brazil. This study was conducted under synthetic air and nitrogen purge gases. The present work presents two different samples of HDPE geomembranes, with similar thicknesses. The evaluation of the exhumed sample is, therefore, valid for comparison purposes. It is important to mention that there are no regulations in terms of sampling of the product applied on site. Thus, the use of reference materials is limited to similar materials.

Figures 60 and 61 show the TG and DTG curves under synthetic air for the exhumed and reference samples, respectively. It can be observed that the TG curves at 5-10 ºC min^{-1} and 20-30 ºC min^{-1} are similar. This behavior is not seen in the TG curves for the exhumed sample because the 5 ºC min^{-1} analysis showed a different behavior to the others. For both samples, this behavior is attributed to the effect of the reaction time due to the different heating rates, highlighting the reference sample which showed that the reaction was only for the heating rate of 5 ºC min^{-1}. Figures 60B and 61B showed the DTG curves and the reactions occurring for different heating rates. The DTG behavior for the exhumed sample shows that when the heating rate is increased, the overlapping reactions tend to decrease gradually. For the reference sample, the thermal behavior showed the tendency to decrease the number of decomposition reactions. The reference sample evaluated in this paper has a synthetic air thermal decomposition similar to that observed in the study by Valentin *et al.* (2018). Besides that, the TG/DTG-DTA curves were performed in triplicate to verify the repeatability of the obtained curves. Table 42 shows the values of the mass variation obtained under synthetic air for both samples.

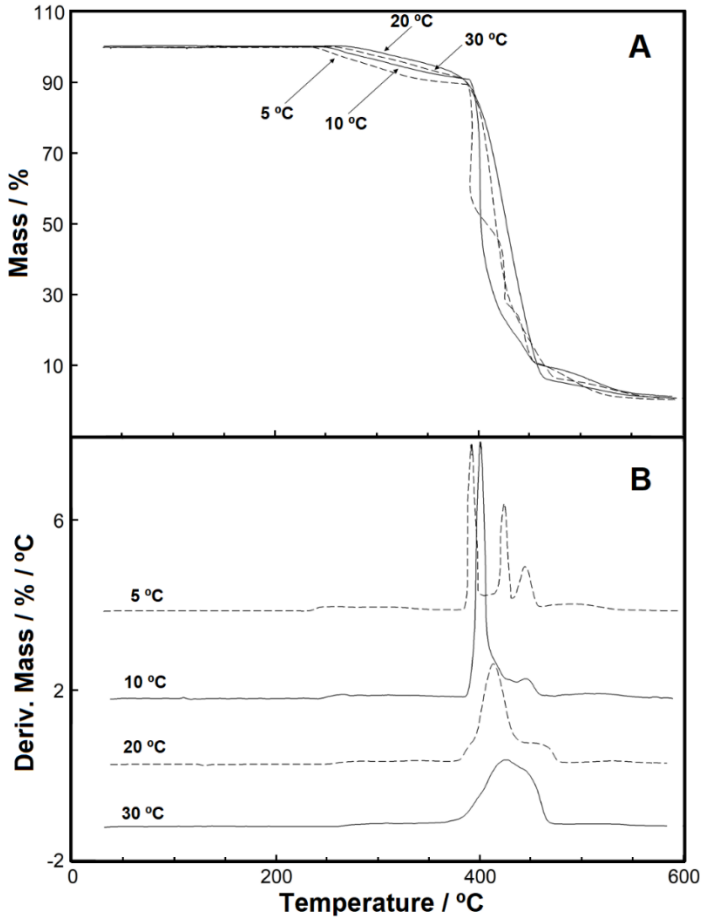

Figure 60. (A) TG curves under synthetic air purge gas, and (B) DTG curves of TG curves, under synthetic air purge gas for the exhumed sample

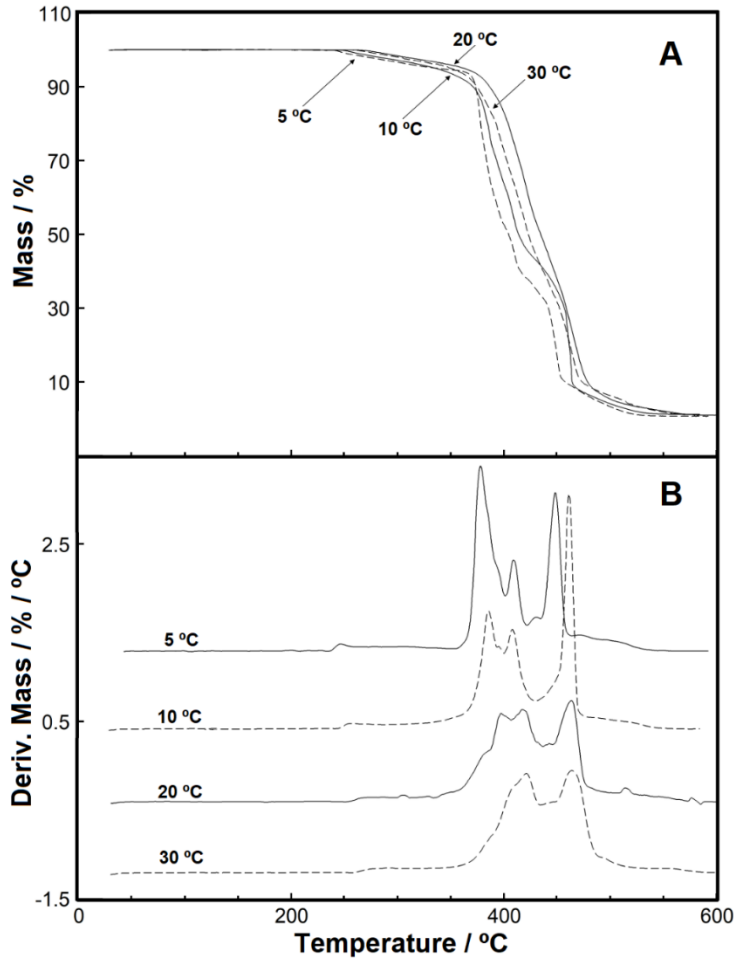

Figure 61. (A) TG curves under synthetic air purge gas, and (B) DTG curves of TG curves, under synthetic air purge gas for the reference sample

Table 42. Temperature range obtained by DTG curves for the thermal decomposition stages under synthetic air purge gas, with heating rates of 5, 10, 20 and 30 ºC min^{-1}

Compound/purge gas	**Stage**	**Heating rate/ ºC min^{-1}**	**ΔT/ºC**	**Mass loss/%**
Reference sample (synthetic air)	1	5	233 – 254	5.53
	2		254 – 401	42.11
	3		401 – 434	19.00
	4		434 – 463	24.44
	5		463 – 550	8.30
	Residue		550	0.62
Exhumed sample (synthetic air)	1	5	232 – 383	10.67
	2		383 – 405	38.52
	3		405 – 432	25.02
	4		432 – 460	15.71
	5		460 – 475	10.08
	Residue		475	0.00
Reference sample (synthetic air)	1	10	243 – 356	7.12
	2		356 – 428	49.10
	3		428 – 475	36.60
	4		475 – 550	5.83
	Residue		550	1.35
Exhumed sample (synthetic air)	1	10	236 – 385	9.00
	2		385 – 435	72.37
	3		435 – 463	8.76
	4		463 – 585	8.63
	Residue		585	1.24
Reference sample (synthetic air)	1	20	251 – 345	4.52
	2		345 – 443	59.15
	3		443 – 484	28.13
	4		484 – 590	7.17
	Residue		590	1.03
Exhumed sample (synthetic air)	1	20	244 – 375	8.35
	2		375 – 446	73.03
	3		446 – 481	12.75
	4		481 – 575	5.23
	Residue		575	0.65
Reference sample (synthetic air)	1	30	257 – 340	3.55
	2		340 – 434	46.16
	3		434 – 535	47.46
	4		535 – 590	1.82
	Residue		590	1.01
Exhumed sample (synthetic air)	1	30	256 – 364	6.47
	2		364 – 476	88.47
	3		476 – 590	4.67
	Residue		590	0.39

The TG/DTG curves for the thermal decomposition study for the exhumed sample and reference sample under carbonic gas are shown in Figures 62A and B, respectively. In both samples, there was thermal behavior which presented a shoulder at the beginning of the thermal decomposition for the heating rate of 5 ºC min^{-1}, and additionally for the heating rate of 10 ºC min^{-1} for the reference sample. As an exception to these reactions, the other heating rates presented a one-stage of heating, without a change in the DTG curves, which indicates a homogeneous kinetic behavior of the decomposition thermal reaction. Table 43 shows the mass variation values for each heating rate studied.

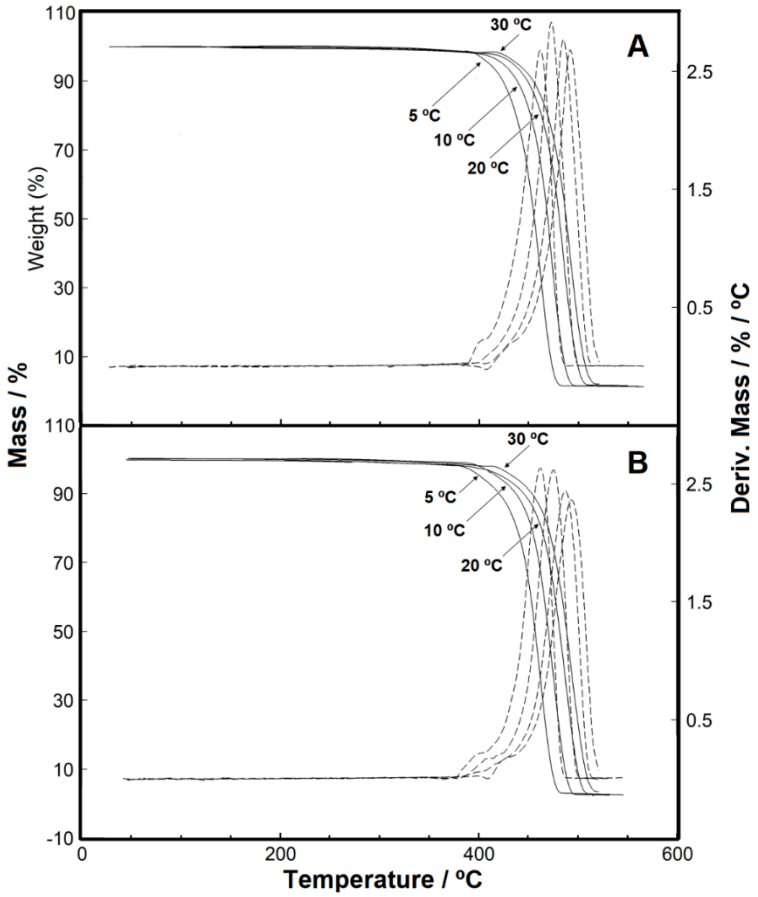

Figure 62. TG/DTG exhumed sample curve (A) and reference sample curve (B), under carbonic gas purge gas with a flow through to 110 mL min^{-1}, using different heating rates

Table 43. Temperature range obtained by DTG curves for the thermal decomposition stages under carbonic gas purge gas, with heating rates of 5, 10, 20 and 30 ºC min^{-1}

Compound/purge gas	Stage	Heating rate/ ºC min^{-1}	ΔT/ºC	Mass loss/%
Reference sample (carbonic gas)	1 Residue	5	376 – 490 490	95.75 4.25
Exhumed sample (carbonic gas)	2 Residue	5	389 – 489 489	97.17 2.83
Reference sample (carbonic gas)	1 Residue	10	382 – 498 498	96,01 3.99
Exhumed sample (carbonic gas)	4 Residue	10	397 – 507 507	96.78 3.22
Reference sample (carbonic gas)	4 Residue	20	391 – 518 518	95.68 4.32
Exhumed sample (carbonic gas)	4 Residue	20	408 – 516 516	96.36 3.64
Reference sample (carbonic gas)	3 Residue	30	409 – 530 530	94.92 5.08
Exhumed sample (carbonic gas)	1 Residue	30	412 – 522 522	96.59 3.41

Additionally, Figures 63A and B show the DTA curves respectively for the exhumed and reference samples for different heating rates. For both samples, the endothermic peak can be seen between 120 and 140 ºC due to the material melting, and according to the behavior seen in the DSC curves (Figures 64 and 65). The first stage of thermal decomposition shows that there is an exothermic event between 230 and 290 ºC, while from the second stage of decomposition, there are different DTA curve behaviors. As can be seen in the exhumed sample at 5 ºC min^{-1}, from the second stage of mass loss there is a combustion behavior of the sample, which caused the DTA curve to distort in the first peak and rise in the second peak. The third peak shows that the last stage is a decomposition final material exothermic reaction. For the reference sample, the peaks showed no combustion, which was attributed to exothermic reactions of the sample. Besides that, for the reference sample, the fact that a reaction could not be seen can be attributed to the combustion for different heating rates. In this sample, the presence of different exothermic peaks can be observed during the thermal decomposition.

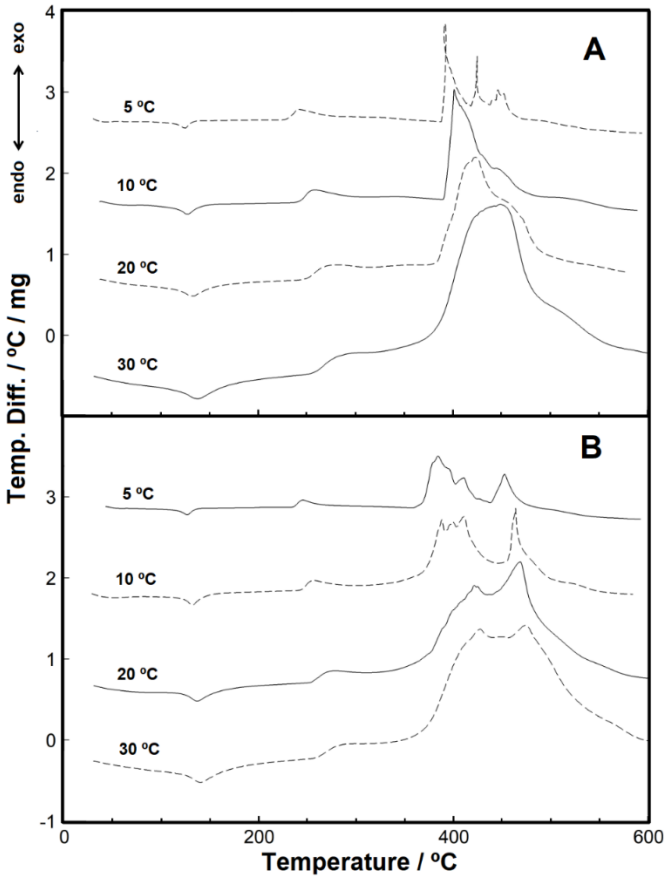

Figure 63. DTA curves of the samples for different heating rates. (A) exhumed sample and (B) reference sample

Figures 64 and 65 show the DSC curves of heating and cooling, respectively, in the temperature range from -80 to 200 ºC in two heating rates. The aim of using two heating rates was to verify the glass transition. Figure 64 shows, for the 10 °C min^{-1} analysis, that there was a change between -70 to -60 °C at the baseline, which was attributed to the glass transition in both samples. This change in the baseline can be seen for the analysis of 30 ºC min^{-1}, but in the temperature range from -56 to 24 ºC. For the melting point, it can be observed for the analysis of 10 ºC min^{-1} that the exhumed sample has an overlapping reaction while the same sample does not have an overlapping reaction for the analysis of 30 ºC min^{-1}. It can be observed that there was no overlapping reaction for the reference sample. In addition, there was an increase in melting peaks, which is usually explained by high heating rates. Figure 65 shows that the crystallization behavior for both samples is coincident and can be seen for both samples.

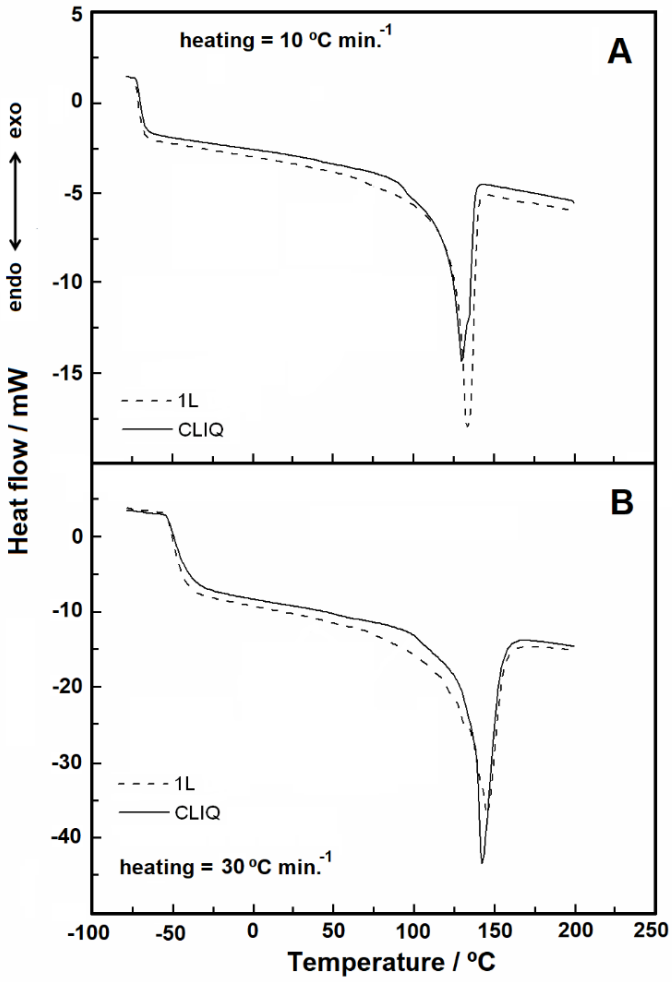

Figure 64. DSC curves showing the samples' melting point for heating rates of 10 and 30 ºC min^{-1} under nitrogen purge gas with a flow through to 50 mL min^{-1}

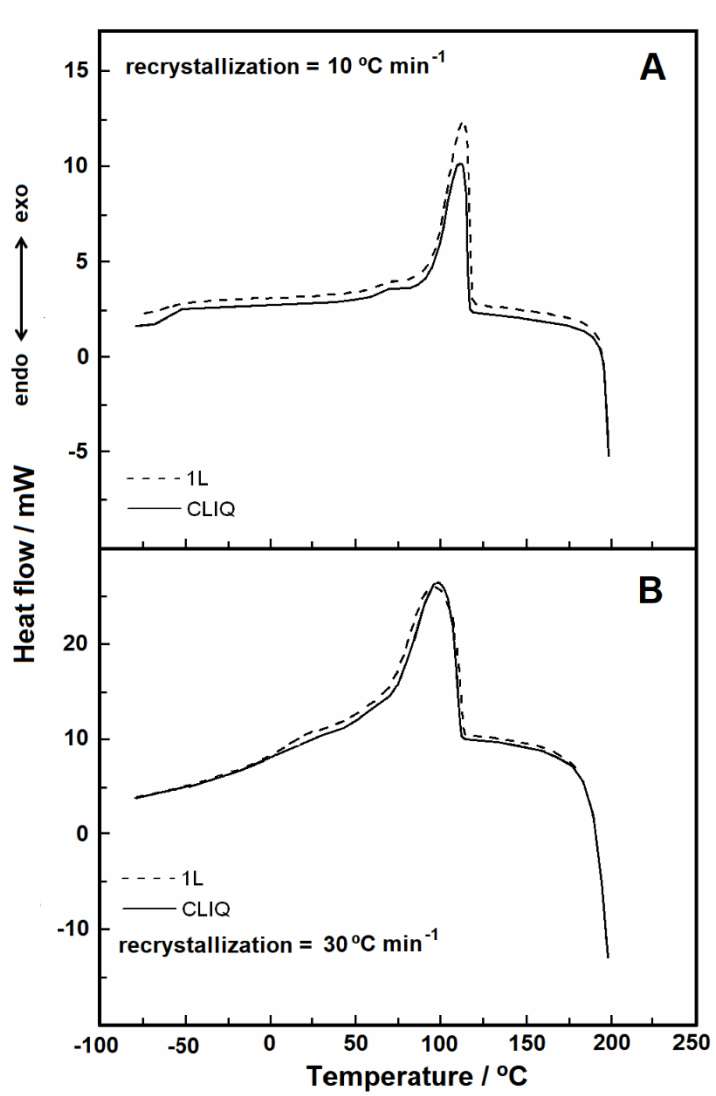

Figure 65. Crystallization DSC curves for heating rates of 10 and 30 ºC min^{-1} under nitrogen purge gas with a flow through to 50 mL min^{-1}

Figure 66 shows the TMA curves obtained under synthetic air purge gas and without purge gas. It is important to highlight that each sample was set in the equipment oven for 10 minutes before starting the analyses in order to homogenize the thermal behavior. Moreover, it can be observed that both samples, without purge gas, have thermal stability until a temperature of about 30 ºC. From this temperature, it can be seen that both samples have a thickness decrease until 110 ºC. It was observed that the reference sample has a range between 30 and 65 ºC, which is attributed to a molecular relaxation. The same effect was not observed for the exhumed sample because it was subjected to severe environmental conditions, and therefore due to continuous exposure of the sample, relaxation no longer occurred.

Both samples present a distinct behavior without a purge gas condition. As can be seen in the dynamic purge gas, in this condition both samples show no change in thickness, which was attributed to the cooling effect of the sample during heating. Due to the possibility of reaction between the sample and the synthetic air purge gas, the analysis was repeated under nitrogen purge gas and the result was strictly the same, indicating the behavior of the samples.

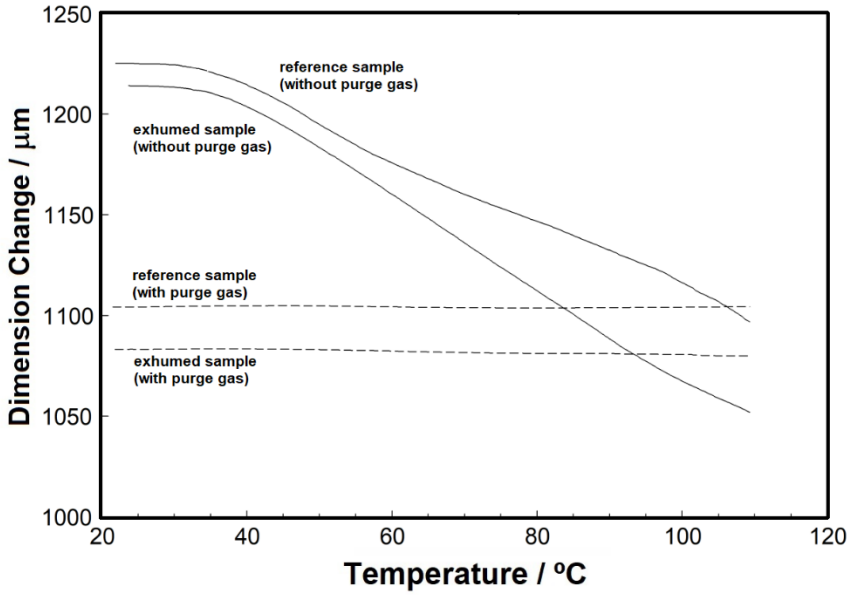

Figure 66. TMA curves for heating rate of 5 ºC min^{-1} under nitrogen purge gas

4.2.2 Sanitation ponds: LCH and LTE samples

Two different high-density polyethylene geomembrane samples were evaluated exhumed from sanitation construction works. The first sample was exhumed from a sewage treatment aeration pond (LTE) after 2.75 years of operation. Another sample was exhumed from a municipal landfill leachate pond (LCH) after 5.17 years of operation.

An experiment series were systematically proceeded using TG-DTA analysis simultaneously, with heating rates of 5, 10, 20 and 30 °C min^{-1}. The obtained results from both HDPE geomembrane samples are shown in the Figures 67 and 68.

Figure 67 shows the TG, DTG and DTA curves of the LTE sample in synthetic air with different heating rates. It was observed that the thermal stability of the LTE sample (TG curves in Figure 67A), which was in contact with the sewage, reached 238 °C for the heating rate of 5 °C min^{-1} and gradually increased to 262 °C for the heating rate of 30 °C min^{-1}. The first sample's mass variation for the heating rate of 5 °C min^{-1} occurs in one stage only, in the range of 248-

369 °C, as seen in the TG curve, whereas in the DTG curve (Figure 67B) only a small deviation from the baseline is seen. The second stage, attributed to the material's thermal decomposition process, occurs with overlapping reactions, which have presented variations in the intensity of the reactions for the different heating rates, as seen in the TG curves. Furthermore, in the DTG curves it can be observed that with the increase in the heating rate, there is a widening in the decomposition events. For the verification of the mass variations and the respective temperature ranges, the values of each stage are shown in Table 44. For both LTE and LCH samples, at the end of the analyses, the ash formation was observed, which was easily removed from the crucible by a breath. From the DTA curves (Figure 67C) endothermic peaks can be observed at 127, 130, 135 and 140 °C, respectively, for the heating rates of 5, 10, 20 and 30 °C min^{-1}, which were attributed to material melting. This melting point temperature variation is due to the speed of the sample heat absorption, which occurs for different heating rates. The sample's melting point is also seen in the DSC curve (Figure 69). Other exothermic peaks are linked to the different stages of the material's thermal decomposition and, as an effect of the speeds of the different heating rates, the peaks widened.

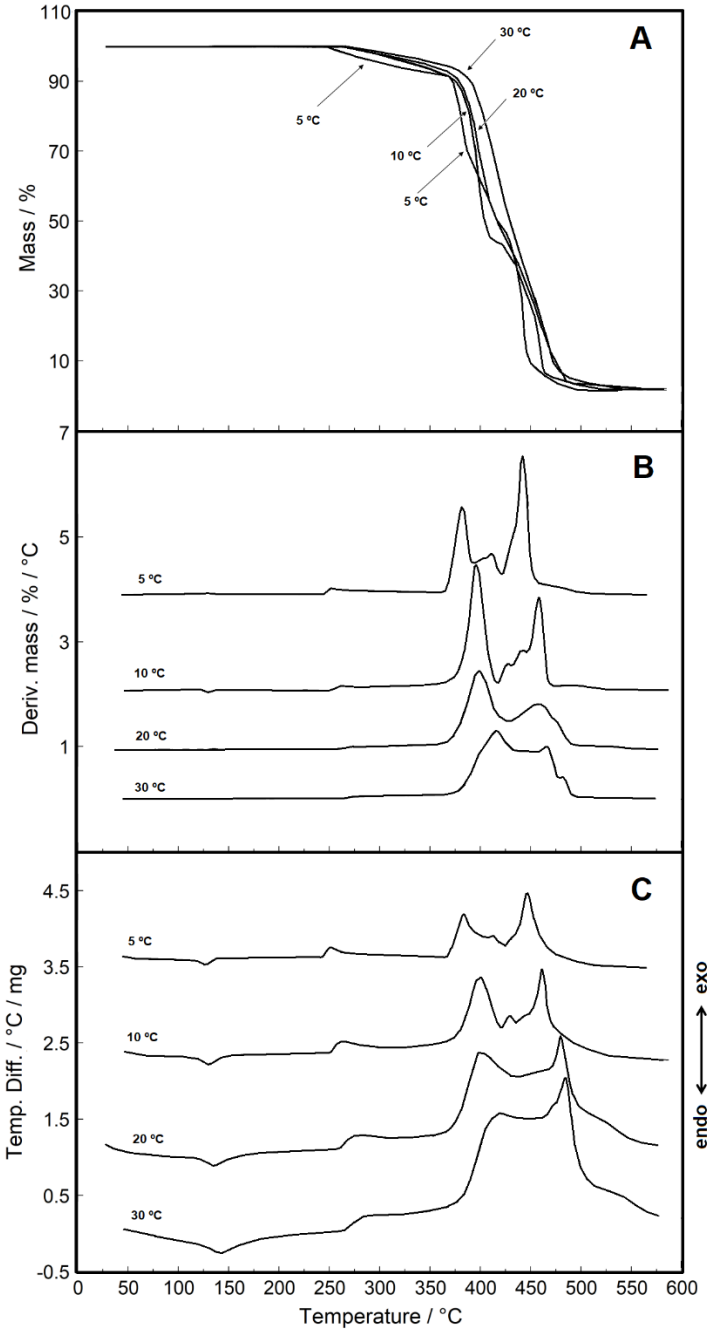

Figure 67. (A) TG curves for LTE sample in the synthetic gas purge; (B) DTG curves for the LTE sample in the synthetic gas purge; (C) DTA curves for the LTE sample in the synthetic gas purge. (all analyses conducted with heating rates of 5, 10, 20 and 30 °C min^{-1} with the flow of 110 mL min^{-1})

In the LTE sample analysis, there were no changes in the thermal behavior of the geomembrane, despite the contact of the sample with the sewage for 2.75 years. However, for the LCH sample evaluation which had been in contact with the leachate for 5.17 years, it was observed that the thermogravimetric behavior presented significant changes in the sample's thermal decomposition. To ensure this result, two other TG curves were performed in each

heating rate to verify again the thermal behavior observed once again. Indeed, the other analyses showed that there had been undoubtedly a change in the sample's thermal behavior due to contact with the leachate. The leachate is a highly concentrated organic substance and this fact added to the 5.17 years of sample exposure can explain the changes in the sample's thermal behavior. Thus, as seen in the TG curves (Figure 68A), the organic material absorption by the geomembrane probably changed the material's behavior, causing interaction reactions between the polymer and the leachate. Figure 68A shows that the heating rate of 10 °C min^{-1} is different from the other curves. In this specific curve, the first mass variation occurs between 259-406 °C and the second mass variation occurs from 406 °C, in two stages, which can be seen in the DTG curve (Figure 68B). The 5 °C min^{-1} heating rate curve shows three stages of mass variation, in the temperature ranges of 248-369 °C, 369-392 °C and 392-459 °C. For the heating rates of 20 and 30 °C min^{-1} from the second mass variation, the DTG curves are wider, which indicates that the decomposition occurs with overlapping reactions. The mass variation data for each thermal decomposition stage are shown in Table 44, presenting the results from synthetic air and carbonic gas analyses.

The obtained results from the DTA curves are shown in Figure 68C for the LCH sample. It can be observed that the first event is an endothermic reaction (without mass variation in the TG/DTG curves), which occurs at temperatures of 127, 132, 138 and 150 °C, for the four heating rates, respectively, representing the samples' melting point. As both samples (LTE and LCH) were produced with the same type of polymer, the melting point values differ slightly from each other probably due to their different uses of the conditions. Moreover, this melting reaction follows what was observed in the DSC curve (Figure 70). The following stages of thermal decomposition are exothermic reactions for the four heating rates. The heating rate of 5 °C min^{-1} showed a sharp peak in the second stage of thermal decomposition, which is attributed to a sample combustion reaction. In addition, as with the LTE sample, it can be observed that with the increase in the heating rate, there is a widening effect of the exothermic reactions due to the overlapping reactions.

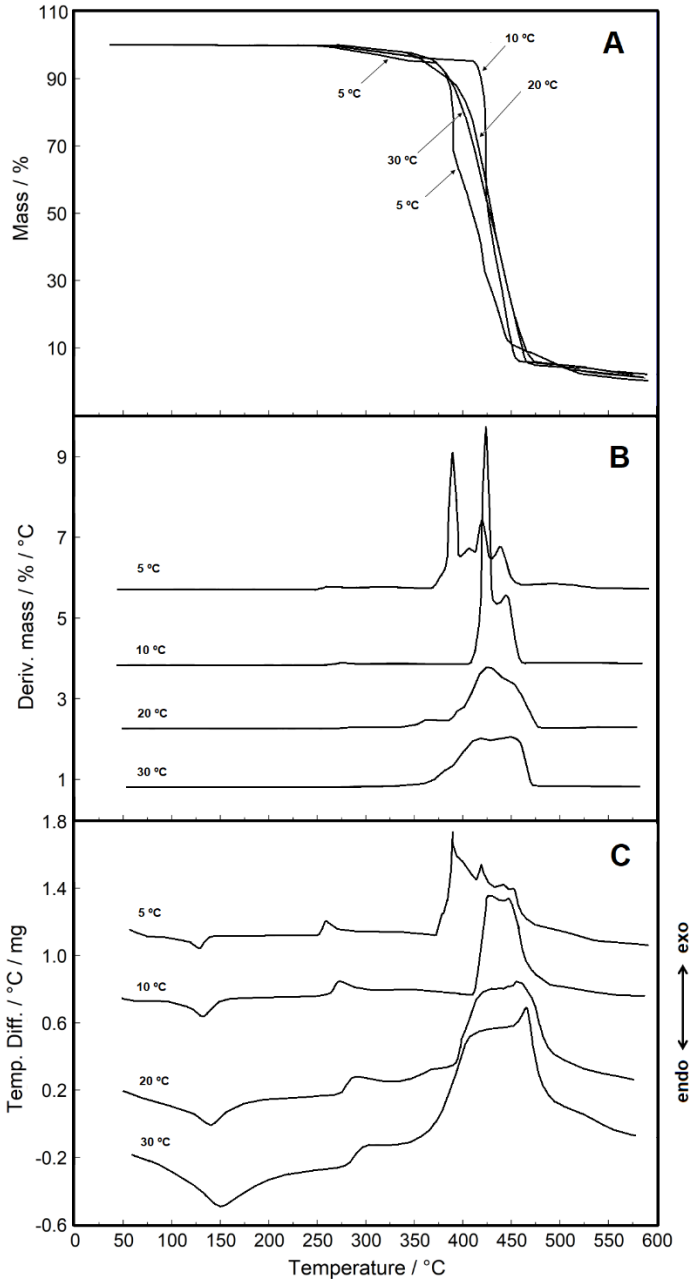

Figure 68. (A) TG curves for LCH sample in synthetic gas purge; (B) DTG curves for the LCH sample in synthetic gas purge; (C) DTA curves for the LCH sample in synthetic gas purge. (all analyses conducted with heating rates of 5, 10, 20 and 30 °C min^{-1} with the flow of 110 mL min^{-1})

Table 44. Temperature intervals (°C) obtained from TG/DTG curves for the thermal decomposition stages in synthetic air and carbonic gas, with heat flow rates of 5, 10, 20 and 30 °C min^{-1}

Sample	5 °C min^{-1}	10 °C min^{-1}	20 °C min^{-1}	30 °C min^{-1}
LCH Synthetic air	248-369 °C 5.33 % 369-392 °C 29.15 % 392-459 °C 55.77 °C 459-600 ºC 9.51 % Residue 0.24 %	259-406 °C 4.64 % 406-465 °C 89.52 % 465-600 °C 4.85 % ---- ---- residue 0.99 %	264-352 °C 3.47 % 352-392 °C 8.68 % 392-484 °C 82.48% 484-600 °C 3.35 % Residue 2.95%	264-358 °C 2.95 % 358-578 °C 91.89 % 578-600 °C 2.72 % ---- ---- Residue 2.44 %
LTE Synthetic air	238-363 °C 7.89 % 363-422 °C 44.09 % 422-468 °C 42.77 % 468-600 °C 3.77 % Residue 1.48 %	241-364 °C 8.40 % 364-417 °C 48.08 % 417-475 °C 38.92 % 475-592 °C 3.46 % Residue 1.14 %	249-362 °C 6.33 % 362-426 °C 49.29 % 426-497 °C 39.65 % 497-586 °C 2.85 % Residue 1.88 %	262-372 °C 6.01 % 372-500 °C 90.57 % 500-580 °C 1.34 % ---- ---- Residue 2.08 %
LCH Carbonic gas	378-498 °C 96.38 % ---- ---- Residue 3.62 %	383-435 °C 3.66 % 435-508 °C 92.93 % Residue 3.41 %	387-443 °C 1.33 % 443-523 °C 94.89 % Residue 3.78 %	401-451 °C 3.00 % 451-530 °C 93.48 % Residue 3.52 %
LTE Carbonic gas	376-496 °C 94.04 % Residue 5.96 %	381-507 °C 94.28 % Residue 5.72 %	405-518 °C 94.97 % Residue 5.03 %	410-525 °C 96.15 % Residue 3.85 %

Figures 69 and 70 show, respectively, the LTE and LCH samples analyses under heating and cooling conditions performed to verify the materials' transitions.

Figure 69A shows that during the first cooling there was a decrease in the LTE sample heat flow, which coincides with the baseline of the second cooling between 5 to -28 °C. The first heating of the sample (Figure 69B) shows that there had been a change in the baseline of the curve between -55 to -25 °C. For the second cooling, there was a heat flow decrease in the range of -28 to -40 °C, which is attributed to a difference in the heat capacity of the sample. However, in the second and third heatings, there was an inverse behavior, that is, there was an

increase in the material’s heat flow. These changes in the sample’s heat flow occurred due to the behavior of the material's molecules, which during cooling, the polymer molecules undergo contraction due to low temperature, getting closer to one another, and consequently changing the sample dimensions. During heating, the molecules tend to distance themselves from each other, and thus, the heat capacity changes, causing the accumulated energy to be released. In contrast, in the first heating, the material melted and then there was a crystallization, where there is a molecular reorganization and a temperature decrease. Then the molecular structure experiences a decrease in the heat flow between -25 and -39 °C, which shows an energy loss that corresponds to a material’s molecular approximation. As the material was heated and recrystallized again, there was an even more random molecular reorganization, which causes the change in the heat flow. When reheating this sample again, in the second heating (Figure 69B) there is an increase in the sample’s heat flow, and then the new fusion, which has a wider peak area than the first fusion. When recrystallizing again, as seen in the third cooling, the peak is also smaller and wider. However, as seen, there was a small change in the baseline between -4 to -19 °C. Finally, in the third heating, there was an overlap with the event observed in the second cooling, attributed to the molecular distance.

For the LCH sample, the behavior seen in the LTE sample was not observed. It indicates that there was probably an effect of leachate in the sample, causing a change in the heat flow. As seen in Figure 70A, the first cooling and the first heating have the same behavior observed for the LTE sample. After the melting and the first crystallization, a slight change in the baseline is seen in the second cooling (17 to 8 °C) and the third cooling (7 to -2 °C), both in agreement with what is seen in the third cooling of the LTE sample. It is important to note that during the heating of this sample, there was no change in the material's baseline between (-54 to -16 °C). Thus, it can be reaffirmed that the effect caused on the DSC curve for the LCH sample is attributed to the presence of leachate molecules, which altered the material’s behavior after the melting process.

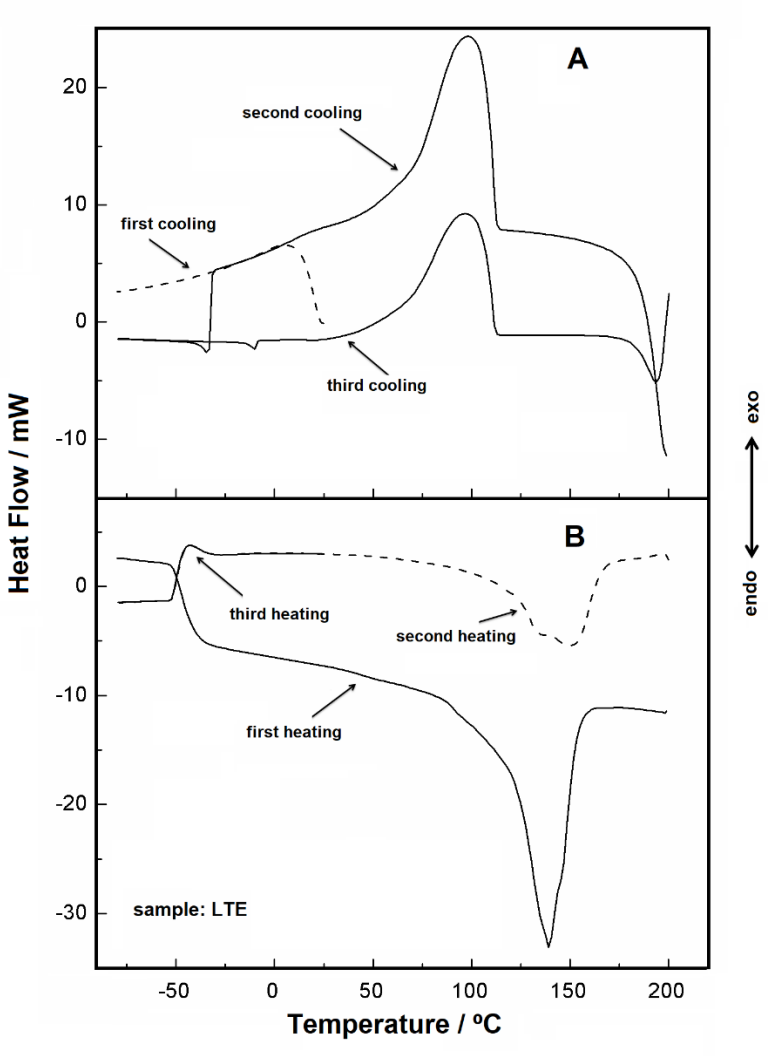

Figure 69. LTE sample DSC curves with a heating rate of 30 °C min^{-1} under nitrogen gas purge with the flow of 50 mL min^{-1}: (A) cooling and (B) heating

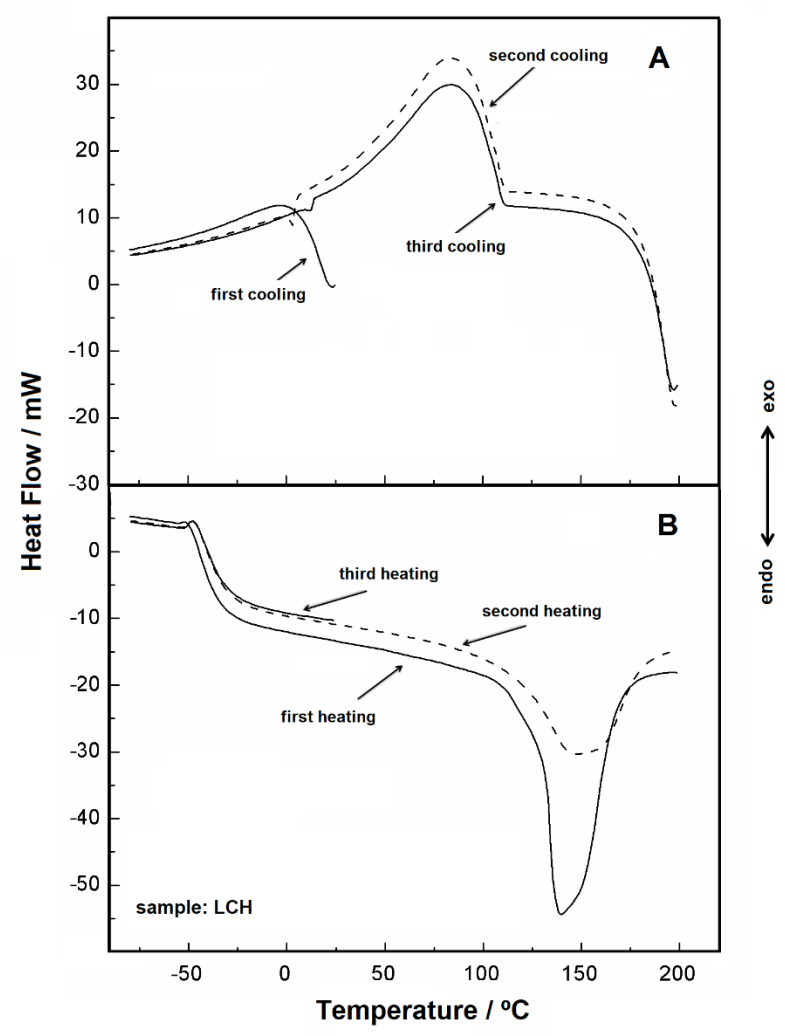

Figure 70. LCH sample DSC curves with a heating rate of 30 °C min^{-1} under nitrogen gas purge with the flow of 50 mL min^{-1}: (A) cooling and (B) heating

DMA was used to track changes in the molecular relaxation of the materials, to learn whether these changes were a function of the time in operation and an indication of the material's degradation, and to learn about the effects of leachate and sewage on the material. DMA analysis usually have different modulus, which allow a better characterization of the material, that is, the material's capacity to store energy (storage modulus), its capacity to lose energy (loss modulus) and the proportion of these effects (tan-δ), which is called damping (damping factor) (GABBOTT, 2008).

Figure 71 shows the DMA analysis under nitrogen purge gas, at a range temperature of -80 to 120 °C for both samples, where it is possible to verify that both samples have different behavior between each other. The temperature range utilized in this analysis is situated above the glass transition temperature, which is a region of high hardness and therefore, the information obtained from the temperature of -80 °C refers to the transition region performed

in this work (MENARD, 2008). The behavior of the LTE sample storage modulus (Figure 71A) shows that this sample has a higher value than for the LCH sample, which means that the LCH sample is less brittle, that is, more elastic. The basic definition of the storage modulus is given as a measure of the mechanical energy that the material is capable of storing, in the form of potential or elastic energy (CASSU AND FELISBERTI, 2005). This result shows that the potential energy of the LTE sample decreases gradually until the temperature of 32 °C, and after this temperature, this sample increases its potential energy again until the temperature of 78 °C. This effect is attributed to the simultaneous effect of raising the temperature and the interaction of the geomembrane polymer with molecules from the sewage which were impregnated in the geomembrane, which causes an increase in stiffness (becomes less elastic). The same effect is observed for the LCH sample, but to a lower degree. The expected trend would be an increase in the elasticity of the material and a consequent decrease in stiffness.

These results show that the geomembranes' contact with the sewer and leachate caused the alteration in elastic potential, which is attributed to the molecular interaction in the structure of the polymeric matrix. Furthermore, from temperatures of 72 °C for the LTE sample and 85 °C for the LCH sample, both samples tend to increase viscosity since the increase in temperature leads to the melting stage, that is, the polymer chains start to have a greater movement due to the increase of the temperature with loss of stored energy, until the consequent fusion.

The loss modulus (E") is shown in Figure 71B, which presents that the LTE sample has a much higher curve behavior than the LCH sample curve in the same temperature range (32 to 125 °C). This information indicates that the LTE sample, when dissipating the energy stored in this interval, shows that its elasticity decreases again, while the LCH sample has a constant behavior, showing variations in different temperature ranges (Hatakeyama *et al.* 1999).

In Figure 71C, tan-δ is shown, which is a relationship between the material's elastic/stiffness behavior (GABBOTT, 2008; MENARD, 2008). As both materials are more rigid at low temperatures, tan-δ tends to increase with the temperature increasing. Thus, at the peak temperature of tan-δ (32 °C) for the LTE sample, there was a peak in the decrease in the material's stiffness and after this temperature there was a decrease in the tan-δ, indicating an increase in stiffness. For the LCH sample there was the same behavior but with the tan-δ peak at 63 °C, which corresponds to the temperature at which is the value of the lowest potential energy of this sample (Fig. 71A), that is, after this temperature, this sample increases its potential energy up to 82 °C. As with the LTE sample, there was an increase in the LCH stiffness, and therefore, the tan-δ peak (63 °C) corresponds to this situation. Tan-δ decreases

with increasing stiffness, that is, if the material is rigid, tan-δ will be constant (will have a zero value) (KRONGAUZ, 2010; SUCESKA *et al.*, 2010).

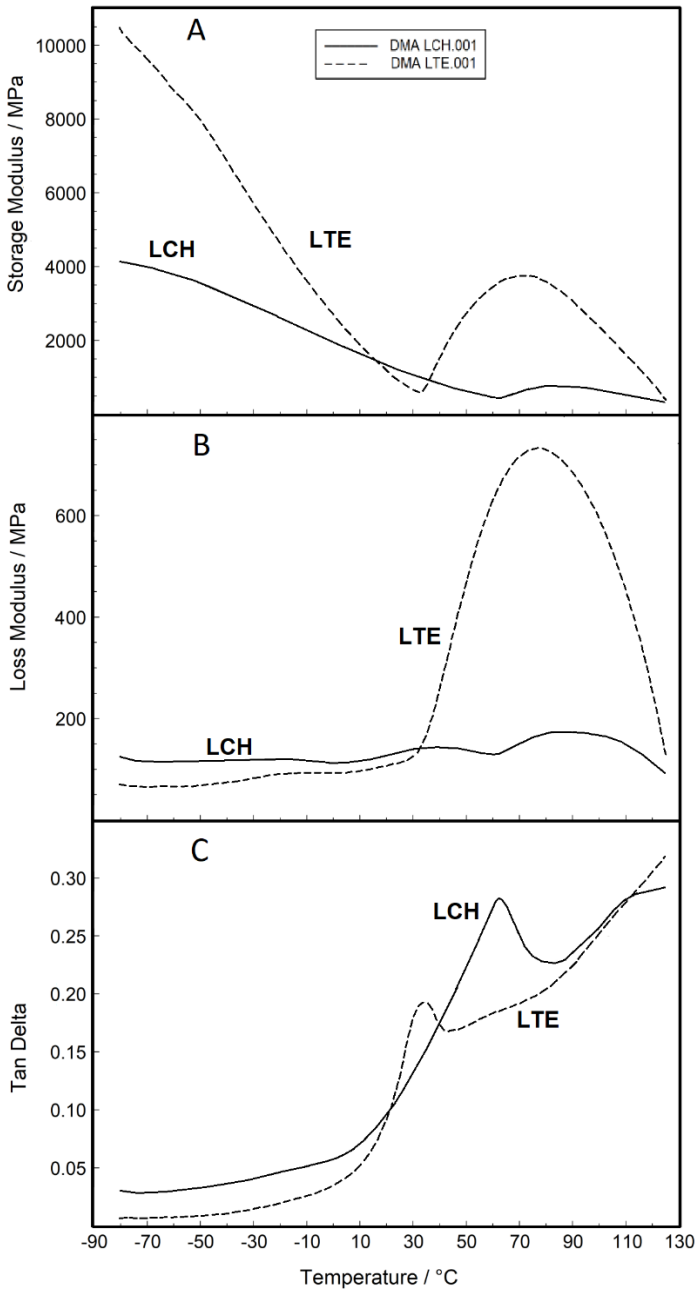

Figure 71. DMA curves of LCH and LTE samples with a heating rate of 10 °C min^{-1} under nitrogen gas purge with a flow of 50 mL min^{-1}

4.2.3 Mining facility constructions: MIN and MIN2 samples

Figure 72 shows the TG/DTG curves with 10 °C min^{-1} of heating rate using synthetic air purge gas for the MIN and MIN2 samples. It can be observed that both samples did not show mass variation between the initial temperature and 245 °C. The MIN2 sample presented the first mass variation of 9.81 % (until 380 °C), while the MIN sample presented the first mass variation of 8.18 % (until 390 °C). The second mass variation occurred until 445 °C and showed variations of 76.13 % and 74.22 %, respectively, for the MIN and MIN2 samples. Furthermore, the MIN sample's DTG curve at the second mass variation presented an acute behavior and a wider curve than the MIN2 sample. The mass variations' difference observed can be attributed to the different field exposures between the samples. The final decomposition presented a similar behavior, with a mass variation of 14.97 % and 14.54 %, respectively, for the MIN and MIN2 samples. At the end of the decomposition, carbonaceous material was observed on the crucible for both samples.

Figure 73 shows the DTA curves for both samples. The endothermic peak can be observed in both curves, at 128 °C and 131 °C, respectively, for the MIN and MIN2 samples. This peak is attributed to the melting point of the materials in concordance with the DSC curves. The exothermic peaks can be seen at 260 °C (MIN2 sample) and 267 °C (MIN sample). These peaks are related to the samples' first decomposition step. After 380 °C, there are two exothermic peaks for both samples at 417 °C and 462 °C due to the third and fourth thermal decomposition steps. These peaks represent the oxidative process of these materials and do not represent the materials' combustion because the peaks are wide. The combustion process would present the acute peak in the curves.

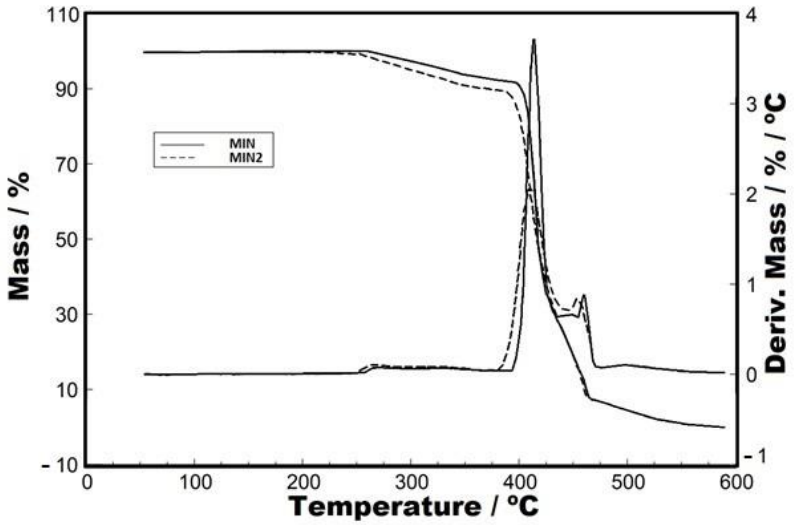

Figure 72. TG/DTG curves for both samples, MIN sample (solid line) and MIN2 sample (dotted line), under synthetic air purge gas with a flow through to 110 mL min^{-1}, using 10 °C min^{-1} as heating rate

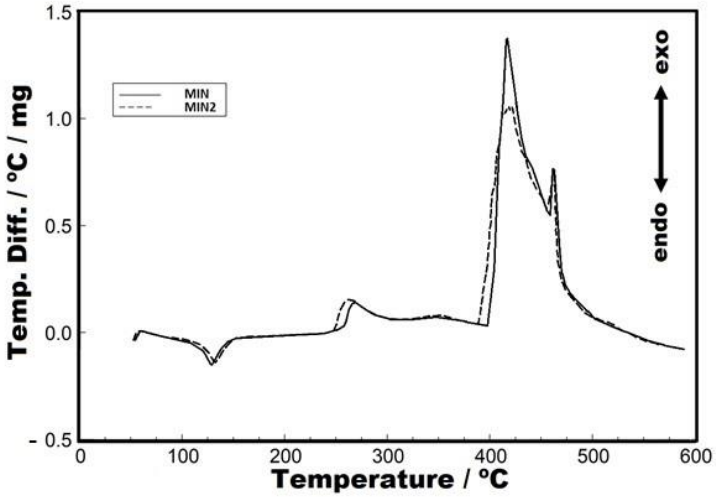

Figure 73. DTA curves for both samples, MIN sample (solid line) and MIN2 sample (dotted line), under synthetic air purge gas with a flow through to 110 mL min^{-1}, using 10 °C min^{-1} as heating rate

Figures 74 and 75 show the DSC curves for the heating and cooling, respectively, at temperature ranges from −80 to 200 °C and 200 to 25 °C, with 10 °C·min^{-1} as a heating rate. The purpose of using two temperature ranges was to verify the melting point and crystallization. For the melting point (Figure 74), it can be observed that the difference between the peaks is low (134 °C for the MIN sample and 133 °C for the MIN2 sample), which shows that the geomembranes' exposure conditions did not change the fusion behavior. Likewise, the samples' crystallization peaks, seen in Figure 75, present both peaks with temperatures of 110 °C for the MIN sample and 111 °C for the MIN2 sample.

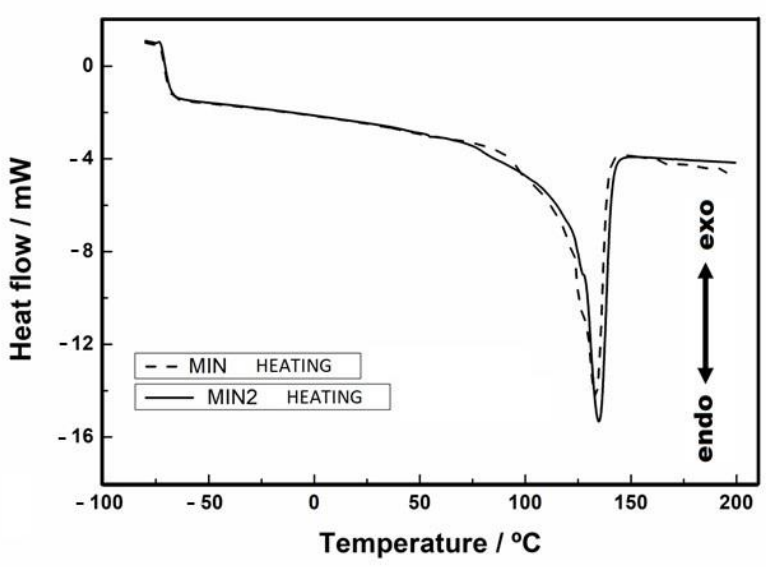

Figure 74. DSC curves for both samples, MIN sample (solid line) and MIN2 sample (dotted line), showing the samples' melting point for a heating rate of 10 °C min^{-1} under nitrogen purge gas with a flow through to 50 mL min^{-1}

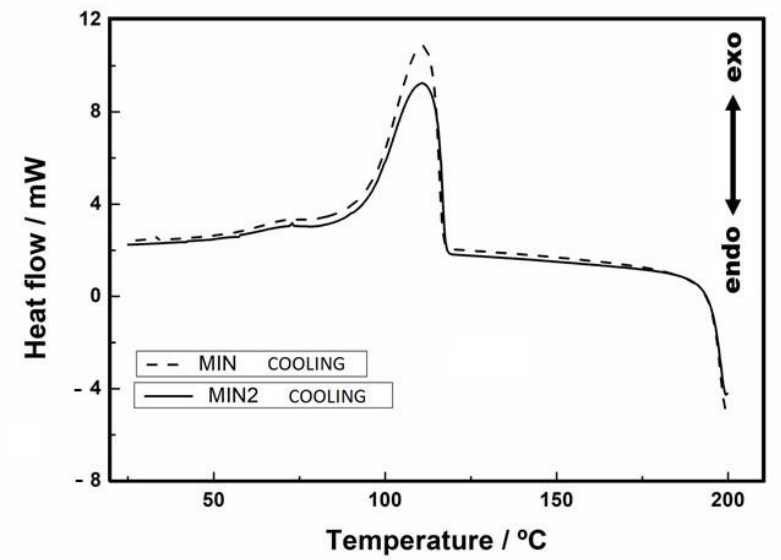

Figure 75. Crystallization DSC curves for both samples, MIN sample (solid line) and MIN2 sample (dotted line), for a heating rate of 10 °C min^{-1} under nitrogen purge gas with a flow through to 50 mL min^{-1}

4.2.4 Biodegradable waste pond: LDO sample

Figure 76 presents the DSC curves for heating (A) and cooling (B) conditions. DSC curve 76A shows that from the temperature of 90 °C, there is a baseline change of the curve that indicates the tendency to soften due to the continuous increase in temperature until it

reaches its melting point, which occurred at 129 °C. After the melting point, the sample was cooled (Figure 76B), and the result showed that the crystallization peak occurred at 115 °C. It can be observed that there is an indication of overlapped reactions in both peaks (melting and crystallization points), which is attributed to the presence of inorganic impurities in the material. The enthalpy value for the melting point was 162 J g^{-1}, while the value for the crystallization point was 139 J g^{-1}. The deduction of the polymer's crystallinity is determined by the ratio between the practical and theoretical enthalpy, where the theoretical enthalpy, according to Rollin and Rigo (1991), has a value of 285 J g^{-1}. In this study, the sample crystallinity value obtained was 57 % for the melting enthalpy. According to Hsuan (2000), the HDPE geomembranes present relatively high crystallinity, between 40 % to 50 %. The crystallization enthalpy was determined at the peak area, which corresponds to 139 J g^{-1}. It is important to note that the crystallization enthalpy is not the same as the melting temperature because the intervals and conditions of physical change are different. Furthermore, crystallization occurs in a state where the resulting material is quickly reorganized because of the material being molten (GU *et al.*, 2014).

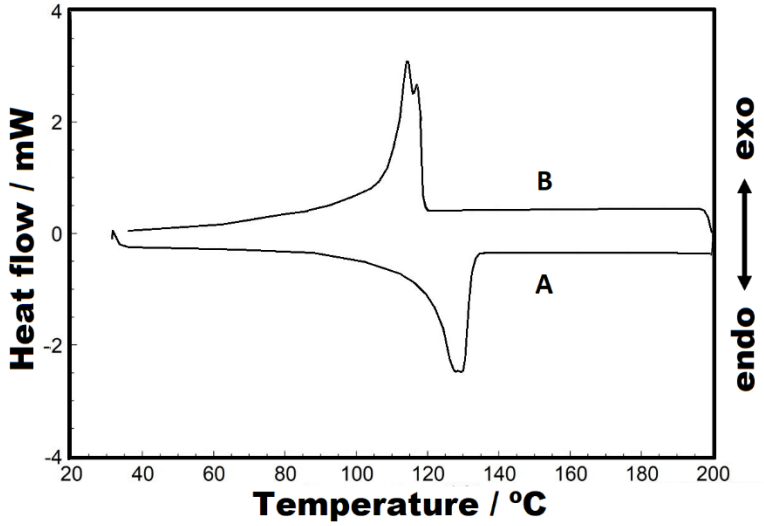

Figure 76. DSC curves: (A) heating and (B) cooling, with a heating rate of 10 °C min^{-1}, under nitrogen purge gas (50 mL min^{-1})

Figure 77 shows the storage modulus (A), loss modulus (B) and tan-δ (C) curves. The storage modulus represents the material's capacity to store energy (elastic energy), while the loss modulus represents the energy loss capacity. Tan-δ is known as the damping factor, as it represents the proportion of the effects of storage and loss modulus (VALENTIN *et al.*, 2018).

The material's behavior, when cooled, is to have its molecules closer together, and therefore, the tendency is to stiffen, and, because of that, the storage modulus is high. When the temperature increases, molecular vibrations increase, and therefore, stiffness decreases and consequently, the polymer reaches a relaxed state of energy dissipation. However, there is an increase in the storage modulus (Figure 77A) value between 7 ºC and 60 ºC, which is attributed to the interaction of the impregnated material with the polymer. This state is seen in the loss modulus curve, where the energy loss point (Figure 77B) coincides with the storage modulus point (Figure 77A), considering that the expected trend would be an increase in the elasticity of the material and a consequent decrease in stiffness. After 65 ºC, there is a decrease in storage modulus and loss modulus, which is attributed to the material softening stage, that is, the material goes into a viscoelastic state.

The tan-δ is a relation that indicates the elastic/stiffness behavior of the material. This behavior is linked to the stiffness of the material, that is, with the increase in temperature, there is a gradual increase in the tan-δ. Thus, Figure 77C shows the peak temperature of tan-δ at 7 ºC, which represents the apex in the stiffness' decrease of this material and, after this temperature, due to the interaction of the particles present in the polymer, there was again an increase in the tan-δ, indicating a decrease in stiffness up to the temperature of 65 °C, where an inflexion in the tan-δ curve can be observed. After this inflexion, the material passes to a viscoelastic state (LAVOIE *et al.*, 2020-2).

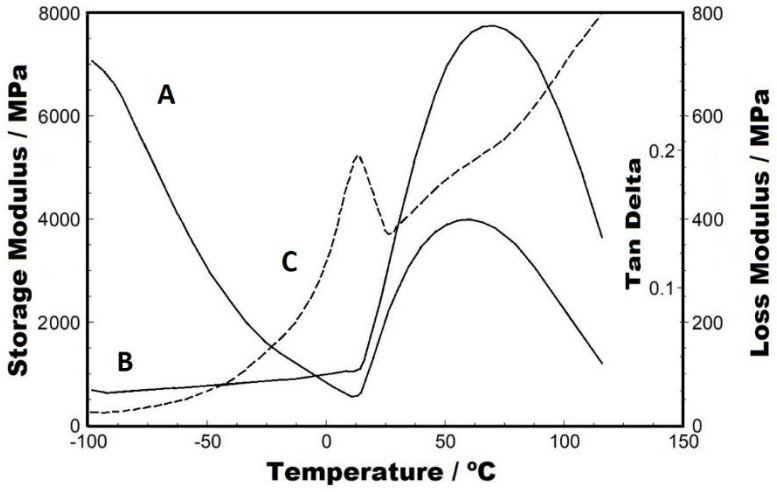

Figure 77. DMA curves: (A) storage modulus, (B) loss modulus and (C) tan-δ, with a heating rate of 10 ºC min^{-1}

4.2.5 Shrimp farming ponds: CAM, CAM1 and CAM2 samples

Figure 78 shows the TG/DTG curves for the CAM, CAM1 and CAM2 samples. It can be observed that the CAM and CAM1 samples have similar thermal behavior, while the CAM2 sample, which was taken from a shrimp farming pond after 3 years of service, shows noticeably different behavior. As mentioned, the CAM2 sample was exhumed from an area protected directly from the sunlight. It is interesting to note that for all these samples, there is thermal stability up to a temperature of 248 °C.

For the CAM2 sample, the first thermal decomposition step occurs from 248 to 396 ºC, with a total loss in this range of 10.46 %, as seen in the DTG curve. The second stage of thermal decomposition occurs between 396 ºC and 427 ºC, with a mass loss of 55.21 %, which shows a single stage, as seen in the DTG curve. The third and fourth stages occur in the intervals of 427–490 ºC and 490–605 ºC, and show mass variations of 24.87 % and 8.19 %, respectively.

The CAM and CAM1 samples (Figures 78A and B) have similar thermal behavior up to a temperature of 347 ºC. However, they show different behavior after that in the TG/DTG curves. The CAM sample, which was underwater throughout the entire service time, presented a higher thermal decomposition than the other two samples, while the CAM1 sample, exposed to UV radiation at the pond's slope shows a slightly smaller decomposition. This effect is attributed to the different conditions in which both materials were found. Mass variations are best observed in the DTG curves, where it can be observed that CAM and CAM1 samples have five main mass variation ranges. For the CAM sample, the loss and temperature ranges are as follows: 5.27 % (235–349 °C), 5.40 % (349–381 °C), 16.18 % (381–408°C), 43.34 % (408–451 °C) and 28.75 % (451–590 °C). The CAM1 sample shows the following mass losses and respective temperature ranges: 5.83 % (235–349 °C), 7.51 % (349–381 °C), 28.67 % (381–403 °C), 24.67 % (403–448 °C), 31.58 % (448–590 °C).

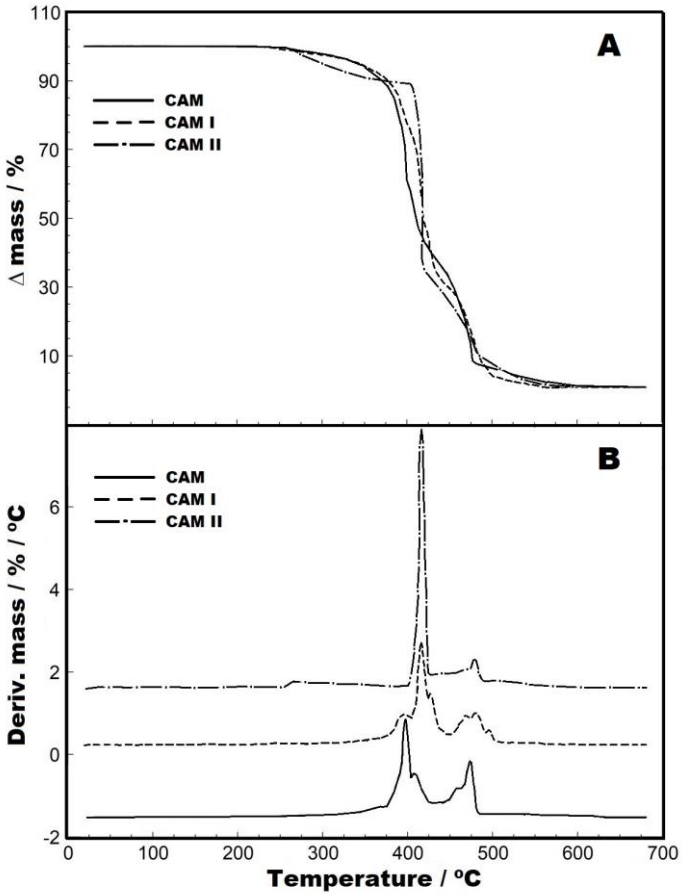

Figure 78. TG/DTG curves for the samples, CAM sample (solid line), CAM1 sample (dashed line), and CAM2 sample (dotted line) under nitrogen purge gas with a flow through to 90 mL min^{-1}, using 10 °C min^{-1} as heating rate. (A) samples' TG curves. (B) samples' DTG curves

The DSC curves are shown in Figure 79. Three analysis conditions can be observed: (A) first heating, (B) second heating, and (C) cooling (after the first heating).

The first heating (Figure 79A) shows the samples' melting point in the condition in which they were collected in the respective ponds and locations. Note that all samples have a melting peak at a temperature of 126 °C. Before the melting point, there were baseline change events between 75 and 90 °C for the CAM sample, 90–102 °C for CAM1, and 71–82 °C for the CAM2 sample. Moreover, the melting peak of the CAM2 sample shows a shoulder, which is not seen in the other samples. Valentin et al. (2018) performed the DSC characterization of HDPE geomembrane samples of different thicknesses and manufacturers. The events observed before and during melting in the samples in this work were also observed events that shifted the baseline and the presence of shoulders as the one seen here. Furthermore, Figure 79B shows the second heating of these materials. It can be observed that in all the samples, the events observed in the first heating disappear because, with the heating, the molecular history

disappeared due to the formation of a homogeneous material. This fact shows that the use of the melting point for quality control analysis is not adequate, as the molecular relaxation of the polymer causes melting events. However, it should be noted that the evaluation of the melting point of pure substances presents sharper peaks in DSC curves, and the presence of impurity can be detected or evaluated by the peak area. As HDPE polymers are not pure but with different additives, melting peaks are not suitable for evaluation via DSC (KSIQCZAK *et al.*, 2004). Figure 79C shows the crystallization peaks, which are obtained after the first heating. It can be observed that the crystallization peaks are coincident (115 °C), attributed to the effect caused by the fusion (homogenization of the material).

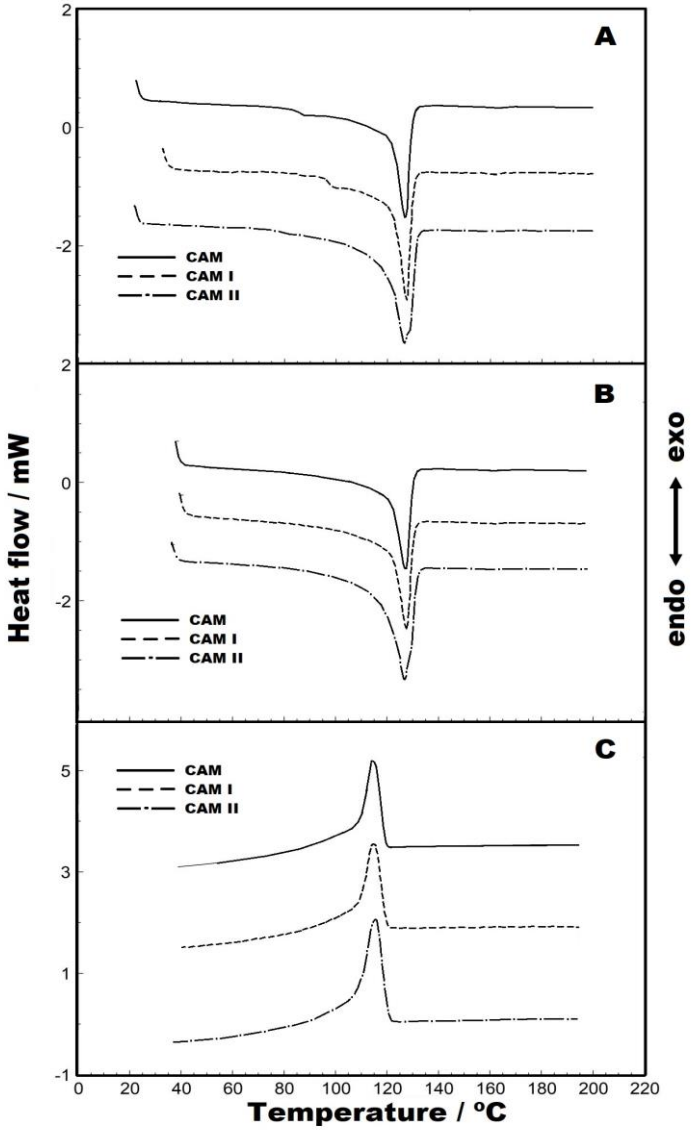

Figure 79. DSC curves for the samples, CAM sample (solid line), CAM1 sample (dashed line), and CAM2 sample (dotted line) under nitrogen purge gas with a flow through to 50 mL min^{-1}, using 10 °C min^{-1} as heating rate. (A) first heating. (B) second heating. (C) cooling (after the first heating)

The results obtained from the DMA analyses are shown in Figure 80. In the literature, the studies and the DMA results focus on three main concepts: storage modulus, loss modulus, and viscoelastic material information (tan-δ), which are calculated from the material's response to the sine wave (MENARD, 1999; KHONAKDAR *et al.*, 2003).

The variations in the storage modulus (Figure 80A) show the degree of crosslinking in the materials' molecules. At low temperatures, the polymer has a rigid behavior, while at high temperatures, the stiffness decreases. Thus, it can be observed that the CAM and CAM1 samples are similar. In contrast, the CAM2 sample presents an event between -44 and 32 ºC, which shows a significant increase in stiffness. After 32 ºC, there is a decrease in the storage modulus, attributed to the increase in the materials' viscoelastic behavior. The evaluation of loss modulus (Figure 80B) can succinctly be attributed to the energy loss due to polymer's molecular vibrations. The molecular vibration causes heat loss. In this case, it can be understood that the CAM and CAM1 samples presented similar behavior. Finally, the evaluation of tan-δ, seen in Figure 80C, presents a continuous increase, which shows information about the materials' viscoelastic behavior because it is a relationship between the loss and storage modulus. An increase in temperature causes the polymeric material to absorb energy and tends to molecular disassembly, which effectively occurs at the melting point, where the material has a viscous behavior.

Valentin *et al.* (2018) evaluated virgin samples of different HDPE geomembranes, and no noted changes in the performed analyses. Therefore, the material's exposure in construction work changes the initial conditions of the polymer (KHONAKDAR *et al.*, 2003).

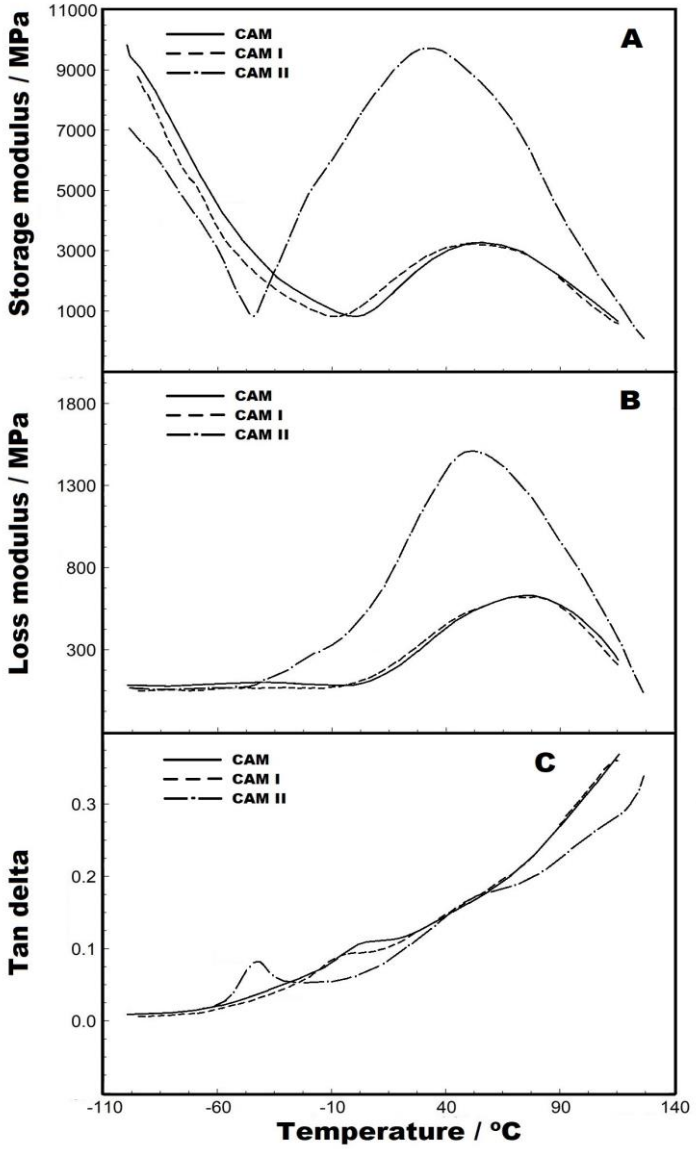

Figure 80. DMA curves for the samples, CAM sample (solid line), CAM1 sample (dashed line), and CAM2 sample (dotted line) using 10 °C min^{-1} as heating rate. (A) storage modulus. (B) loss modulus. (C) tan-δ

4.2.6 UV fluorescent and xenon arc exposures: 1L sample

Figure 81 shows the samples' DSC curves of heating (A) and cooling (B). A curves' overlap adjustment was performed to coincide with the peaks. Initially, the samples were heated up to 200 °C, where a peak attributed to the melting point was observed (Figure 81A). For all samples, the melting point essentially has the same behavior, without presenting any displacement or overlapping reactions due to the different exposure time of the samples analyzed. This behavior can be explained because the polymer under melting does not present

crystallinity, predominating the disordered molecular material. The degraded molecules by ultraviolet radiation or other radiation are involved in the melting process, making it difficult to identify the degradation of the molecules. The crystallization of the different samples can be seen in Figure 81B. The crystallization process tends to ordinate the polymer's melted molecules, leading to an exothermic process. Thus, the molecules' degradation was hidden by the molecules' reorientation, obtaining coincident crystallization points at the DSC curves. The glass transition behavior depends on a cooling system and was not obtained in this work. This analysis is necessary for future evaluations.

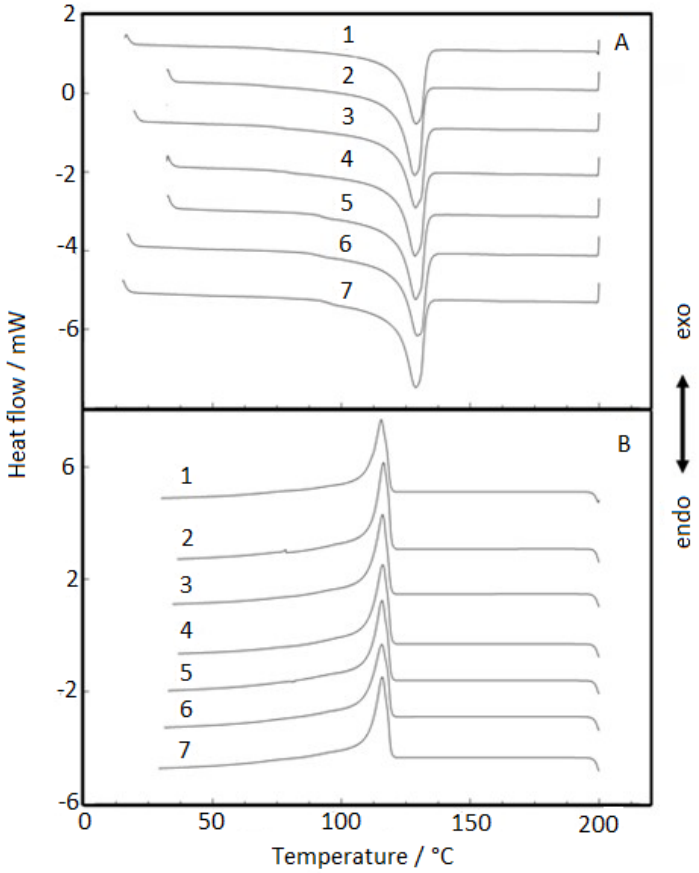

Figure 81. DSC curves: (A) melting point stage and (B) crystallization stage. 1—virgin sample; 2—960 h xenon arc sample; 3—1639 h xenon arc sample; 4—2160 h xenon arc sample; 5—960 h UV fluorescent sample; 6—4380 h UV fluorescent sample; and 7—8760 h UV fluorescent sample

4.2.7 UV fluorescent exposure: 1.5L sample

Figure 82 shows the DSC curves for the first and second heating (Figure 82A) to verify the melting point behavior and cooling (Figure 82B) to understand the crystallization point

behavior. It can be observed, in the first heating (except for the virgin sample), that there is a deviation in the DSC curve before the melting point, in the following temperature ranges: 96-105 °C for the 8760 h sample; 82-93 ºC for the 4380 h sample, and 80-89 ºC for the 960 h sample, which is attributed to the effect of exposure of the material to the UV radiation, considering that the virgin sample did not show any change in the DSC curve. On the second heating, it is possible to note that the samples have a unique curve behavior due to the homogenization effect of the material after the first heating. In Figure 82B, it can be observed that the crystallization is similar among the samples due to the homogenization after melting. The homogenization caused by the material's melting started a new polymeric configuration, considering that the crystallization points are coincident; besides, the second evaluation of the melting point is also coincident. The essential DSC evaluation was the first heating analysis, where it was possible to observe that there was a deviation from the samples' baseline.

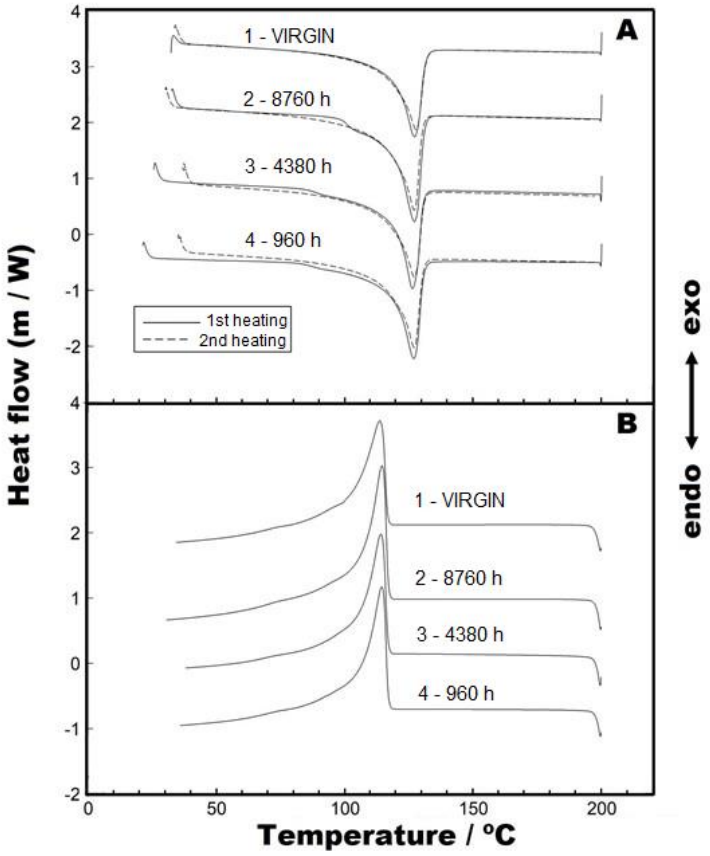

Figure 82. DSC curves: (A) melting point stage and (B) crystallization stage. 1—virgin sample; 2—8760 h UV fluorescent sample; 3—4380 h UV fluorescent sample; and 4—960 h UV fluorescent sample.

4.2.8 Results of thermal exposure and synergic exposure to UV radiation and thermal aging

Figures 83, 84 and 85 show the storage modulus (A), loss modulus (B) and tan-δ (C) curves, respectively, for 1L, 1.5L and 2L virgin samples and the samples after the thermal exposure and the synergic effect between UV radiation and thermal aging.

The analysis is conducted applying a cycle deformation through a sinusoidal deformation to a sample of known geometry, measuring the deformation suffered by the material. This application makes the material respond to the deformation, which gives information about its stiffness and damping (HAINES, 2002).

In the dynamic mechanic analysis, it is possible to express the storage modulus (E''), loss modulus and tan-δ. The storage modulus is related to stored mechanical energy when the response of the solid material is elastic. The loss modulus indicates the dissipated energy attributed to the movement of the molecular chain. The tan-δ (mechanical loss factor) shows the material's ability to convert mechanical energy into heat (BROWN, 1988).

When the polymer is cooled, the molecules tend to get closer to each other due to a decrease in the molecular energy of attraction. The material becomes stiffener, and thus its storage modulus is raised. Likewise, as the temperature increases, the storage module tends to decrease as the molecules tend to move away from each other. Three distinct behaviors were observed in three temperature ranges in the storage modulus, as seen in Figures 83A, 84A and 85A. The first behavior of the storage modulus was different for each of the sample sets. For the 1L sample set (Figure 83A), the 1L virgin sample temperature range was between -110 to -32 °C, and for the other samples, the ranges were variable: 1L (960 h) was -48°C, 1L (4380 h) was -63 °C, 1L (8760 h) was -49 to -22 °C, 1L (8760 UV – 4380 TE) was -48 °C. The second behavior observed for the virgin samples showed an increase in the storage modulus. The storage modulus intensity for the 1L sample was higher than the other two virgin samples. This fact is attributed to the molecules' distancing during heating, and it is suggested that the 1L sample shows more susceptibility to malleability (more elastic) than the other two virgin samples, which is, in fact, true, because the thickness of this 1L sample is the lowest among the virgin samples. The highest storage modulus was observed for 37 ºC (1L virgin sample), 26 °C (1L 960 h), 31 °C (1L 4380 h), 42 °C (1L 8760 h), and 28 °C 1L (8760 UV – 4380 TE). After the maximum peak of the second behavior, the third phase occurred a decrease in the storage modulus. When the temperature is elevated and is close to the melting point, there is an increase in molecular vibrations, passing to the viscoelastic phase. The effect of the thickness is decisive,

given the differences among the evaluated samples. Valentin et al. (2018) studied different HDPE geomembrane samples from different Brazilian manufacturers and thicknesses. The authors concluded that the samples had the same final storage temperature. The behavior observed in the 2L virgin sample (Figure 85A) is similar to the samples studied by Valentin et al. (2018).

Figures 83B, 84B and 85B present the loss modulus of the studied samples. These curves showed that the loss modulus was different for each set of the samples. For 1L and 1.5L samples sets, the loss modulus energy coincided with the storage modulus, considering that there is an increase in the elasticity of the material and a consequent decrease in stiffness. For the 1L sample set, there was stability in the loss modulus. However, for 1.5L and 2L samples sets, there was an oscillatory behavior in the curves. The 1L and 1.5L samples sets show that after the maximum temperatures (average for the sample set) of 55 ºC (1L sample) and 70 ºC (1.5L sample), there was a decrease in the loss modulus, which is coincident with the storage modulus and was attributed to the passage to the viscoelastic stage. The oscillation observed for the 1.5L and 2L samples sets were attributed to lost energy. One explanation for these oscillations is attributed to the thickness. In the sample with the lowest thickness, the energy loss is faster and therefore, the sample's stability is noted, while the 1.5L and 2L samples sets, both with higher thicknesses than the 1L sample, have a greater tendency to have a longer molecular rearrangement that is detectable by the DMA equipment. Thus, molecules tend to occupy the intermolecular space better; that is, the molecules, when moving, dissipate internal energy (ABDEEN, 2012).

Figures 83C, 84C and 85C show the tan-δ behavior of the samples. The tan-δ is a relationship that indicates the behavior between the energy dissipated per cycle by the stored energy. This behavior is linked to material stiffness, as stiffer materials will have lower tan-δ values. Thus, with increasing temperature, there is a gradual increase in tan-δ. In Figure 83C it was observed that the tan-δ peak is practically coincident with the end of the first stage observed in the storage module (Figure 83A). Likewise, the tan-δ peaks of 1.5L and 2L samples sets were also coincident. This behavior shows that at the end of the higher storage temperature, there is a change in the behavior of the polymer, as it is no longer stiff and passes to an elastic stage. Consequently, when passing to the viscoelastic state, the tan-δ will have high values (FIRMINO *et al.*, 2017).

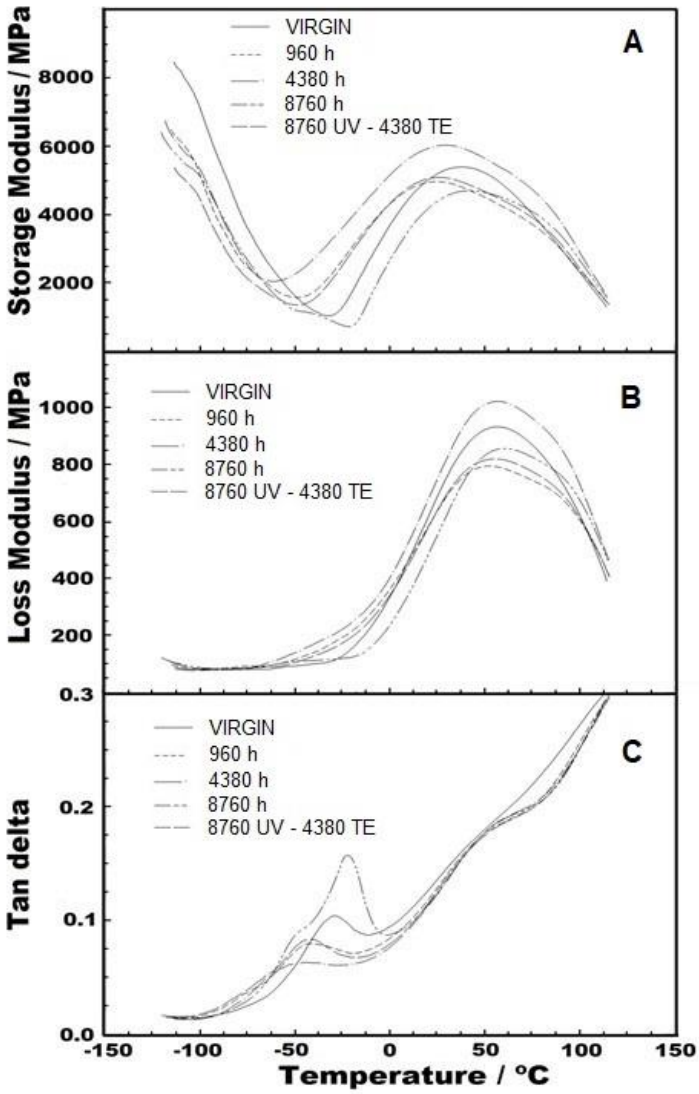

Figure 83. DMA curves of 1L sample set: (A) storage modulus, (B) loss modulus and (C) tan-δ, with a heating rate of 10 ºC min^{-1}

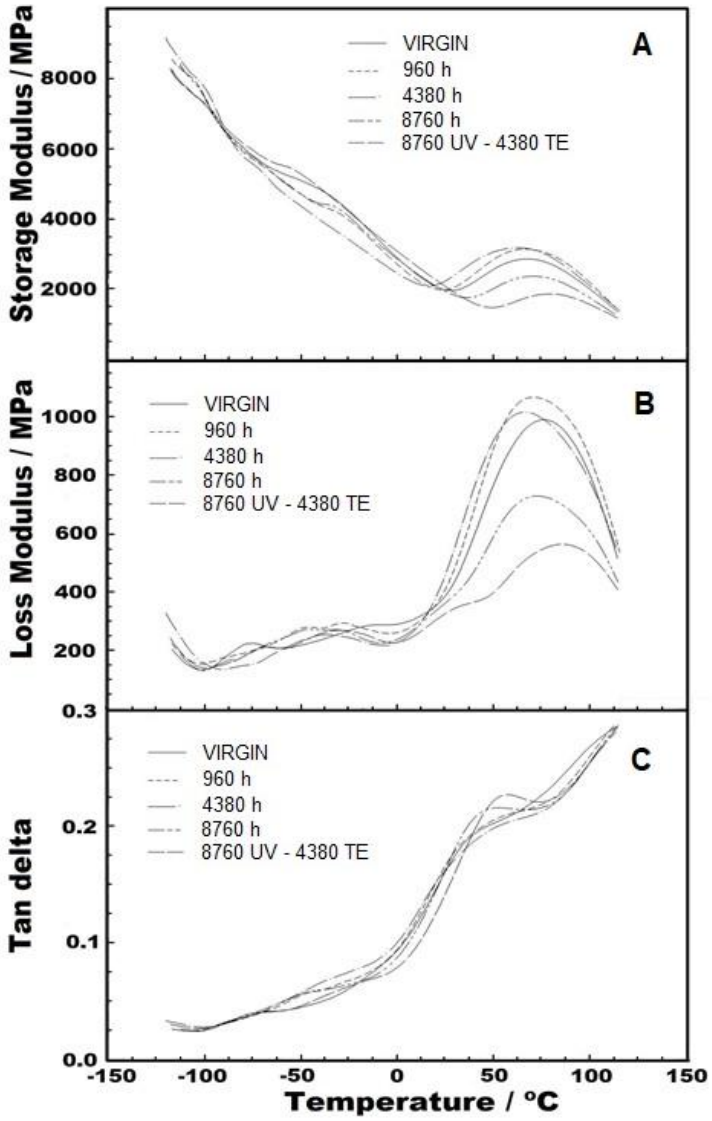

Figure 84. DMA curves of 1.5L sample set: (A) storage modulus, (B) loss modulus and (C) tan-δ, with a heating rate of 10 ºC min^{-1}

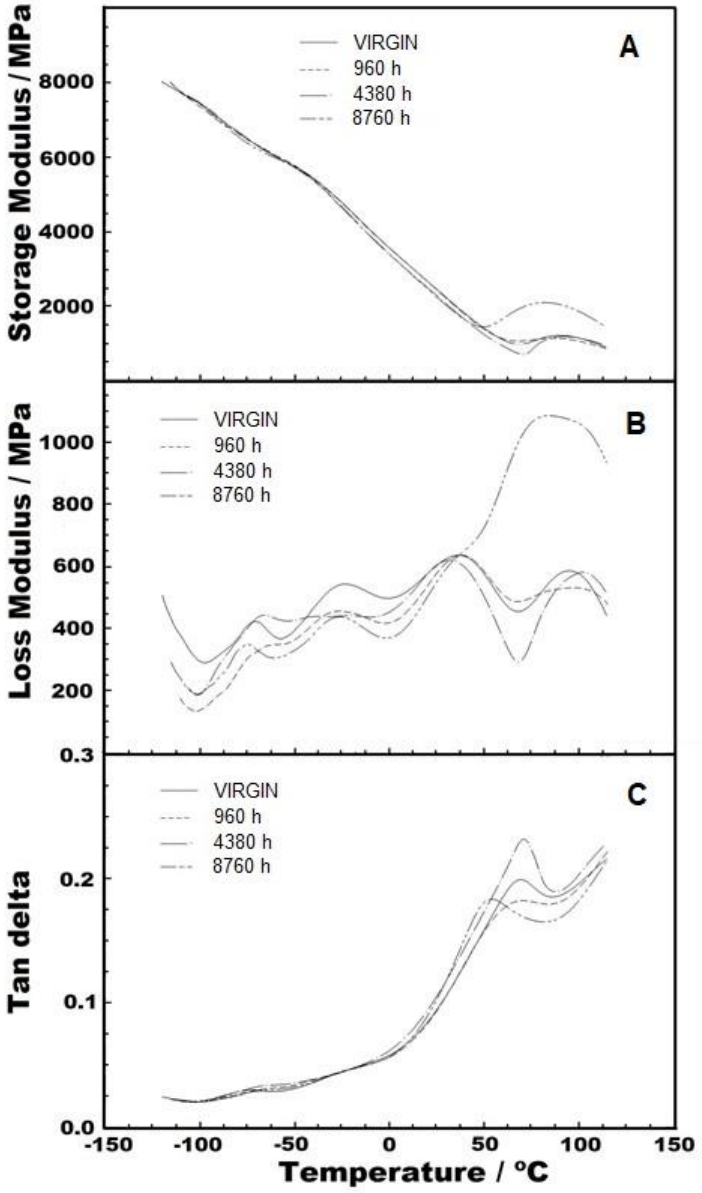

Figure 85. DMA curves of 2L sample set: (A) storage modulus, (B) loss modulus and (C) tan-δ, with a heating rate of 10 ºC min^{-1}

4.3 Complementary analysis

Figure 86 shows the FTIR analysis for the UV fluorescent exposure device and the xenon arc exposure chamber (1L sample), highlighting the range from 600 to 3100 cm^{-1} to check the possibility of formations, breaks in the functional groups, and oxidative reactions. The analyzed samples are formed by repetitions of CH_2 groups. Consequently, the appearance of absorbance bands characteristic of simple C–H bonds and Covalent C–C bonds is expected using this technique (COLTHUP *et al.*, 1990; KOENIG, 1999).

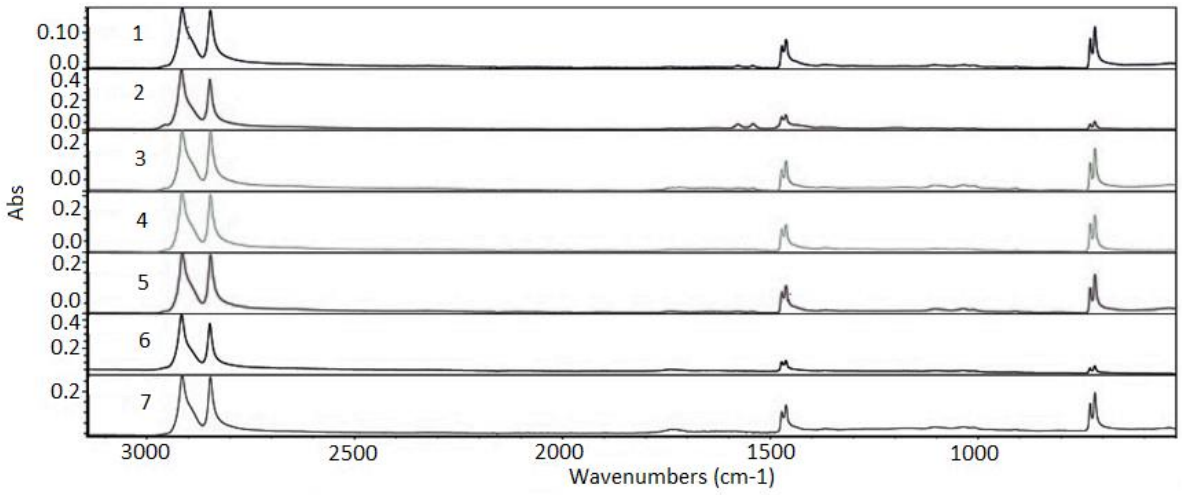

Figure 86. Absorption spectra region from 600 to 3100 cm^{-1}. 1—virgin sample (1L); 2—960 h xenon arc sample; 3—1639 h xenon arc sample; 4—2160 h xenon arc sample; 5—960 h UV fluorescent sample; 6—4380 h UV fluorescent sample; and 7—8760 h UV fluorescent sample

The three modes of the C–H link vibration can be observed through the spectrum. The bands observed in the range of 2800 to 3000 cm^{-1} refer to axial deformations C-H (Figure 87). The angular vibration of CH_2 was observed in the range of 1400 to 1500 cm^{-1} (Figure 88) and the bands referring to the asymmetric deformation of CH_2 were noted in the region of 700–730 cm^{-1} (Figure 89) (KOENIG, 1999). The low-intensity bands observed in the region between 1000–1250 cm^{-1} refer to the link's vibrations C–C (Figure 90) (STUART, 2004). It was not possible to notice a significant variation in the obtained spectra, since the absorption intensities of the bands were close.

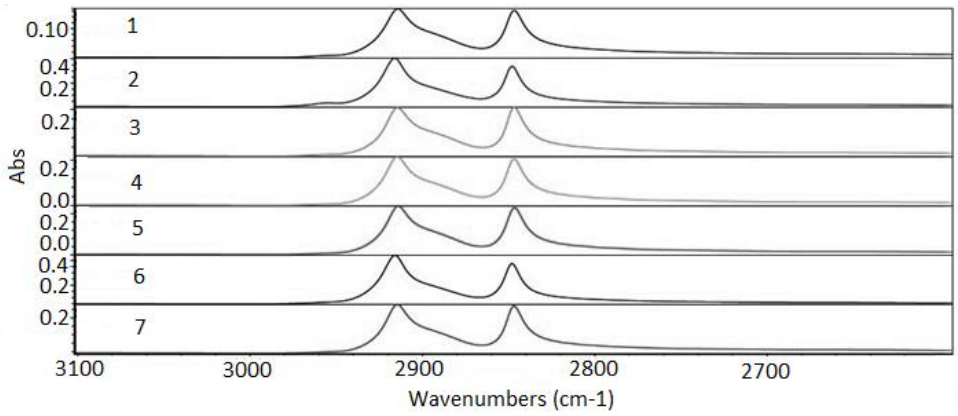

Figure 87. Absorption spectra region from 3100 to 2600 cm^{-1}. 1—virgin sample (1L); 2—960 h xenon arc sample; 3—1639 h xenon arc sample; 4—2160 h xenon arc sample; 5—960 h UV fluorescent sample; 6—4380 h UV fluorescent sample; and 7—8760 h UV fluorescent sample

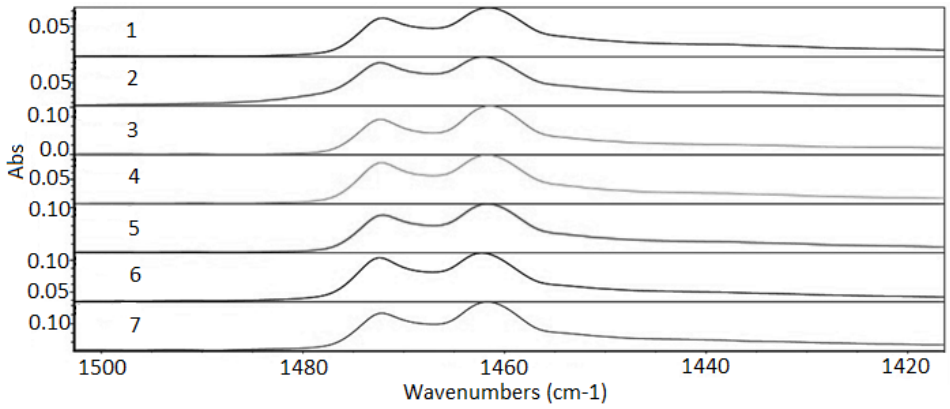

Figure 88. Absorption spectra region from 1420 to 1500 cm^{-1}. 1—virgin sample (1L); 2—960 h xenon arc sample; 3—1639 h xenon arc sample; 4—2160 h xenon arc sample; 5—960 h UV fluorescent sample; 6—4380 h UV fluorescent sample; and 7—8760 h UV fluorescent sample

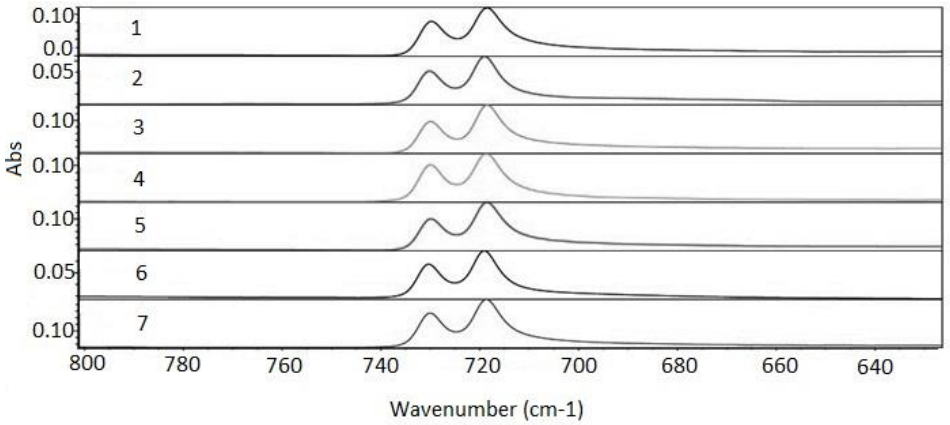

Figure 89. Absorption spectra region from 620 to 800 cm^{-1}. 1—virgin sample (1L); 2—960 h xenon arc sample; 3—1639 h xenon arc sample; 4—2160 h xenon arc sample; 5—960 h UV fluorescent sample; 6—4380 h UV fluorescent sample; and 7—8760 h UV fluorescent sample

It can be observed that all the functional groups characteristic of the polymer were preserved showing that the exposures carried out under different conditions did not cause the departure of any functional group and no reaction was also observed.

Variations in samples' absolute absorbance values were observed, probably related to the different conditions that samples were exposed to compared with the virgin sample. The degradations caused by the exposures can indicate small morphological changes in the polymers that did not present a trend. However, greater absolute absorbances can be observed in the total spectrum (region of 600–3100 cm^{-1}) for the exposed samples compared with the virgin sample. Moynihan (1959) also observed changes in the infrared spectra for the PTFE polymer with different morphologies and related this change to the intensity of the peaks. The intensity of the

peaks decreased with the increase in crystallinity caused by the exposure of the samples in different degradation conditions. The changes were not sufficient to cause breaks in the functional group or other reactions and did not follow a trend compared with the virgin sample.

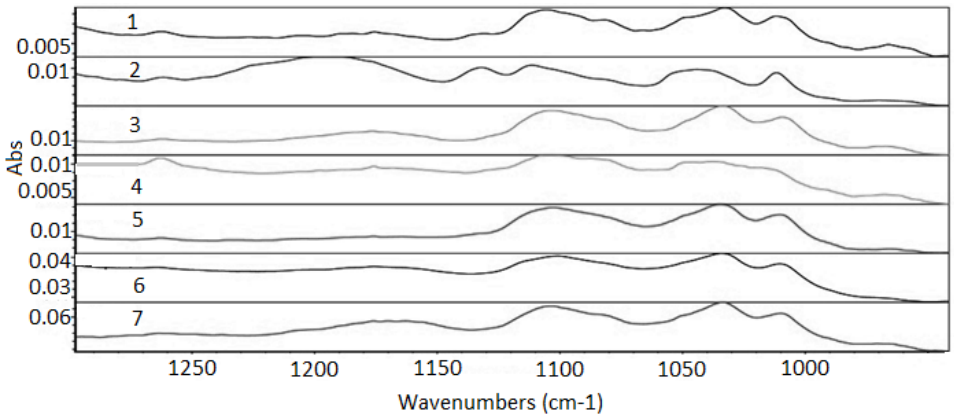

Figure 90. Absorption spectra region from 1300 to 950 cm^{-1}. 1—virgin sample (1L); 2—960 h xenon arc sample; 3—1639 h xenon arc sample; 4—2160 h xenon arc sample; 5—960 h UV fluorescent sample; 6—4380 h UV fluorescent sample; and 7—8760 h UV fluorescent sample

4.4 Comparison among exhumed and exposed samples results

The performance of the analyzed HDPE geomembrane samples in this research was verified by many properties as viscosity, SCR, tensile elongation, antioxidant depletion (Std. OIT) and thermal behavior. The comparison among exhumed and exposed samples can be possible from these properties results. Table 45 shows the behavior of the samples through the analysis of the property's values for the exhumed samples and the increase or decrease of the property's values for the exposed samples compared to the virgin sample values.

Table 45. The behavior of the exhumed and exposed samples

Sample	Viscosity	SCR Behavior	Tensile Behavior	Antioxidant Depletion	Thermal Behavior
CLIQ	High	High	TBB	High	CB; OVL
LCH	High	High	Ductile	Low	CTD; CB; INT
LTE	High	TBF	Ductile	Low	INT
MIN	High	TBF	BB	High	Normal
MIN2	Low	TBF	TBB	ATAC	Normal
LDO	Low	TBF	BB	ATAC	OVL; INT
CAM	Low	High	Ductile	ATAC	BCE
CAM1	Low	TBF	Ductile	ATAC	BCE
CAM2	High	TBF	BB	Low	BCE; CTD
1L UV fluorescent	Retained	-	Ductile	ATAC	Normal
1L Xenon arc	Decreased	-	-	Low	Normal
1L Thermal Exposure	Increased	TBF	Ductile	ATAC	DTB
1L Synergic Effect	Increased	TBF	TBB	ATAC	DTB
1.5L UV fluorescent	Retained	Decreased	Ductile	ATAC	DEV
1.5L Thermal Exposure	Retained	Decreased	Ductile	ATAC	DTB
1.5L Synergic Effect	Increased	TBF	Ductile	High	DTB
2L Thermal Exposure	Increased	TBF	Ductile	Low	DTB

ATAC – Almost the total antioxidant consumption

BB – Brittle behavior

BCE – Baseline change event

CB – Combustion

CTD – Changes in thermal decomposition

DEV – Deviation in DSC curve

DTB – Distinct Thermal Behavior

INT – Interaction between the polymer and the solution

OVL – Overlapped reactions

TBB – Tendency to brittle behavior

TBF – Tendency to brittle failure

It was observed that the antioxidant depletion is related to the geomembrane's thickness, that is, the thicker samples, LCH and 2L after 8760 h of thermal exposure, presented the highest Std. OIT values and the minor Std. OIT values decrease. Otherwise, the CAM, CAM1, LDO,

MIN2 samples presented the lowest Std. OIT values and the samples 1L after thermal exposure and 1L after the synergic effect presented the major Std. OIT values decrease.

The exhumed samples showed different changes in thermal behavior due to the environmental agents and the contact with the residues during the exposure time. The LCH sample, which was in contact with the leachate, was the sample that presented the major thermal changes. Other exhumed samples still presented significant changes in thermal behavior, as LDO, CAM2, CLIQ and LTE samples. On the other hand, the samples exposed in laboratory did not present several thermal behavior changes.

The tendency to viscosity's decrease was verified for the 1L sample after the xenon arc exposure. The high MFI values (low viscosity) were either noted for MIN2, LDO, CAM and CAM1 samples. For others exposed samples, the MFI values were retained or decreased, showing the maintenance or increased viscosity. The CLIQ, LCH, LTE, MIN and CAM2 followed the same tendency, presenting low MFI values.

Only the 1L sample after the synergic effect presented a tendency to brittle behavior. Nonetheless, some exhumed samples showed brittle behavior (MIN, LDO and CAM2 samples), and CLIQ and MIN2 samples presented a tendency to brittle behavior. The loss in the ductility there is a high impact on the geomembrane's performance.

The SCR results demonstrated low values for the exhumed samples compared to the GRI-GM13 and several decreases for the exposed samples compared to the results of the virgin samples. The LTE, MIN, MIN2, LDO, CAM1 and CAM2 samples presented the tendency to brittle failure. For the exhumed samples, only the CLIQ, LCH and CAM samples demonstrated high SCR results. The samples 1L and 2L under thermal exposure showed the tendency to brittle failure. The synergic effect also affected the SCR behavior for both samples (1L and 1.5L). According to Rowe and Sangam (2002), the time to reach the failure level of degradation of a particular property occurs for 50 % of the retained property. Some exposed samples reached 50 % of the retained SCR, as 1.5L sample after 8760 h of UV exposure (47.52 %) and after the synergic effect (7.63 %), the 1L sample after 8760 h of thermal exposure (30.36 %), and the 2L sample after 8760 h of thermal exposure (13.98 %).

5 CONCLUSIONS

5.1 Summary and main conclusion

This work aimed to understand the final conditions of nine exhumed HDPE smooth geomembranes applied in geotechnics and environment Brazilian facilities and analyzed the behavior of three virgin HDPE smooth geomembranes with different thicknesses after laboratory exposure.

The analyzed exhumed geomembranes demonstrated several changes in their properties, except for the LCH sample, the thicker sample, which presented good performance in the physical properties, but some changes in thermal decomposition. The LTE sample is changing its physical properties and could conduct a liner rupture in a short-term. The MIN, MIN2, LDO, and CAM2 samples showed brittle tensile behavior, low SCR values, low Std. OIT values and could culminate in a system failure. The CAM1 sample presented an atypical viscosity, low SCR result, unprotection from the additives against the oxidative degradation, certainly reaching the lifetime. The CLIQ and CAM samples changed their physical and thermal behavior and could provoke a liner rupture in the short-term.

The initial conditions of the virgin samples showed that none of the samples presented HP OIT values equal to or higher than 400 min. Probably none of the virgin samples presented HALS in their additive package. The 2L sample showed SCR about 60 % of the minimum required value. Highlighted for the 1L sample, which represents a geomembrane commonly used in the Brazilian market, presented a high-density value, which is incompatible with a modern HDPE geomembrane. Moreover, the same sample showed a high MFI value, low SCR, and low OIT values. The 1L sample behavior shows that this geomembrane may not have a good performance in the field.

The virgin geomembrane samples with 1.0 mm and 1.5 mm thicknesses presented some changes in their properties after the UV radiation exposure. After 2160 h of xenon arc exposure, the 1L sample showed an increase in the MFI value and a significant antioxidant depletion decrease. For the UV fluorescent radiation, after 8760 h of exposure, the same sample demonstrated losses in tensile properties and a considerable antioxidant depletion, changing its performance as a liner. This geomembrane used as a liner can compromise the engineering system. It was possible to note that the 1.5 mm-thick HDPE geomembrane, after 8760 h of UV fluorescent exposure, had losses in SCR, high antioxidant consumption, a change in the thermal behavior before the melting point, but maintained the viscosity of the polymer and preserved

the ductility, still presenting an acceptable performance as an engineering product applied as an environmental protection liner.

The samples presented several changes in some evaluated properties after the thermal exposure and the synergy exposure to UV radiation and thermal aging, highlighting for the MFI results, which demonstrated the occurrence of cross-linking reactions for all samples. Moreover, all samples presented considerable changes in SCR behavior, especially for the 1.5L sample after the synergy exposure to UV radiation and thermal aging that presented the retained SCR value lower than 10 %, and for the 2L sample after the thermal exposure, demonstrating the SCR susceptibility of these samples. Analyzing the Std. OIT results, it was observed that all of the samples presented high antioxidant depletion, especially for the 1L sample under the synergic effect exposure, which caused almost the total antioxidants' consumption, unprotecting the resin against the oxidative degradation. Finally, the 1L sample presented the most severe property's losses among the studied samples and can fail in the field after short-term under thermal exposure or a combination between UV radiation and high temperatures. The 1.5L and 2L samples still present an acceptable performance as an engineering product applied as an environmental protection liner even under the effect of the studied exposures.

Based on the obtained results of this work, the following conclusions can be detailed:

- The comparison between the CLIQ and the reference sample (1L) showed that the exhumed sample presented a different behavior in the TG curve for a heating rate of 5 $^{o}C\ min^{-1}$. The DTA curve observed that the exhumed sample presented combustion from the second mass loss stage at the same heating rate. The TMA curves without purge gas showed a range of thermal stability between 30 and 65 ^{o}C for the reference sample, attributed to molecular relaxation. The exhumed sample did not have the same relaxation. For the exhumed sample, the physical properties values showed lower MFI result, higher SCR result, and tensile brittle behavior trend. The differences between the samples verified in those analyses can indicate that changes probably occurred in the polymer structure for the exposed sample.

- For the LTE and LCH samples comparison, the TG analyses showed significant changes in the LCH sample's thermal decomposition. The organic material absorption by the geomembrane probably changed the material's behavior, causing interaction reactions between the polymer and the leachate. For the DSC analyses, the behavior seen in the

LTE sample was not observed in the LCH sample. It indicates that there was probably an effect of leachate in the sample, causing a change in the heat flow. The DMA analyses showed that the LCH sample is less brittle than the LTE sample, that is, more elastic. These results follow the physical results because the LTE sample presented low stress crack resistance and low tensile elongation at break. Meanwhile, the physical results of the LCH sample showed that this sample demonstrated good performance, even after the field exposure.

- The MIN and MIN2 samples, during the exposure time, could experience exposure to environmental agents and chemical contact with mining effluents. The MIN2 sample obtained the highest MFI value, which was double the value of the MIN sample. The samples presented high antioxidant depletion at 200 °C, verified by the Std. OIT results. The MIN2 sample had the lowest Std. OIT value; the longer exposure time may have influenced this result. Both samples presented similar stress cracking and tensile behaviors, with low tensile elongation values (brittle behavior) and low-stress crack resistance. Thus, the analyses conducted on the geomembrane samples, especially for the tensile, stress cracking, and viscosity properties, demonstrate that changes occurred in the polymer's structure after exposures in the field, indicating that the product had reached the end of its lifespan.

- For the LDO sample, it was observed that the high value of the sample's density is related to its crystallinity. The sample's crystallinity is considered higher than the crystallinity of the HDPE geomembranes. The low SCR value of the sample is associated with a high MFI value and high crystallinity. The tensile behavior of the sample presented a brittle tendency, observed by the low tensile elongation, which corroborates with the low SCR value. The results still demonstrated that the antioxidants were almost completely depleted, and the morphological changes in the polymer were happening. The DMA results showed an interaction of the impregnated material with the polymer. Therefore, the analyzed HDPE exhumed geomembrane showed changes in its properties due to aging mechanisms and the waste contact at the site. Thus, this material applied as an environmental protection liner can cause a system failure, compromising the environmental protection of the area.

- The comparison of three HDPE geomembrane samples exhumed from two shrimp farming ponds showed that the first heating of the DSC analysis, which represents the samples' final conditions in the field, demonstrated events before the melting point for all the samples. The CAM1 sample presented an atypical MFI result because the result was high, and the material melted fast. The OIT test results for the CAM1 sample demonstrated the unprotection from the additives to the polymer against thermo-oxidative degradation after exposure. Changes in viscosity, stress crack resistance, and polymer protection by the antioxidants demonstrated that the environmental exposure in the field changed the initial conditions of the CAM1 sample. Moreover, the CAM2 sample presented a high-density value, brittle tensile behavior, and a different thermal behavior than the other samples. Finally, the CAM1 and CAM2 samples presented several changes in their properties due to the field exposure, demonstrating that applying these geomembranes as liners can culminate in financial and environmental losses.

- The behavior of 1.0 mm-thick HDPE virgin geomembrane under exposures to two ultraviolet radiation devices for different exposure times was studied. The sample under the xenon arc exposure chamber showed a trend to increase the MFI's values during the exposure time. This increasing trend can indicate changes in the polymer's morphology. The tensile behavior analysis showed a sample's trend to lose its ductileness (resistance and elongation decreased about 30 %) without presenting brittle behavior. The samples' OIT test results under both device exposures showed faster antioxidant depletion for the standard OIT test than the high-pressure OIT test. After 8760 h of exposure, the sample under UV fluorescent device exposure decreased 75 % for the Std. OIT test and 36 % for the HP OIT test. For the xenon arc exposure chamber, the sample tested demonstrated a decrease of 35 % for the Std. OIT test and 8% for the HP OIT test after 2160 h of exposure.

- The analyses of an HDPE geomembrane sample with 1.5 mm of thickness exposed by UV radiation in the laboratory showed decreases of 11.60 % and 7.20 % after 8760 h of exposure, respectively, for the tensile resistance and tensile elongation. The geomembrane maintained the ductile behavior after the UV exposure. The sample showed SCR's final decrease of 52.48 % compared to the virgin SCR result. The tensile and SCR results demonstrated the higher susceptibility of the sample for the stress cracking than the ductility losses. It was observed that there was a considerable

antioxidant depletion after 8760 h of exposure, evidenced by the Std. OIT results, reaching a decrease of 89.19 % compared to the virgin Std. OIT result. This antioxidant depletion behavior showed that, after 8760 h of UV laboratory exposure, the geomembrane's resin is almost unprotected against oxidative degradation. For the exposed samples, a deviation in the DSC curves was observed before the melting point, attributed to the effect of exposure of the material to the UV radiation.

- The samples after laboratory thermal exposure and after the synergy exposure to UV radiation and thermal aging presented decreases in the MFI values, demonstrating the occurrence of cross-linking reactions. After 8760 h of thermal exposure, the evaluated samples presented tensile resistance result decreases between 10 and 25 %, demonstrating changes in this property due to the exposure. It was observed that the 1.5L sample demonstrated the highest retained tensile elongation among the samples tested for both exposures, of 88.06 % (thermal) and 85.85 % (synergic). Otherwise, the 1L sample presented the lowest retained tensile elongation of the samples evaluated of 69.08 % (thermal) and 59.0 % (synergic). This sample demonstrated a considerable ductility loss, almost reaching 50 %. It was possible to note that all samples presented considerable changes in SCR behavior after 8760 h of thermal exposure, highlighted for the 2L sample, which presented the highest SCR value decrease (86.02 %). After the synergy exposure to UV radiation and thermal aging, the 1.5L sample presented a high SCR value decrease (92.37 %). The samples tested presented several decreases in the Std. OIT values. The 1L sample showed the highest antioxidant depletion among the samples analyzed. The thicker sample (2L) demonstrated the lowest antioxidant depletion after the thermal exposure. The 1L sample obtained a decrease of 72.09 % after 8760 h of UV exposure in the Std. OIT value. The synergic effect between the UV (8760 h) and thermal (4380 h) exposures caused almost the total antioxidants' consumption (Std. OIT value decrease of 98.44 %). The general retained HP OIT results showed values higher than 40 %, demonstrating a tendency to stabilize. The DMA results showed three distinct behaviors observed in three temperature ranges in the storage modulus for the analyzed samples sets. For the 1L sample set, there was stability in the loss modulus. However, for 1.5L and 2L samples sets, there was an oscillatory behavior in the loss modulus curves, attributed to lost energy.

Unfortunately, in Brazil it is not common to save and store geomembrane samples to the product installed in the field to monitor the properties of the material during the service life of the work. Furthermore, it is important to specify the quality control and inspection by the contractor during the delivery of the product at the field. This inspection collaborates to the verification of the product's conformance to the project's specification. In addition to excellent resin, a suitable additive package, good industrial processability, good manufacturing quality control, satisfactory material specification for applications and good installation practice must be specified and supervised in the field by the designer. The implications of bad installation procedures can lead to a short-term service life of high-density polyethylene geomembranes. In Brazil, there is a technical standard concerning geomembrane installation practice. This document includes the importance of the type of application to protect the product and good workmanship such as proper welding equipment, field seam testing, destructive seam testing, and avoiding damage and stress concentration in the product.

It was noted that the HDPE geomembranes in Brazil do not present HALS in their additive package. Moreover, the initial SCR values demonstrated the susceptibility of the virgin geomembranes to this common phenomenon for semicrystalline polymers. After the laboratory exposure, highlighted the high reduction of the SCR values for all samples. The absence of HALS and the low initial SCR values decrease the product's durability and reduce the geomembrane's lifetime. The exhumed samples results showed the vulnerability of the Brazilian HDPE geomembranes and demonstrated, in general, the short-term durability of this product. Finally, this research evidenced the necessity to homogenise the resins and additives of the Brazilian HDPE geomembranes to guarantee products with long-term durability, avoiding losses in terms of human lives, environmental impacts, and financial costs.

5.2 Recommendations for future work

The study at the laboratory of the textured HDPE geomembranes is recommended due to the increase in the use, especially in landfills. The durability analysis of these geomembranes does not present many published papers around the world. It is interesting to conduct the chemical compatibility analysis with leachate and other substances beyond the UV and thermal exposures analyses.

It interesting to carry on exhumed seams samples analysis to understand the seams behavior after the field exposure, for thermo-fusion technique by hot wedge and hot air,

including different geomembrane thicknesses, applications, and exposure times. This issue presents a lack of information in the scientific area.

Beyond using physical and thermal analyses to understand the final conditions of the HDPE geomembranes, it recommends performing permeability tests with the HDPE geomembrane samples after the exhumation or the laboratory exposure.

REFERENCES

ABDELAAL, F. B. *et al.* Antioxidant depletion from HDPE and LLDPE geomembranes without HALS in an extremely low pH solution. *In*: 2ND PAN AMERICAN CONFERENCE ON GEOSYNTHETICS, 2012, Lima.

ABDELAAL, F. B.; ROWE, R. K. Effect of chlorinated water on the antioxidant depletion of HDPE geomembrane without HALS, *In*:10TH INTERNATIONAL CONFERENCE ON GEOSYNTHETICS, 2014, Berlin.

ABDELAAL, F. B.; ROWE, R. K. Effect of high temperatures on antioxidant depletion from different HDPE geomembranes. **Geotextiles and Geomembranes**, n. 42, p. 284-301, 2014. Doi: http://dx.doi.org/10.1016/j.geotexmem.2014.05.002.

ABDELAAL, F. B.; ROWE, R. K.; ISLAM, M. Z. Effect of leachate composition on the long-term performance of a HDPE geomembrane. **Geotextiles and Geomembranes**, n. 42, p. 348-362, 2014. Doi: http://dx.doi.org/10.1016/j.geotexmem.2014.06.001.

ABDELAAL, F. B. *et al.* Effect of high temperatures on the physical and mechanical properties of HDPE geomembranes in air. **Geosynthetics International**, n. 22, p. 207-224, 2015. Doi: https://doi.org/10.1680/gein.15.00006.

ABDELAAL, F. B.; MORSY, M. S.; ROWE, R.K. Long-term performance of a HDPE geomembrane stabilized with HALS in chlorinated water. **Geotextiles and Geomembranes**, n. 47, p. 815-830, 2019. Doi: https://doi.org/10.1016/j.geotexmem.2019.103497.

ABDELAAL, F. B.; ROWE, R. K. Degradation of an HDPE geomembrane without HALS in chlorinated water. **Geosynthetics International**, n. 26, p. 354-370, 2019. Doi: https://doi.org/10.1680/jgein.19.00016.

ABDEEN, M. A. Static and dynamic mechanical properties of poly (vinyl chloride) loaded with aluminum oxide nano powder. **Materials and Design**, n. 33, p. 523–528, 2012. Doi: 10.1016/j.matdes.2011.04.059.

ADAMS, M.W.; WAGNER, N. Evaluating physical property integrity of a geomembrane used at a wastewater treatment facility for 11 years. **Geotechnical Fabrics Report**, n. 18, p. 36-39, 2000.

AMINABHAVI, T. M.; NAIK, H. G. Chemical compatibility testing of geomembranes - sorption/desorption, diffusion, permeation and swelling phenomena. **Geotextiles and**

Geomembranes, n. 16, p. 333-354, 1998. Doi: https://doi.org/10.1016/S02661144(98)00017-X.

AMERICAN SOCIETY FOR TESTING AND MATERIALS. **ASTM D792:** standard test methods for density and specific gravity (relative density) of plastics by displacement. West Conshohocken: ASTM, 2020.

AMERICAN SOCIETY FOR TESTING AND MATERIALS. **ASTM D1004:** standard test method for tear resistance (graves tear) of plastic film and sheeting. West Conshohocken: ASTM, 2021.

AMERICAN SOCIETY FOR TESTING AND MATERIALS. **ASTM D1238:** standard test method for melt flow rates of thermoplastics by extrusion plastometer. West Conshohocken: ASTM, 2020.

AMERICAN SOCIETY FOR TESTING AND MATERIALS. **ASTM D3895:** standard test method for oxidative-induction time of polyolefins by differential scanning calorimetry. West Conshohocken: ASTM, 2019.

AMERICAN SOCIETY FOR TESTING AND MATERIALS. **ASTM D4218:** standard test method for determination of carbon black content in polyethylene compounds by the muffle-furnace technique. West Conshohocken: ASTM, 2020.

AMERICAN SOCIETY FOR TESTING AND MATERIALS. **ASTM D4833:** Standard Test Method for Index Puncture Resistance of Geomembranes and Related Products. West Conshohocken: ASTM, 2020.

AMERICAN SOCIETY FOR TESTING AND MATERIALS. **ASTM D5199:** standard test method for measuring the nominal thickness of geosynthetics. West Conshohocken: ASTM, 2019.

AMERICAN SOCIETY FOR TESTING AND MATERIALS. **ASTM D5397:** standard test method for evaluation of stress crack resistance of polyolefin geomembranes using notched constant tensile load test. West Conshohocken: ASTM, 2020.

AMERICAN SOCIETY FOR TESTING AND MATERIALS. **ASTM D5596:** standard test method for microscopic evaluation of the dispersion of carbon black in polyolefin geosynthetics. West Conshohocken: ASTM, 2021.

AMERICAN SOCIETY FOR TESTING AND MATERIALS. **ASTM D5721:** standard

practice for air-oven aging of polyolefin geomembranes. West Conshohocken: ASTM, 2018.

AMERICAN SOCIETY FOR TESTING AND MATERIALS. **ASTM D5885:** standard test method for oxidative induction time of polyolefin geosynthetics by high-pressure differential scanning calorimetry. West Conshohocken: ASTM, 2020.

AMERICAN SOCIETY FOR TESTING AND MATERIALS. **ASTM D6693:** standard test method for determining tensile properties of nonreinforced polyethylene and nonreinforced flexible polypropylene geomembranes. West Conshohocken: ASTM, 2020.

AMERICAN SOCIETY FOR TESTING AND MATERIALS. **ASTM D7238:** standard test method for effect of exposure of unreinforced polyolefin geomembrane using fluorescent uv condensation apparatus. West Conshohocken: ASTM, 2020.

AMERICAN SOCIETY FOR TESTING AND MATERIALS. **ASTM G155:** standard practice for operating xenon arc light apparatus for exposure of non-metallic materials. West Conshohocken: ASTM, 2013.

BENSON, C. H.; KUCUKKIRCA, I. E.; SCALIA, J. Properties of geosynthetics exhumed from a final cover at a solid waste landfill. **Geotextiles and Geomembranes**, n. 28, p. 536-546, 2010. Doi: http://dx.doi.org/10.1016/j.geotexmem.2010.03.001.

BROWN, M. E. **Introduction to thermal analysis**. 1st ed. New York: Chapman and Hall, 1988.

BUASZCZYK, G. **Durabilidade de polietileno em vinhaça quente e fresca em usina de açúcar e álcool**. 2013. Dissertação de Mestrado – Departamento de Engenharia de Materiais, Universidade Federal de São Carlos, São Carlos, 2013.

BUENO, M. T. N. S. **Durabilidade Análise da degradação de alguns geossintéticos em contato com fluidos agressivos**. 2007. Tese de Doutorado – Departamento de Engenharia Civil, Universidade de Brasília, Brasília, 2007.

CALABRIA, C. R.; PEGGS, I. D. Investigation of geomembrane destructive field seam test failures: landfill cover. **Geotextiles and Geomembranes**, n. 15, p. 419-440, 1997. Doi: https://doi.org/10.1016/S0266-1144(97)10019-X.

CASSU, S. N.; FELISBERTI, M. I. Comportamento dinâmico-mecânico e relaxações em polímeros e blendas poliméricas. **Química Nova**, n. 28, p. 255-263, 2005. Doi: http://dx.doi.org/10.1590/S0100-40422005000200017.

CAZZUFFI, D.; GIOFFRÈ, D. Lifetime assessment of exposed PVC-P geomembranes installed on Italian dams. **Geotextiles and Geomembranes**, n. 48, p. 130-136, 2020. Doi: https://doi.org/10.1016/j.geotexmem.2019.11.015.

CHIRINOS-PADRÓN, A. J.; ALLEN, N. S. Aspects of polymer stabilization. In: HAMID, A. H.; AMIN, M. B.; MAADHAH, A. G. (Ed.). **Handbook of polymer degradation**. New York: Marcel Dekker, 1992.

COELHO, M. F. L.; LAVOIE, F. L. Comportamento da geomembrana de PEAD exposta ao envelhecimento acelerado. *In*: 14º CONGRESSO BRASILEIRO DE POLÍMEROS, 2017, Águas de Lindóia.

COLTHUP, N.B.; DALY, L. H.; WIBERLEY, S. E. **Introduction to infrared and raman spectroscopy**, 3rd ed. Cambridge: Academic Press, 1990.

DIX, J. S.; BURKINSHAW, J. S. HDPE resin developments. **Geotextiles and Geomembranes**, n. 10, p. 621-624, 1991. Doi: https://doi.org/10.1016/B978-1-85166-644-7.50027-6.

DOLEZ, P. I. *et al.* Reduction in hdpe geomembrane thermal expansion using nanoclay particles. **Advanced Materials: TechConnect Briefs**, n. 1, p. 296-299, 2016.

DOLEZ, P. I.; WELTROWSKI, M.; DAVID, E. Study of the Parameters Controlling Nanoparticle Dispersion for Nanocomposite Geomembrane Applications. *In*: GEOTECHNICAL FRONTIERS, 2017, Orlando.

EITH, A. W.; KOERNER, G. R. Assessment of HDPE geomembrane performance in a municipal waste landfill double liner system after eight years of service. **Geotextiles and Geomembranes**, n. 15, p. 277-287, 1997. Doi: https://doi.org/10.1016/S0266-1144(97)10010-3.

EWAIS, A. M. R.; ROWE, R. K.; SCHEIRS, J. Degradation behaviour of HDPE geomembranes with high and low initial high-pressure oxidative induction time. **Geotextiles and Geomembranes**, n. 42, p. 111-126, 2014. Doi: http://dx.doi.org/10.1016/j.geotexmem.2014.01.004.

EWAIS, A. M. R.; ROWE, R. K.; BRACHMAN, R. W. I. Effect of gravel deterioration on the time to failure of an HDPE geomembrane aged under simulated landfill liner conditions. *In*: 3RD PAN AMERICAN CONFERENCE ON GEOSYNTHETICS, 2016, Miami.

EWAIS, A. M. R. *et al.* 17-year elevated temperature study of HDPE geomembrane longevity in air, water and leachate. **Geosynthetics International**, n. 25, p. 525-544, 2018. Doi: https://doi.org/10.1680/jgein.18.00016.

FAY, J. J.; KING, R. E. In: Antioxidants for geosynthetic resins and applications. HSUAN, Y. G.; KOERNER, R. M. (Ed.). **Geosynthetic resins, formulations and manufacturing**. St Paul: Industrial Fabric Assn Intl, 1994.

FERREIRA, L. C.; REIS, E. C.; VIEIRA, N. M. R. Caracterização do Efluente da Etapa de Filtragem de um Concentrado de Minério de Ferro. *In*: 70º CONGRESSO ANUAL DA ABM (ASSOCIAÇÃO BRASILEIRA DE METALURGIA, MATERIAIS E MINERAÇÃO), 2015, Rio de Janeiro.

FIRMINO, H. C. T.; DAS CHAGAS, T. F.; DE MELO, P. M. A.; Da Silva, L. B. Characterization of the particulate composites of high density polyethylene/mollusk shell powder. **Revista Materia**. n. 22, p. 1-12, 2017. Doi: 10.1590/S1517-707620170002.0164.

GABBOTT, P. **Principles and applications of thermal analysis**. 1st ed. Oxford: Blackwell Publishing Ltd., 2008.

GEOSYNTHETICS RESEARCH INSTITUTE. **GRI—GM13:** test methods, test properties and testing frequency for high density polyethylene (HDPE) smooth and textured geomembranes. Folsom: GRI, 2021.

GIROUD, J. P. Relationship between geomembrane density and carbon black content. **Geosynthetics International**, n. 1, p. 93-98, 1994. Doi: https://doi.org/10.1680/gein.1.0005.

GRASSIE, N.; SCOTT, G. **Polymer degradation and stabilization**. 1st ed. New York: Cambridge University Press, 1985.

GREENWOOD, J. H.; SCHROEDER, H. F.; VOSKAMP, W. **Durability of geosynthetics**. 1st ed. Gouda: Curnet, 2012.

GU, J., XU, H., WU, C. Thermal and crystallization properties of HDPE and HDPE/PP blends modified with DCP. **Advances in Polymer Technology**, n. 33**,** p. 21384-21389, 2014. Doi: https://doi.org/10.1002/adv.21384.

GULEC, S. B.; EDIL, T. B.; BENSON, C. H. Effect of acidic mine drainage on the polymer

properties of an HDPE geomembrane. **Geosynthetics International**, n. 11, p. 60-72, 2004. Doi: https://doi.org/10.1680/gein.2004.11.2.60.

HAINES, P. J. (Ed.). **Principles of thermal analysis and calorimetry**. 1st ed. London: RSC, 2002.

HALSE, Y. H.; KOERNER, R. M.; LORD Jr., A. E. In: Laboratory evaluation of stress cracking in HDPE geomembrane seams. KOERNER, R. M. (Ed.). **Durability and aging of geosynthetics**. London: Elsevier, 1989.

HALSE, Y. H.; LORD Jr., A. E.; KOERNER, R. M. In: Ductile-to-brittle transition time in polyethylene geomembrane sheet. KOERNER, R. M. (Ed.). **Geosynthetic testing for waste containment applications**. West Conshohocken: ASTM International, 1990.

HATAKEYAMA, T.; QUINN, F. X. **Thermal analysis:** fundamentals and applications to polymer science. 2nd ed. Baffins Lane Chichester: John Wiley & Sons Ltd., 1999.

HOU, J. *et al.* A DEM analysis of geomembrane-lined landfill subject to vertical loading. **Geotextiles and Geomembranes**, n. 49, p. 369-375, 2021. Doi: https://doi.org/10.1016/j.geotexmem.2020.10.008.

HSUAN, Y. G., KOERNER, R. M., LORD JR., A. E. Stress-cracking resistance of high-density polyethylene geomembranes. **Journal of Geotechnical Engineering**, n. 119, p. 1840-1855, 1993. Doi: https://doi.org/10.1061/(ASCE)0733-9410(1993)119:11(1840).

HSUAN, Y. G.; KOERNER, R. M. The single point-notched constant Tension load test: a quality control test for assessing stress crack resistance. **Geosynthetics International**, n. 2, p. 831-843, 1995. Doi: https://doi.org/10.1680/gein.2.0038.

HSUAN, Y. G.; KOERNER, R. M. Antioxidant depletion lifetime in high density polyethylene geomembranes. **Journal of Geotechnical and Geoenvironmental Engineering**, n. 124, p. 532-541, 1998. Doi: https://doi.org/10.1061/(ASCE)1090-0241(1998)124:6(532).

HSUAN, Y. G. Data base of field incidents used to establish HDPE geomembrane stress crack resistance specifications. **Geotextiles and Geomembranes**, n. 18, p. 1-22, 2000. Doi: https://doi.org/10.1016/S0266-1144(99)00018-7.

HSUAN, Y. G. et al. Long-term performance and lifetime prediction of geosynthetics. *In*: EUROGEO 4, THE 4TH EUROPEAN GEOSYNTHETICS CONFERENCE, 2008,

Edinburgh.

IBRA INSTITUTO BRASILEIRO DE ANÁLISES. **Relatório de Ensaios nº 130467**, Sumaré, 2019.

ISLAM, M. Z.; ROWE, R. K. Effect of HDPE geomembrane thickness on the depletion of antioxidants. *In*: 60TH CANADIAN GEOTECHNICAL CONFERENCE AND THE 8TH JOINT CGS/IAH-CNC GROUNDWATER CONFERENCE, 2007, Ottawa.

ISLAM, M. Z.; GROSS, B. A.; ROWE, R. K. Degradation of exposed LLDPE and HDPE geomembranes: a review. *In*: GEO-FRONTIERS 2011: ADVANCES IN GEOTECHNICAL ENGINEERING, 2011, Dallas.

JESSBERGER, H. L.; HEIBROCK, G.; Development of a safety concept for landfill liner systems. In: AUGUST, H.; HOLZLOHNER, U.; MEGGYES, T. (Eds.). **Advanced Landfill Liner Systems**. London: Thomas Telford: London, 1997.

JIANG, T. *et al.* Application of antioxidant and ultraviolet absorber into HDPE: enhanced resistance to UV irradiation. **e-Polymers**, n. 19, p. 499–510, 2019. Doi: https://doi.org/10.1515/epoly-2019-0053.

KAY, D.; BLOND, E.; MLYNAREK, J. Geosynthetics durability: a polymer chemistry issue. *In*: 57TH CANADIAN GEOTECHNICAL CONFERENCE, 2004, Quebec.

KELEN, T. **Polymer degradation**. 1st ed. New York: Van Nostrand Reinhold Co., 1983.

KHONAKDAR, H. A. *et al.* An investigation of chemical crosslinking effect on properties of high-density polyethylene. **Polymer**, n. 44, p. 4301–4309, 2003, Doi: https://doi.org/10.1016/S0032-3861(03)00363-X.

KOENIG, J. L. **Spectroscopy of polymers**. 2nd ed. Washington: American Chemical Society, 1999.

KOERNER, R. M.; LORD Jr., A. E.; HSUAN, Y. H. Arrhenius modelling to predict geosynthetics degradation. **Geotextiles and Geomembranes**, n. 11, p. 151-183, 1992. Doi: https://doi.org/10.1016/0266-1144(92)90042-9.

KOERNER, G. R.; EITH, A. W.; TANESE, M. Properties of exhumed HDPE field waves. **Geotextiles and Geomembranes**, n. 17, p. 247-261, 1999. Doi:

https://doi.org/10.1016/S0266-1144(98)00024-7.

KOERNER, R. M. **Designing with geosynthetics**. 5th ed. New Jersey: Prentice Hall, 2005.

KOERNER, G. R.; KOERNER, R. M. Long-term temperature monitoring of geomembranes at dry and wet landfills. **Geotextiles and Geomembranes**, n. 24, p. 72-77, 2006. Doi: https://doi.org/10.1016/j.geotexmem.2004.11.003.

KOERNER, G. R.; HSUAN, Y. G.; KOERNER, R. M. The durability of geosynthetics. In: SARSBY, R. W. (Ed.). **Geosynthetics in civil engineering**. Cambridge: Woodhead Published, 2007.

KOERNER, R. M.; HSUAN, Y. G.; KOERNER, G. R. Freshwater and geosynthetics; a perfect marriage. *In*: 1ST PAN AMERICAN CONFERENCE ON GEOSYNTHETICS, 2008, Cancun.

KOERNER, R. M.; HSUAN, Y. G.; KOERNER, G. R. Lifetime predictions of exposed geotextiles and geomembranes. **Geosynthetics International**, n. 24, p. 198-212, 2017. Doi: https://doi.org/10.1680/jgein.16.00026.

KRONGAUZ, V. V. Diffusion in polymers dependence on crosslink density. Eyring approach to mechanism. **Journal of Thermal Analysis and Calorimetry**, n. 102, p. 435–445, 2010. Doi: http://dx.doi.org/10.1007/s10973-010-0922-6.

KSIQCZAK, A.; KSIQCZAK, T.; ZIELENKIEWICZ, T. Influence of purity on the thermal stability of solid organic compounds. **Journal of Thermal Analysis and Calorimetry**, n. 77, p. 233–242, 2004. Doi: http://dx.doi.org/10.1023/B:JTAN.0000033208.42367.97.

LAVOIE, F. L.; BUENO, B. S.; LODI, P. C. Influence of the degradation on the stress cracking values of high-density polyethylene (HDPE) geomembranes after different exposures. **The Electronic Journal of Geotechnical Engineering**, n. 17, p. 3097-3104, 2012.

LAVOIE, F. L.; BUENO, B. S.; LODI, P. C. Degradação de membrana impermeabilizante de polietileno de alta densidade usada em tanques de armazenamento de vinhaça. **Polímeros**, n. 23**,** p. 690-695, 2013. Doi: http://dx.doi.org/10.4322/polimeros.2013.010.

LAVOIE, F. L.; BUENO, B. S.; LODI, P. C. Evaluation of stress cracking on geomembranes after accelerated tests. **Dyna**, n. 183, p. 215-220, 2014. Doi: http://dx.doi.org/10.15446/dyna.v81n183.34447.

LAVOIE, F. L. *et al.* Durability of HDPE geomembranes: an overview, **Química Nova**, n. 43(5), p. 656-667, 2020. Doi: https://doi.org/10.21577/0100-4042.20170540.

LAVOIE, F. L. *et al.* Study of an exhumed HDPE geomembrane used in an industrial water pond: physical and thermoanalytical characterisations. **Results in Materials**, n. 8 (100131), p. 1-9, 2020-1. Doi: https://doi.org/10.1016/j.rinma.2020.100131.

LAVOIE, F. L. *et al.* HDPE geomembranes for environmental protection: two case studies. **Sustainability**, n. 12 (8682), p. 1-19, 2020-2. Doi: https://doi.org/10.3390/su12208682.

LAVOIE, F. L. *et al.* Laboratory study of the ultraviolet radiation effect on an HDPE geomembrane. **Membranes**, n. 11 (390), p. 1-14, 2021. Doi: https://doi.org/10.3390/membranes11060390.

LAVOIE, F. L. *et al.* Environmental protection with HDPE geomembranes in mining facility constructions. **Construction Materials**, n. 1, p. 122-133, 2021-1. Doi: https://doi.org/10.3390/constrmater1020009.

LEITE, A. F. R.; LIGEIRO, L. P. M. **Características, tratamento e potencial utilização de esgoto produzido em shopping centers: estudo de caso do Catarina Fashion Outlet**. 2017. Trabalho de Graduação – Departamento de Engenharia Hidráulica e Ambiental, Universidade de São Paulo, São Paulo, 2017.

LODI, P. C.; BUENO, B. S.; ZORNBERG, J. G. Considerations about weathering exposure and UV degradation of polymeric geomembranes. **Revista Minerva – Pesquisa e Tecnologia**, n. 4(2), p. 201-205, 2008.

LODI, P. C.; BUENO, B. S. Thermo-gravimetric analysis (TGA) after different exposures of high-density polyethylene (HDPE) and polyvinyl chloride (PVC) geomembranes. **The Electronic Journal of Geotechnical Engineering,** n. 17, p. 3339-3349, 2012.

LODI, P. C.; BUENO, B. S.; VILAR, O. M. The effects of weathering exposure on the physical, mechanical, and thermal properties of high-density polyethylene and poly (vinyl chloride). **Materials Research**, n. 16, p. 1331-1335, 2013. Doi: https://doi.org/10.1590/S1516-14392013005000137.

LODI, P. C. *et al.* Evaluation of mechanical and thermal properties after chemical degradation of PVC and HDPE geomembranes. **The Electronic Journal of Geotechnical Engineering**, n. 18, p. 1227-1236, 2013.

LOPES, M. P.; LOPES, M. L. **A durabilidade dos geossintéticos**. 1ª ed. Porto: FEUP Edições, 2010.

MARCOTTE, B. A.; FLEMING, I. R. Damage to geomembrane liners from tire derived aggregate. **Geotextiles and Geomembranes**, n. 48, p. 198-209, 2020. Doi: https://doi.org/10.1016/j.geotexmem.2019.11.005.

MARTÍNEZ-ROMO, A. *et al.* Investigating the degradability of HDPE, LDPE, PE-BIO, and PE-OXO films under UV-B radiation. **Journal of Spectroscopy**, n. 586514, p. 1-6, 2015. Doi: https://doi.org/10.1155/2015/586514.

MENARD, K. P. **Dynamic mechanical analysis**: a practical introduction. 1st ed. New York: CRC Press, 1999.

MENARD, K. P. **Dynamic mechanical analysis**: a practical introduction. 2nd ed. Boca Raton: CRC Press Taylor & Francis Group., 2008.

MENDES, L. C. et al. Mechanical, thermal and microstructure evaluation of HDPE after weathering in Rio de Janeiro city. **Polymer Degradation and Stability**, n. 79, p. 371-383, 2003. Doi: https://doi.org/10.1016/S0141-3910(02)00337-3.

MERRY, S. M.; BRAY, J. D.; YOSHITOMI, S. Axisymmetric temperature- and stress-dependent creep response of ‘new’ and ‘old’ HDPE geomembranes. **Geosynthetics International**, n. 12, p. 156-161, 2005. Doi: https://doi.org/10.1680/gein.2005.12.3.156.

MITCHELL, D. H. Geomembrane compatibility tests using uranium acid leachate. **Geotextiles and Geomembranes**, n. 2, p. 111-127, 1985. Doi: https://doi.org/10.1016/0266-1144(85)90002-0.

MORSY, M. S.; ROWE, R. K. Antioxidant depletion from HDPE and LLDPE geomembranes in chlorinated water. *In*: 3RD PAN AMERICAN CONFERENCE ON GEOSYNTHETICS, 2016, Miami.

MORSY, M. S.; ROWE, R. K. Effect of texturing on antioxidant depletion rate from HDPE geomembranes. *In*: 19TH INTERNATIONAL CONFERENCE ON SOIL MECHANICS AND GEOTECHNICAL ENGINEERING, 2017, Seoul.

MOYNIHAN, R. The molecular structure of perfluorocarbon polymers. Infrared studies on polytetrafluoroethylene. **Journal of the American Chemical Society**, n. 81, p. 1045–1050,

1959.

MUELLER, W.; JAKOB, I. Oxidative resistance of high-density polyethylene geomembranes. **Polymer Degradation and Stability**, n. 79, p. 161-172, 2003. Doi: http://dx.doi.org/10.1016/S0141-3910(02)00269-0.

MUÑOZ GÓMEZ, M. Geomembrane stress cracking resistance using various polymers. *In*: 3RD PAN AMERICAN CONFERENCE ON GEOSYNTHETICS, 2016, Miami.

NOVAL, A. M. *et al.* Long-term performance of the HDPE geomembrane at the "San Isidro" reservoir. *In*: 10TH INTERNATIONAL CONFERENCE ON GEOSYNTHETICS, 2014, Berlin.

PALMEIRA, E. M. **Geossintéticos em geotecnia e meio ambiente**. 1ª ed. São Paulo: Oficina de Textos, 2018.

PEGGS, I. D.; CARLSON, D. S. 1989. Stress cracking of polyethylene geomembrane: field experience. In: KOERNER, R. M. (Ed.). **Durability and aging of geosynthetics**. London: Elsevier, 1989.

PEGGS, I. D.; KANNINEN, M. F. HDPE geosynthetics: premature failures and their prediction. **Geosynthetics International**, n. 2, p. 327-339, 1995. Doi: https://doi.org/10.1680/gein.2.0013.

PERKINS, S. W. The material properties of geosynthetics. In: SARSBY, R. W. (Ed.). **Geosynthetics in civil engineering**. Cambridge: Woodhead Published, 2007.

QUÍMICA PURA LABORATÓRIO DE ANÁLISES QUÍMICAS. **Relatório de Ensaios nº 49808/18**, Giruá, 2018.

QURESHI, F. S. *et al.* Weather induced degradation of linear low-density polyethylene: mechanical properties. **Polymer-Plastics Technology and Engineering**, n. 28, p. 649-662, 1989. Doi: https://doi.org/10.1080/03602558908049820.

REIS, R. K.; BARROSO, M.; LOPES, M. G. Evolução de cinco geomembranas expostas a condições climáticas em Portugal durante 12 anos. **Geotecnia**, n. 141, p. 41-58, 2017. Doi: http://dx.doi.org/10.24849/j.geot.2017.141.03.

RICHGELS, C. M. HDPE daily degradation cycle due to ultraviolet and thermal oxidation.

In: 3RD PAN AMERICAN CONFERENCE ON GEOSYNTHETICS, 2016, Miami.

RIMAL, S.; ROWE, R. K. Ageing of HDPE geomembranes in jet fuel A-1. **Geosynthetics International**, n. 16, p. 482-499, 2009. Doi: https://doi.org/10.1680/gein.2009.16.6.482.

ROLLIN, A. R.; RIGO, J. M. **Geomembranes** - identification and performance testing. 1st ed. London: Chapman and Hall., 1991.

ROLLIN, A. L. *et al.* Leak location in exposed geomembrane liners using an electrical leak detection technique. *In*: GEOSYNTHETIC'99, 1999, Boston.
Proceedings of Geosynthetic'99, vol. 2. Industrial Fabrics Association International, p. 615–626.

ROWE, R. K. Liner Systems. In: ROWE, R. K. (Ed.). **Geotechnical and geoenvironmental engineering handbook**. Norwell: Kluwer Academic, 2001.

ROWE, R. K.; SANGAM, H. P. Durability of HDPE geomembranes. **Geotextiles and Geomembranes**, n. 20, p. 77-95, 2002. Doi: https://doi.org/10.1016/S0266-1144(02)00005-5.

ROWE, R. K. Long-term performance of contaminant barrier systems. **Geotechnique**, n. 55, p. 631-678, 2005. Doi: https://doi.org/10.1680/geot.2005.55.9.631.

ROWE, R. K.; ISLAM, M. Z.; HSUAN, Y. G. Leachate chemical composition effects on OIT depletion in an HDPE geomembrane. **Geosynthetics International**, n. 15, p. 136-151, 2008. Doi: https://doi.org/10.1680/gein.2008.15.2.136.

ROWE, R. K.; RIMAL, S.; SANGAM, H. Ageing of HDPE geomembrane exposed to air, water and leachate at different temperatures. **Geotextiles and Geomembranes**, n. 27, p. 137-151, 2009. Doi: https://doi.org/10.1016/j.geotexmem.2008.09.007.

ROWE, R. K.; HOOR, A. Predicted temperatures and service lives of secondary geomembrane landfill liners. **Geosynthetics International**, n. 16, p. 71-82, 2009. Doi: https://doi.org/10.1680/gein.2009.16.2.71.

ROWE, R. K. *et al.* Durability of fluorinated high density polyethylene geomembrane in the Arctic. **Geotextiles and Geomembranes**, n. 28, p. 100-107, 2010. Doi: http://dx.doi.org/10.1016/j.geotexmem.2009.10.012.

ROWE, R. K. Short- and long-term leakage through composite liners. **Canadian**

Geotechnical Journal, n. 49, p. 141-169, 2012. Doi: https://doi.org/10.1139/t11-092.

ROWE, R. K.; ABDELAAL, F. B.; BRACHMAN, R. W. I. Antioxidant depletion of HDPE geomembrane with sand protection layer. **Geosynthetics International**, n. 20, p. 73-89, 2013. Doi: https://doi.org/10.1680/gein.13.00003.

ROWE, R. K.; EWAIS, A. M. R. Ageing of exposed geomembranes at locations with different climatological conditions. **Canadian Geotechnical Journal**, n. 52, p. 326-343, 2015. Doi: https://dx.doi.org/10.1139/cgj-2014-0131.

ROWE, R. K.; SHOAIB, M. Effect of brine on long-term performance of four HDPE geomembranes. **Geosynthetics International**, n. 24, p. 508-523, 2017. Doi: http://dx.doi.org/10.1680/jgein.17.00018.

ROWE, R. K.; SHOAIB, M. Long-term performance of high-density polyethylene (HDPE) geomembrane seams in municipal solid waste (MSW) leachate. **Canadian Geotechnical Journal**, n. 54, p. 1623-1636, 2017. Doi: https://doi.org/10.1139/cgj-2017-0049.

ROWE, R. K.; MORSY, M. S.; EWAIS, A. M. R. Representative stress crack resistance of polyolefin geomembranes used in waste management. **Waste Management**, n. 100, p. 18-27, 2019. Doi: https://doi.org/10.1016/j.wasman.2019.08.028.

SAFARI, E.; ROWE, R. K.; MARKLE, J. Antioxidants in an HDPE geomembrane used in a bottom liner and cover in a PCB containment landfill for 25 years. *In*: PAN AM CGS GEOTECHNICAL CONFERENCE, 2011, Toronto.

SAHU, A. K.; SUDHAKAR, K.; SARVIYA, R. M. Influence of U.V light on the thermal properties of HDPE/carbon black composites. **Case Studies in Thermal Engineering**, n. 15 (100534), p. 1-7, 2019. Doi: https://doi.org/10.1016/j.csite.2019.100534.

SANTOS, L. S. **Estudo da durabilidade de geomembranas utilizadas na impermeabilização de reservatórios das barragens de rejeito de mineração de ouro**. 2014. Dissertação de Mestrado – Escola de Engenharia da UFMG - Universidade Federal de Minas Gerais, Belo Horizonte, 2014.

SANTOS, L. S., GARDONI, M. G. A. Evaluation of geomembranes degradation aged in the laboratory and exposure to weathering. *In*: 3RD PAN AMERICAN CONFERENCE ON GEOSYNTHETICS, 2016, Miami.

SAHELI, P. T. *et al.* Diffusion of multiwall carbon nanotubes (MWCNTs) through a high

density polyethylene (HDPE) geomembrane. **Geosynthetics International**, n. 24(2), p. 184-197, 2017. Doi: http://dx.doi.org/10.1680/jgein.16.00025.

SCHEIRS, J. **A guide to polymeric geomembranes:** a practical approach. 1st ed. London: Wiley, 2009.

SCHOENBECK, M. A. Durability of chiorosulfonated polyethylene geomembrane seams after accelerated aging tests. **Geotextiles and Geomembranes**, n. 9, p. 337-341, 1990. Doi: https://doi.org/10.1016/0266-1144(90)90024-7.

SHARMA, H. D.; LEWIS, S. P. **Waste containment system, waste stabilization and landfills**: design and evaluation. 1st ed. New York: Wiley, 1994.

SHIMOTORI, T.; CUSSIER, E. L.; ARNOLD, W. A. High-density polyethylene membrane containing Fe^0 as a contaminant barrier. **Journal of Environmental Engineering**, n. 132, p. 803-809, 2006. Doi: http://dx.doi.org/10.1061/(ASCE)0733-9372(2006)132:7(803).

SOFRI, F. L. **Influência do negro de fumo na absorção da radiação na região do infravermelho para o reaquecimento do copolímero de poli (tereftalato de etileno) - PET**. 2005. Dissertação de Mestrado – Departamento de Engenharia de Materiais, Universidade Federal de São Carlos, São Carlos, 2005.

SOSA, E. R. **Caracterização e aproveitamento dos rejeitos oriundos de processos hidrometalúrgicos do níquel e cobalto com um enfoque geoambiental**. 2016. Tese de Doutorado – Departamento de Engenharia Civil e Ambiental, Universidade de Brasília, Brasília, 2016.

SPELTA, A. C. F. **Caracterização e avaliação da qualidade da água de sistema intensivo de produção de camarão com bioflocos em diferentes salinidades**. 2016. Dissertação de Mestrado – Escola de Veterinária, Universidade Federal de Minas Gerais, Belo Horizonte, 2016.

STARK, T. D.; HERNANDEZ, M. A.; ROHE, D. S. Geomembrane factory and field thermally welded seams comparison. **Geotextiles and Geomembranes**, n. 48, p. 454-467, 2020. Doi: http://dx.doi.org/10.1016/j.geotexmem.2020.02.004.

STUART, B. **Infrared spectroscopy fundamentals and applications**. 1st ed. New York: John Wiley and Sons, 2004.

SUCESKA, M. *et al.* Numerical modelling of sample–furnace thermal lag in dynamic

mechanical analyser. **Journal of Thermal Analysis and Calorimetry**, n. 100, p. 337–345, 2010. Doi: http://dx.doi.org/10.1007/s10973-009-0447-z.

SUITS, L. D.; HSUAN, Y. G. Assessing the photo-degradation of geosynthetics by outdoor exposure and laboratory weatherometer. **Geotextiles and Geomembranes**, n. 21, p. 111-122, 2003. Doi: https://doi.org/10.1016/S0266-1144(02)00068-7.

TAGHIZADEH-SAHELI, P. et al. Diffusive transport of multiwall carbon nanotubes through an HDPE geomembrane. *In*: 66TH CANADIAN GEOTECHNICAL CONFERENCE, 2013, Montreal.

TAKE, W.A. *et al.* Thermal exposure conditions for a composite liner with a black geomembrane exposed to solar radiation. **Geosynthetics International**, n. 22, p. 93-109, 2015. Doi: https://doi.org/10.1680/gein.14.00034.

TELLES, R. W.; LUBOWITZ, H. R.; UNGER, S. L. **Assessment of environmental stress corrosion of polyethylene liners in landfills and impoundments**. 1st ed. Cincinnati: U.S. EPA, 1984.

TIAN, K. *et al.* Antioxidant depletion and service life prediction for HDPE geomembranes exposed to low-level radioactive waste leachate. **Journal of Geotechnical and Geoenvironmental Engineering**, n. 143, p. 1-11, 2017. Doi: https://doi.org/10.1061/(ASCE)GT.1943-5606.0001643.

TIAN, K. *et al.* Radiation dose and antioxidant depletion in a HDPE geomembrane. **Geotextiles and Geomembranes**, n. 46, p. 426-435, 2018. Doi: https://doi.org/10.1016/j.geotexmem.2018.03.003.

TISINGER, L. G.; GIROUD, J. P. The durability of HDPE geomembranes. **Geotechnical Fabrics Report**, n. 11, p. 4-8, 1993.

TOUZE, N. Healing the world: a geosynthetics solution. **Geosynthetics International**, n. 28, p. 1-31, 2021. Doi: https://doi.org/10.1680/jgein.20.00023.

TOUZE-FOLTZ, N.; XIE, H.; STOLTZ, G. Performance issues of barrier systems for landfills: A review. **Geotextiles and Geomembranes**, n. 49, p. 475-488, 2021. Doi: https://doi.org/10.1016/j.geotexmem.2020.10.016.

VAHIDI, S.; HSUAN, G.; ELSAFTY, A. Predicting the depletion of antioxidants in high density polyethylene (HDPE) under sunlight using the reciprocity law. **Geotextiles and**

Geomembranes, n. 48, p. 170-175, 2020. Doi: https://doi.org/10.1016/j.geotexmem.2019.11.009.

VAN SANTVOORT, G. **Geotextiles and geomembranes in civil engineering**. 1st ed. Rotterdam: A.A. Balkema, 1994.

VALENTIN, C.A. *et al.* Thermoanalytical and dynamic mechanical analysis of commercial geomembranes used for fluid retention of leaching in sanitary landfills. **Journal of Thermal Analysis and Calorimetry**, n. 136, p. 471–481, 2018. Doi: http://dx.doi.org/10.1007/s10973-018-7690-0.

VILAR, O.M.; BUENO, B.S.; BENVENUTO, C. Aplicações em barreiras impermeabilizantes. In: VERTEMATTI, J.C. (Ed.). **Manual brasileiro de geossintéticos**. 2ª ed. São Paulo: Edgard Blücher, 2015. p.457-503.

ZHANG, L. *et al.* Effects of a very low pH solution on the properties of an HDPE geomembrane. **Geosynthetics International**, n. 25, p. 118-131, 2018. Doi: https://doi.org/10.1680/jgein.17.00037.